



Properties of jet fragmentation using charged particles measured with the ATLAS detector in pp collisions at $\sqrt{s} = 13$ TeV

The ATLAS Collaboration

This paper presents a measurement of quantities related to the formation of jets from high-energy quarks and gluons (fragmentation). Jets with transverse momentum $100 \text{ GeV} < p_T < 2.5 \text{ TeV}$ and pseudorapidity $|\eta| < 2.1$ from an integrated luminosity of 33 fb^{-1} of $\sqrt{s} = 13 \text{ TeV}$ proton–proton collisions are reconstructed with the ATLAS detector at the Large Hadron Collider. Charged-particle tracks with $p_T > 500 \text{ MeV}$ and $|\eta| < 2.5$ are used to probe the detailed structure of the jet. The fragmentation properties of the more forward and the more central of the two leading jets from each event are studied. The data are unfolded to correct for detector resolution and acceptance effects. Comparisons with parton shower Monte Carlo generators indicate that existing models provide a reasonable description of the data across a wide range of phase space, but there are also significant differences. Furthermore, the data are interpreted in the context of quark- and gluon-initiated jets by exploiting the rapidity dependence of the jet flavor fraction. A first measurement of the charged-particle multiplicity using model-independent jet labels (topic modeling) provides a promising alternative to traditional quark and gluon extractions using input from simulation. The simulations provide a reasonable description of the quark-like data across the jet p_T range presented in this measurement, but the gluon-like data have systematically fewer charged particles than the simulation

1 Introduction

Jets are collimated sprays of particles resulting from high-energy quark and gluon production. The details of the process that underlies the *fragmentation* of quarks and gluons with net quantum chromodynamic (QCD) charge into net neutral hadrons is not fully understood. Jet formation is a complex multi-scale problem, including important contributions from QCD effects that cannot be described by perturbation theory. Measuring basic quantities related to fragmentation is therefore essential to furthering our understanding of the emergent properties of QCD.

Perturbative and non-perturbative physically inspired models have free parameters that are tuned to data in order to best describe the radiation pattern inside jets [1]. This is in turn an important input to all analyses at the Large Hadron Collider (LHC) due to the ubiquity of jets. Measurements of jet substructure in proton–proton (pp) collisions at a center-of-mass energy of $\sqrt{s} = 7$ TeV [2–5] have already been used by the ATLAS Collaboration for parameter optimizations (tunes) of the PYTHIA 8 Monte Carlo (MC) generator [6]. A measurement of the average number of charged particles inside jets at $\sqrt{s} = 8$ TeV [7] was also used as input to recent developments in the HERWIG 7 MC program [8]. Further measurements of jet constituent multiplicity and energy sharing will provide powerful constraints for future generator optimizations.

Quark- and gluon-initiated jets (henceforth quark and gluon jets) have different radiation patterns (see e.g. Ref. [9]). As many analyses at the LHC target either quark-enriched or gluon-enriched processes, these radiation-pattern differences can be useful for jet tagging [10, 11]. Measurements of jet structure can be used to calibrate quark-versus-gluon jet taggers. By exploiting the rapidity dependence of the relative quark and gluon jet rates, ATLAS [7] extracted the average charged-particle multiplicity for quark and gluon jets separately. This was then combined with detector-level systematic uncertainties to provide quark/gluon tagger uncertainties at $\sqrt{s} = 13$ TeV [12]. A more complex tagger based on several jet shapes could be calibrated in a similar manner using extended results. The benefit of a particle-level measurement is that a portion of the calibration can be independent of ATLAS and LHC operating conditions. Uncertainties in detector effects can be updated with the changing detector environment. Adding more observables and measuring their differential distributions will improve this calibration.

Although the full radiation pattern inside jets is not calculable from first principles, the energy dependence of many observables can be calculated in perturbation theory. There have been significant theoretical advances in soft-collinear effective theory (SCET) [13–16] to derive factorization theorems that describe the evolution of universal non-perturbative functions [17–20]. This was applied to the measurement of jet charge at $\sqrt{s} = 8$ TeV [21]. There have also been predictions and comparisons with the jet transverse momentum (p_T) dependence of the average number of charged particles inside jets (see Ref. [7] and references therein). This quantity does not have a perturbative expansion in the usual sense (as a series in α_S); instead there is a series expansion in $\sqrt{\alpha_S}$ [22, 23]. This behavior is predicted for a wide class of *Sudakov safe* observables [24]. At least for the case of charged-particle multiplicity, this non-standard expansion seems to be an excellent model of the data [7].

The goal of this paper is to measure properties of jet fragmentation using charged-particle tracks. Such properties have been measured at many colliders at various center-of-mass energies, including the SPS [25–27], PETRA [28, 29], PEP [30–33], TRISTAN [34], CESR [35], LEP [36–47], HERA [48, 49], and the Tevatron [50–53]. Previous measurements by the ATLAS and CMS Collaborations were performed at $\sqrt{s} = 2.76$ TeV [54, 55], $\sqrt{s} = 5.02$ TeV [56–58], $\sqrt{s} = 7$ TeV [2, 59, 60] and $\sqrt{s} = 8$ TeV [7, 21, 61] in pp collisions and are also compared with jet fragmentation measured in Pb+Pb collisions [54, 56–58, 62, 63]

and p+Pb collisions [56]. The measurement presented here represents a significant extension of previous work. In particular, the accessible jet energy range is increased due to the larger $\sqrt{s} = 13$ TeV. There are enough events in the 2016 dataset to probe the substructure of jets with p_T up to 2.5 TeV. Next, the precision of the measurement has improved due to advances in track reconstruction inside jets during the long shutdown between LHC Runs 1 and 2, including the additional insertable B-layer (IBL) detector [64, 65] and new algorithms for tracking inside dense environments [66–68]. Furthermore, detailed experimental studies to derive uncertainties in all aspects of tracking inside jets extend the capabilities of previous measurements to a wider region of phase space and also allow differential analyses [67, 69]. These new data therefore probe broader and deeper aspects of the radiation pattern inside jets across an extended phase space.

The paper is organized as follows. Section 2 introduces the observables to be measured. Then, following a brief description of the ATLAS detector in Section 3, the data and simulation samples are documented in Section 4. Charged-particle track, jet, and event reconstruction are detailed in Section 5. Corrections for detector effects (unfolding) are documented in Section 6. A description of the corresponding systematic uncertainties can be found in Section 7 and the results are presented in Section 8. Section 9 provides conclusions and future outlook.

2 Observables

This analysis builds upon the previous ATLAS jet structure measurements presented in Refs. [7, 21, 59]. The fundamental quantity is the fragmentation function $D_p^h(z, E)$, which describes the probability of finding a hadron h with energy fraction z of the parton p that has energy E . At a hadron collider, the jet transverse momentum, p_T ,¹ is a better proxy for the starting scale (μ) of jet evolution. To avoid confusion with previous measurements of similar observables, the transverse momentum fraction is denoted in this paper by the symbol $\zeta = p_T^{\text{particle}}/p_T^{\text{jet}}$. The fragmentation function itself, like parton distribution functions (PDFs), cannot be calculated from first principles in perturbation theory. However, it has a DGLAP [70–72] evolution and so the p_T dependence of many observables can be calculated. In particular:

$$\mu \frac{\partial}{\partial \mu} D_p^h(\zeta, \mu) = \sum_{p'} \int_{\zeta}^1 \frac{d\zeta'}{\zeta'} \frac{\alpha_S(\mu) P_{p' \leftarrow p}(\zeta', \mu)}{\pi} D_{p'}^h\left(\frac{\zeta}{\zeta'}, \mu\right), \quad (1)$$

where $P_{p' \leftarrow p}(\zeta, \mu)$ are the Altarelli–Parisi splitting functions [70] and depend on the scale μ through α_S . Charged particles are studied because they provide a way to measure single hadrons inside the jet (as opposed to calorimeter energy deposits, which can result from multiple particles) which gives access to $\sum_h D_p^h$. A basic quantity related to the fragmentation function is the charged-particle multiplicity. The average charged-particle multiplicity is an integral over ζ and a sum over h and p of $D_p^h(\zeta)$. An extension of the multiplicity is the set of ζ moments of D . The zeroth moment is the average multiplicity. The full distribution of multiplicity depends on (multi-hadron) fragmentation functions in a complicated way; a more direct probe of D is to measure hadron production as a function of ζ , which is a sum of D over p and

¹ ATLAS uses a right-handed coordinate system with its origin at the nominal interaction point (IP) in the center of the detector and the z -axis along the beam pipe. The x -axis points from the IP to the center of the LHC ring, and the y -axis points upwards. Cylindrical coordinates (r, ϕ) are used in the transverse plane, ϕ being the azimuthal angle around the z -axis. The pseudorapidity is defined in terms of the polar angle θ as $\eta = -\ln \tan(\theta/2)$. Angular distance is measured in units of $\Delta R \equiv \sqrt{(\Delta\eta)^2 + (\Delta\phi)^2}$.

h (but no integral over ζ). Additional observables are also studied in order to probe the angular spread of jet fragmentation beyond the collinear limit. All of the observables are described below.

Charged-particle multiplicity (n_{ch}): The number of charged particles inside a jet with p_T above some threshold. In terms of the fragmentation function:

$$\langle n_{\text{ch}} \rangle(p_T^{\text{jet}}) = \sum_p f_p(p_T^{\text{jet}}) \sum_{h \text{ charged}} \int_{\text{threshold}/p_T^{\text{jet}}}^1 d\zeta D_p^h(\zeta, p_T^{\text{jet}}),$$

where f_p is the fraction of parton type p at a given jet p_T . The multiplicity is not calculable in perturbation theory, but to lowest order in $\sqrt{\alpha_S}$, the ratio of the multiplicity for quark-initiated jets to that for gluon-initiated jets is the ratio of color factors $C_A/C_F = 9/4$. The fraction of quark jets increases with p_T , which decreases the inclusive multiplicity. However, this is compensated by an inherent increase in the multiplicity with p_T for both quark and gluon jets [73]. In addition to the mean, the full $(1/N_{\text{jet}})dN_{\text{jet}}/dn_{\text{ch}}$ distribution is measured.

Summed fragmentation function: The distribution of the momentum fraction ζ is studied inside jets summed over charged-hadron types. The quantity that is measured is $F(\zeta, p_T^{\text{jet}}) = (1/N_{\text{jet}})dn_{\text{ch}}/d\zeta$. In terms of the fragmentation function:

$$F(\zeta, p_T^{\text{jet}}) = \sum_p f_p(p_T^{\text{jet}}) \sum_{h \text{ charged}} D_p^h(\zeta, p_T^{\text{jet}}).$$

By definition, $\int d\zeta F(\zeta) = \langle n_{\text{ch}} \rangle$. In addition to measuring the distribution $F(\zeta)$ in bins of jet p_T , summary statistics of the $F(\zeta)$ distribution are extracted to show how the distribution evolves with jet p_T . The following properties of the ζ distribution are extracted:

- Partial fractions of $F(\zeta)$: $\int_0^X F(\zeta)d\zeta / \int F(\zeta)d\zeta = n_{\text{ch}}(\zeta < X)/n_{\text{ch}}$ to show how much of the jet energy is carried by particles of a given p_T fraction. For illustration, the values considered are $X \in \{0.1, 0.01, 0.001\}$. As $X \rightarrow 1$, these partial fractions become a constant value of 1.0, independent of the jet p_T .
- Moments of $F(\zeta)$: $\langle \zeta^\kappa \rangle = \int \zeta^\kappa F(\zeta)d\zeta / \int F(\zeta)d\zeta$. The distribution of $F(\zeta)$ is nearly normally distributed in $\log(\zeta)$, which means that it is defined by its first two moments [73]. For this reason, $\kappa = 2$ is measured as a function of the jet p_T . For illustration, the case $\kappa = 1/2$ is also considered.
- Weighted sums over the jet: $\langle \sum_{i \in \text{jet}} \zeta_i^\kappa \rangle = \int \zeta^\kappa F(\zeta)d\zeta$. The values considered are $\kappa \in \{1/2, 2\}$. The observable $\sum_{i \in \text{jet}} \zeta_i^2$ is often called p_T^{D} and can be used for quark/gluon jet tagging [74]. For a given jet type, these observables increase monotonically with increasing jet p_T for $\kappa \lesssim 1$ and decrease monotonically for $\kappa \gtrsim 1$ (see Section 8.2); the κ values chosen are representative of these trends.

Each of these derived quantities is extracted from the measured $F(\zeta)$ distribution. More details about the procedure for unfolding these derived quantities are presented in Section 6.

Transverse momentum: $p_T^{\text{rel}} \equiv p_T^{\text{charged particle}} \sin \Delta\phi$, where $\Delta\phi$ is the angle between the momentum of the constituent charged particle and the jet axis in the transverse plane. The quantity that is measured is $f(p_T^{\text{rel}}, p_T^{\text{jet}}) = (1/N_{\text{jet}})dn_{\text{ch}}/dp_T^{\text{rel}}$. The average value is defined by $\langle p_T^{\text{rel}} \rangle = \int p_T^{\text{rel}} f(p_T^{\text{rel}}) / \int f(p_T^{\text{rel}})$.

Radial profile: The number of charged particles in various annuli around the jet axis. The quantity that is measured is $\rho_{\text{ch}}(r, p_{\text{T}}^{\text{jet}}) = (1/N_{\text{jet}})dn_{\text{ch}}/2\pi r dr$, where $r = \Delta R(\text{charged particle, jet})$. The average value is defined by $\langle r \rangle = \int r \rho_{\text{ch}}(r) / \int \rho_{\text{ch}}(r)$.

The last two quantities are not simple derivatives of the fragmentation function as they additionally depend on finite opening angles encoded in the $d\theta/\theta$ emission phase space. Since quantities are measured as a function of jet p_{T} which is defined using charged and neutral particles, the observables are sensitive to the charged-to-neutral fraction inside jets. However, this fraction is robust to mis-modelling as isospin is an approximate symmetry of the strong force.

3 ATLAS detector

The ATLAS detector [75] at the LHC covers nearly the entire solid angle around the collision point. It consists of an inner tracking detector surrounded by a thin superconducting solenoid, electromagnetic and hadronic calorimeters, and a muon spectrometer incorporating three large superconducting toroidal magnets. The inner-detector system (ID) is immersed in a 2 T axial magnetic field and provides charged-particle tracking in the range $|\eta| < 2.5$.

The high-granularity silicon pixel detector covers the vertex region and typically provides four measurements per track, the first hit being normally in the IBL. It is followed by the silicon microstrip tracker (SCT) which usually provides eight measurements per track. These silicon detectors are complemented by the transition radiation tracker (TRT), which enables radially extended track reconstruction up to $|\eta| = 2.0$.

The calorimeter system covers the pseudorapidity range $|\eta| < 4.9$. Within the region $|\eta| < 3.2$, electromagnetic calorimetry is provided by barrel and endcap high-granularity lead/liquid-argon (LAr) calorimeters, with an additional thin LAr presampler covering $|\eta| < 1.8$, to correct for energy loss in material upstream of the calorimeters. Hadronic calorimetry is provided by the steel/scintillating-tile calorimeter, segmented into three barrel structures within $|\eta| < 1.7$, and two copper/LAr hadronic endcap calorimeters. The solid angle coverage is completed with forward copper/LAr and tungsten/LAr calorimeter modules optimised for electromagnetic and hadronic measurements respectively.

Interesting events are selected to be recorded by the first-level trigger system implemented in custom hardware, followed by selections made by algorithms implemented in software in the high-level trigger [76]. The first-level trigger reduces the 40 MHz bunch crossing rate to below 100 kHz, which the high-level trigger further reduces in order to record events to disk at about 1 kHz.

4 Datasets and simulated samples

These measurements use the dataset of pp collisions recorded by the ATLAS detector in 2016, corresponding to an integrated luminosity of 33 fb^{-1} at a center-of-mass-energy of $\sqrt{s} = 13 \text{ TeV}$. Events are only considered if they are collected during stable beam conditions and satisfy all data quality requirements. Due to the high instantaneous luminosity and the large total inelastic proton–proton cross section, on average there are about 25 simultaneous (pileup) collisions in each bunch crossing.

The measurements presented in this paper use a variety of MC samples for estimating correction factors as well as for comparison with the corrected data. Dijet events were generated at leading order (LO) with

PYTHIA 8.186 [77], with the $2 \rightarrow 2$ matrix element convolved with the NNPDF2.3LO PDF set [78] and using the A14 tune of multiple-parton-interaction and shower parameters [6]. PYTHIA uses a p_T -ordered parton shower model. Additional dijet events were simulated using different generators, in order to study the impact of modeling uncertainties. SHERPA 2.1 [79] events were generated using multi-leg $2 \rightarrow 2$ and $2 \rightarrow 3$ matrix elements, which were matched to parton showers following the CKKW prescription [80]. These SHERPA events were simulated using the CT10 PDF set [81] and the default SHERPA event tune. Herwig++ 2.7 [82, 83] was used to provide a sample of events with an angle-ordered parton shower model. These events were generated with the $2 \rightarrow 2$ matrix element, convolved with the CTEQ6L1 PDF set [84] and configured with the UE-EE-5 tune [85].

All simulated events were passed through a full simulation of the ATLAS detector [86] implemented in GEANT 4 [87], which describes the interactions of particles with the detector and the subsequent digitization of analog signals. The effects of multiple simultaneous pp collisions were simulated with inelastic pp collisions using the PYTHIA 8.186 generator with the A2 [88] set of tuned parameters and the MSTW2008LO [89] PDF set; these events were overlaid on the nominal dijet events.

5 Object and event selection

Since the data are unfolded to particle level, it is necessary to define both the particle-level and detector-level objects used in the measurement. The former are chosen to be as close as possible to the latter in order to minimize the model dependence caused by an extrapolation from the measured phase space at detector level to the phase space at particle level. Section 5.1 describes the definition of charged-particle tracks and jets. Following the discussion of objects, Section 5.2 describes the particle-level and detector-level event selection criteria.

5.1 Object reconstruction

While it is not possible to separate the underlying event from the hard scatter at particle level, it is possible to remove the contribution from pileup. Therefore, the unfolding target is particle-level distributions produced in single proton–proton interactions. However, at detector level, there is ambiguity about which pp collision vertex corresponds to the hard-scatter event. Collision vertices are reconstructed from tracks in the inner detector. Each vertex is required to be associated with at least two tracks with $p_T > 0.4$ GeV. The primary hard-scattering vertex of the event is chosen to be the one with the highest $\sum p_T^2$ calculated using all tracks associated with the vertex.

Particle-level jets are built from MC-simulated stable particles ($c\tau > 10$ mm) excluding muons and neutrinos. By definition, particles from pileup and from interactions with the detectors are not included. These jets are clustered using the anti- k_r [90] algorithm with radius parameter $R = 0.4$ as implemented in FastJet [91]. Detector-level jets are built from topological calorimeter-cell energy clusters [92] using the same algorithm as is used at particle level. A series of simulation- and data-based correction and calibration factors are applied to ensure that the resulting jet p_T is the same as the particle-level value on average [93]. Jets are required to have $p_T > 60$ GeV so that the rate of jets originating from pileup is negligible. The detector-level phase space includes one bin at low jet p_T (60–100 GeV) which is not in the fiducial phase space of the measurement due to the large impact of migrations into and out of the acceptance.

Charged particles are used to compute the particle-level definitions of all observables if they are clustered within a particle-level jet and have $p_T > 500$ MeV and $|\eta| < 2.5$. The detector-level analog to charged particles is tracks. Tracks are reconstructed from hits in the inner detector (see e.g. Ref. [67]) and a series of quality criteria are applied to the selected tracks to reject those originating from hits due to multiple charged particles (fake tracks) and from pileup. The transverse momentum resolution is approximately $\sigma(p_T)/p_T \approx 0.05\% \times p_T/\text{GeV} \oplus 1\%$, with a significant degradation in the core of high- p_T jets due to challenges associated with pattern recognition.² Tracks are required to pass the tight primary selection as well as the loose track-to-vertex association [94]. In particular, they must have $p_T > 500$ MeV and $|\eta| < 2.5$, and the number of pixel and strip clusters associated with the track is required to be at least 9 (11) for $|\eta| < 1.65$ (≥ 1.65). In addition, the transverse impact parameter d_0 relative to the beamline must be less than 2 mm and the longitudinal impact parameter, z_0 , is required to satisfy $|z_0 \sin \theta| < 3$ mm. Tracks are matched to jets via ghost association [95]. This matching procedure creates ghost versions of the tracks with the same direction but infinitesimal p_T . Jet clustering is repeated and tracks are assigned to the jet that contains their ghosted version. For the isolated, high p_T jets used in this measurement, ghost association is nearly identical to a geometric matching based on $\Delta R < 0.4$.

5.2 Event selection

Particle-level events are required to have at least two jets with $|\eta| < 2.1$ (within the tracking detector acceptance) and the leading two such jets must satisfy $p_T^{\text{lead}}/p_T^{\text{sublead}} < 1.5$. This jet- p_T balance requirement simplifies the interpretation of the final state in terms of a $2 \rightarrow 2$ scattering process.

Detector-level events are selected using single-jet triggers. Due to the large cross section for jet production, most of the jet triggers are *prescaled*: events that pass the trigger are randomly discarded with a fixed probability. The trigger used for a particular jet p_T is chosen to ensure that the trigger is 100% efficient (for the measurement phase space and prior to prescaling) and has the lowest prescale factor. Events in data are weighted by the prescale. The lowest-threshold unprescaled jet trigger is used for jets with $p_T > 600$ GeV. Detector-level events are required to pass the same selection requirements as particle-level events: there must be at least two offline calibrated jets with $|\eta| < 2.1$ and the leading two of these jets must satisfy $p_T^{\text{lead}}/p_T^{\text{sublead}} < 1.5$. Figure 1 shows the basic kinematic properties of the two leading jets passing this event selection compared with various MC predictions at detector level.

The substructure of the two leading jets is used in the analysis. Figure 2 shows detector-level distributions for a selection of the observables that were introduced in Section 2. For the jets with $p_T \sim 1$ TeV shown in Figure 2, the most probable number of tracks is about 15 and the most probable momentum fraction is about 1%. The radiation pattern is peaked at the center of the jet, so both the p_T^{rel} and r distributions are peaked at zero. The PYTHIA, Herwig++, and SHERPA distributions generally bracket the data and are accurate to within about 20%.

In order to expose differences between quark and gluon jets, the more forward and more central of the two jets are distinguished and measured separately. Figure 3 shows the gluon-jet fraction as a function of jet p_T and jet η (more details about quark/gluon definitions are given in Section 8.2). For a fixed jet p_T , higher- $|\eta|$ jets are more often quark-initiated due to valence quarks scattering off gluons. For a fixed η , the quark fraction increases with jet p_T due to the relative increase in valence-quark scattering off a quark or gluon compared with gluon-gluon scattering.

² For example, the p_T resolution is approximately 30% at 100 GeV when five or more particles are within $\Delta R < 0.015$.

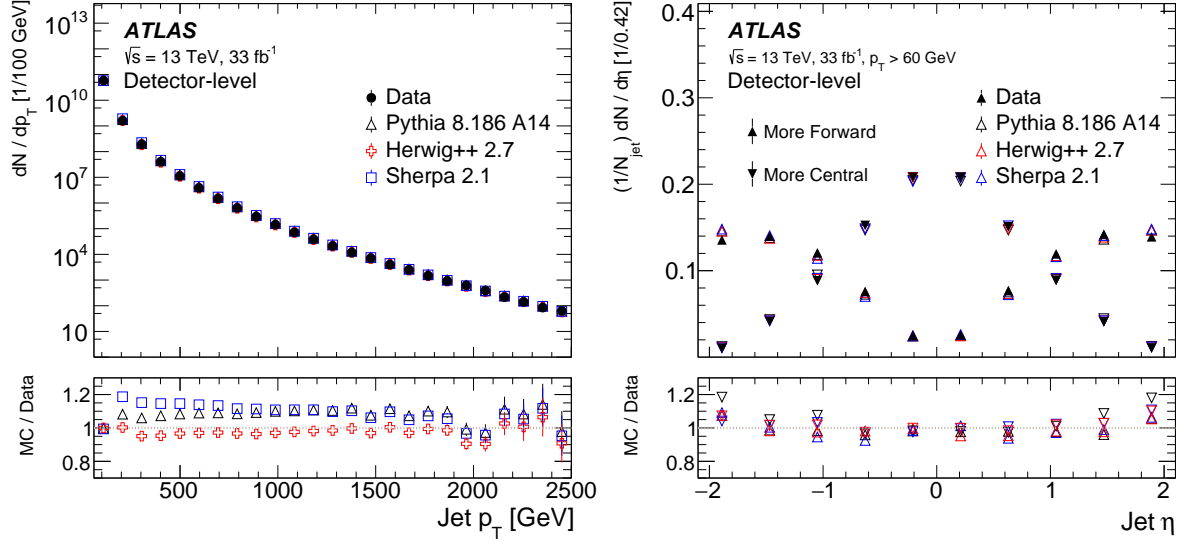


Figure 1: Left: The transverse momentum, p_T , spectrum for the selected jets; the simulation is normalized to the data. The normalization is dominated by the first bin, which accounts for the overall offset in the other bins for some of the predictions. Right: The pseudorapidity, η , distribution for the selected jets, split into the more forward and the more central of the two jets. Error bars only include the statistical uncertainty.

Table 1 summarizes the object and event selections from Section 5.1 and Section 5.2.

Table 1: A summary of the object and event selection criteria at particle level and detector level.

	Particle level	Detector level
Pileup	–	Identify primary vertex
Jet algorithm	Anti- k_t , $R = 0.4$	
Jet requirements	$ \eta < 2.1$	
Jet constituents	Particles with $c\tau > 10$ mm prior to detector interactions excluding μ and ν	Calorimeter energy clusters
Measurement inputs	Charged jet constituents, $p_T > 500$ MeV and $ \eta < 2.5$	Ghost-associated tracks, $p_T > 500$ MeV and $ \eta < 2.5$
Event selection	At least two jets, with the leading two satisfying $p_T^{\text{lead}}/p_T^{\text{sublead}} < 1.5$	
Jet selection	Leading two, separated by η (more forward/central)	

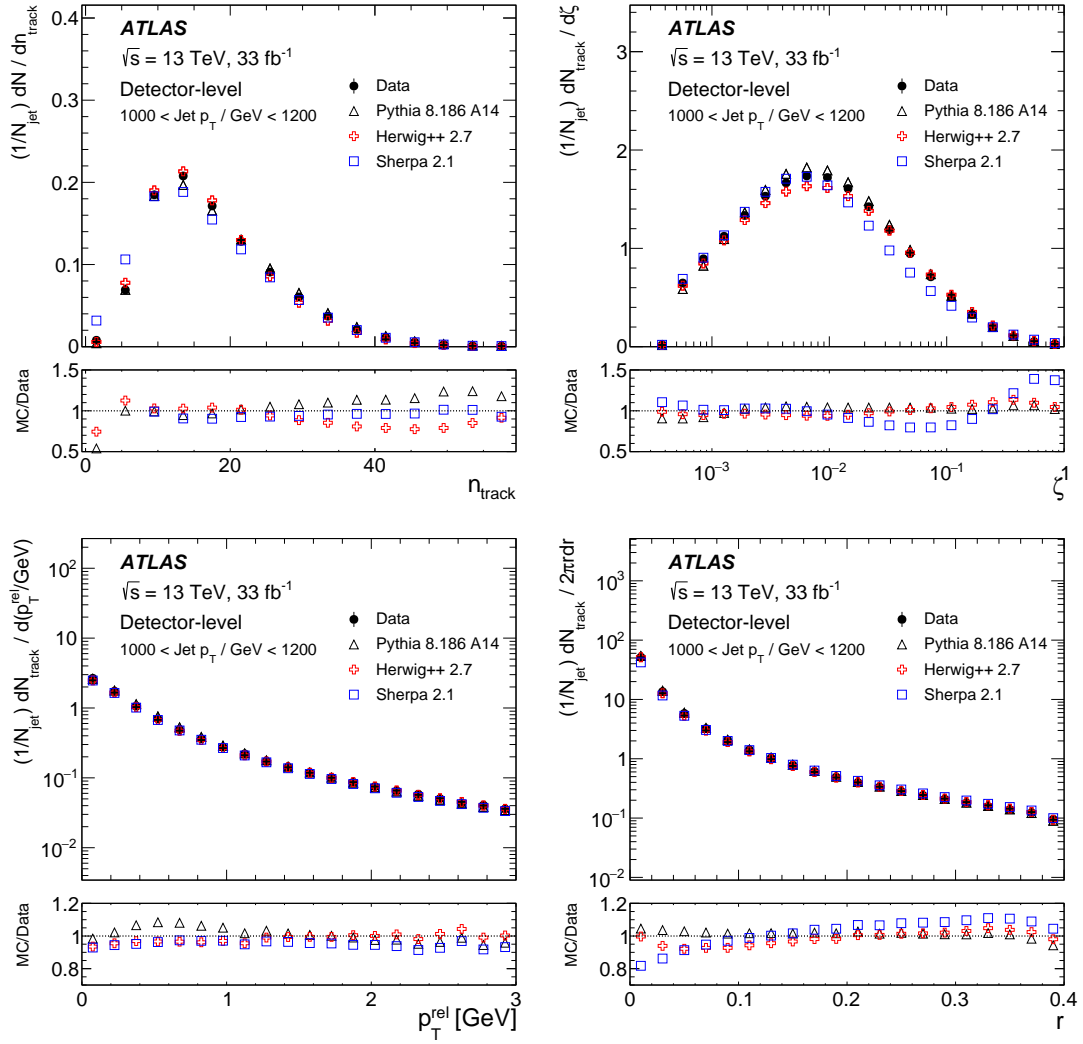


Figure 2: The detector-level distributions of (top left) the number of charged-particle tracks n_{track} , (top right) the transverse momentum fraction ζ , (bottom left) the transverse momentum $p_{\text{T}}^{\text{rel}}$, and (bottom right) the radial profile in bins of the distance r from the jet axis for jets with transverse momentum $1 \text{ TeV} < p_{\text{T}}^{\text{jet}} < 1.2 \text{ TeV}$. Error bars include the statistical uncertainty only.

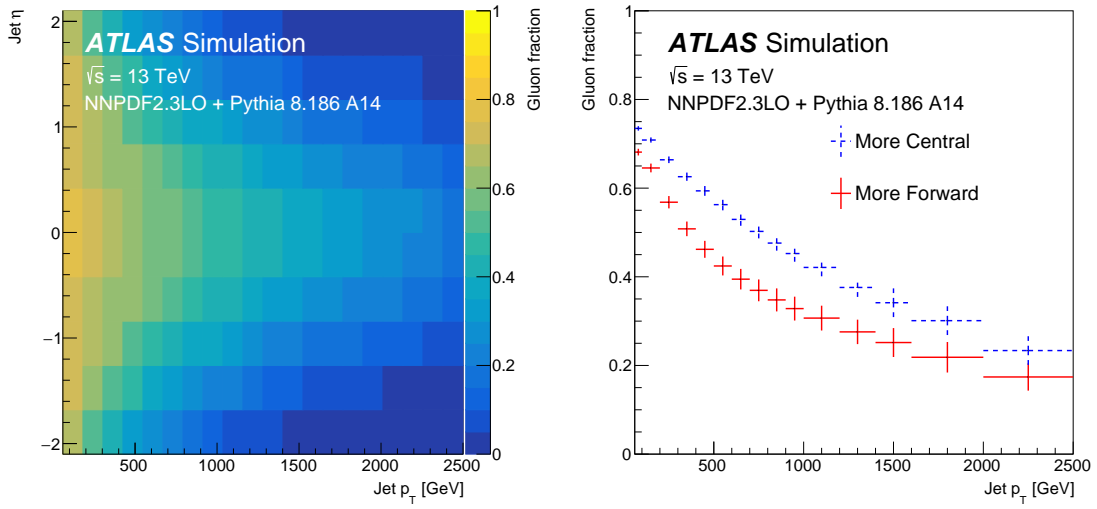


Figure 3: Left: The gluon-jet fraction as a function of jet transverse momentum p_T and jet pseudorapidity η . Right: the fraction of the more forward and the more central jets that are gluon-initiated. The error bars in the right plot represent the uncertainty computed from the 100 NNPDF2.3LO replicas [78]. See Section 8.2 for more details about quark/gluon definitions and uncertainties.

6 Unfolding

The data are corrected for resolution and acceptance effects, and the fiducial phase space of the measurement is described by the particle-level object and event selection in Section 5. Equation (2) symbolically summarizes the unfolding procedure for a binned distribution x :

$$x_{\text{unfolded},i} = \frac{1}{n_{\text{jets, unfolded}}} \sum_{j=1}^{N_{\text{total}}} \theta_{ij} x_{\text{detected},j} \left(\frac{1 - \epsilon_{\text{reco not true},j}}{1 - \epsilon_{\text{true not reco},i}} \right), \quad (2)$$

where $n_{\text{jets, unfolded}}$ is the unfolded number of forward or central jets (depending on the bin), determined by the number of entries in the n_{ch} unfolding (as there is one entry per jet). The symbols θ and ϵ represent the unfolding matrix and correction factors, described in more detail below.

The jet substructure observables are simultaneously unfolded with the jet p_{T} and for the more forward and the more central jets at the same time. For an observable with n_{bins} bins in a given p_{T} bin, this results in a total of $N_{\text{total}} = 2 \times (n_{\text{bins}}) \times (p_{\text{T}} \text{ bins})$ bins. All of these bins are concatenated to form a one-dimensional input. To begin the unfolding, the data are corrected for the fraction of events that pass the detector-level selection but not the particle-level selection, $\epsilon_{\text{reco not true}}$. This also corrects for non-dijet events, but their rate is negligible. Then, an iterative Bayesian (IB) unfolding technique [96] is used as a regularized matrix inversion to correct for the detector resolution in events that pass both the detector-level and particle-level selections. The IB method is implemented in the RooUnfold framework [97] with the unfolding matrix θ and one iteration, is chosen to minimize the total uncertainty. After the application of the response matrix, a final correction is applied to account for the fraction of events that pass the particle-level but not detector-level selection, $\epsilon_{\text{true not reco}}$. The resulting unfolded measurement is reorganized into individual distributions with n_{bins} per p_{T} bin for each of the more forward and more central jet. The jet p_{T} is also unfolded in parallel and each p_{T} bin of the jet substructure observable is normalized by the number of measured jets in that bin. For n_{ch} , this renders the distributions normalized to unity per jet p_{T} bin; for the other observables, the normalization in each p_{T} bin is (up to acceptance effects) $\langle n_{\text{ch}} \rangle$, as discussed in Section 2.

To illustrate the jet- p_{T} dependence of the measured observables, the evolution with the jet p_{T} of various moments (κ) is computed using Eq. (3):

$$\langle x^\kappa \rangle_{\text{unfolded}}(p_{\text{T}} \text{ bin } j) = c_{\text{binning},j}(\kappa) \frac{\sum_{i=1}^{n_{\text{bins}}} x_{\text{unfolded},i} \times (\text{bin center } i)^\kappa}{\sum_{i=1}^{n_{\text{bins}}} x_{\text{unfolded},i}}, \quad (3)$$

where the sum is over all i that correspond to p_{T} bin j . Since the bin center is used to calculate the average, a correction c_{binning} is applied to account for the difference between the bin center and the mean of the distribution within the bin. This correction is calculated using PYTHIA, and is computed by reweighting PYTHIA so that it agrees with the unfolded distribution. For ζ , $p_{\text{T}}^{\text{rel}}$, and r , Eq. (3) represents the κ moment for individual particles. For ζ , the jet-based moments are also computed: $\langle \sum_{i \in \text{jet}} \zeta_i^\kappa \rangle$. For these jet-based moments, Eq. (3) is modified by removing the denominator $\sum_{i=1}^{n_{\text{bins}}} x_{\text{unfolded},i}$. By construction, the $\kappa = 0$ jet-based moment of ζ is the $\kappa = 1$ moment of n_{ch} . The binning correction factor is mostly near unity, deviating by less than 1% for n_{ch} and up to about 10% for the other observables.

Figure 4 shows the response matrix normalized per particle-level bin. As stated above, the observable bins are concatenated with the jet p_T and for both the more forward and more central jets to form a one-dimensional distribution that is unfolded. A diagonal stripe represents events where the detector-level jet p_T is the same as the particle-level value; off-diagonal components represent jet p_T migrations. Within a jet p_T bin, there is a small dependence on ζ , with a worse resolution at high ζ due to the deteriorating momentum resolution at high track p_T . The diagonal strips in the upper left and lower right quadrants correspond to events where the more forward particle-level jet is the more central detector-level jet and vice versa. This migration happens in about 1% of events. Within a given jet p_T bin, the migrations to neighboring ζ bins are small. Except at high ζ and high jet p_T where the migrations can reach 50%, the off-diagonal components of the response matrix are about 10%.

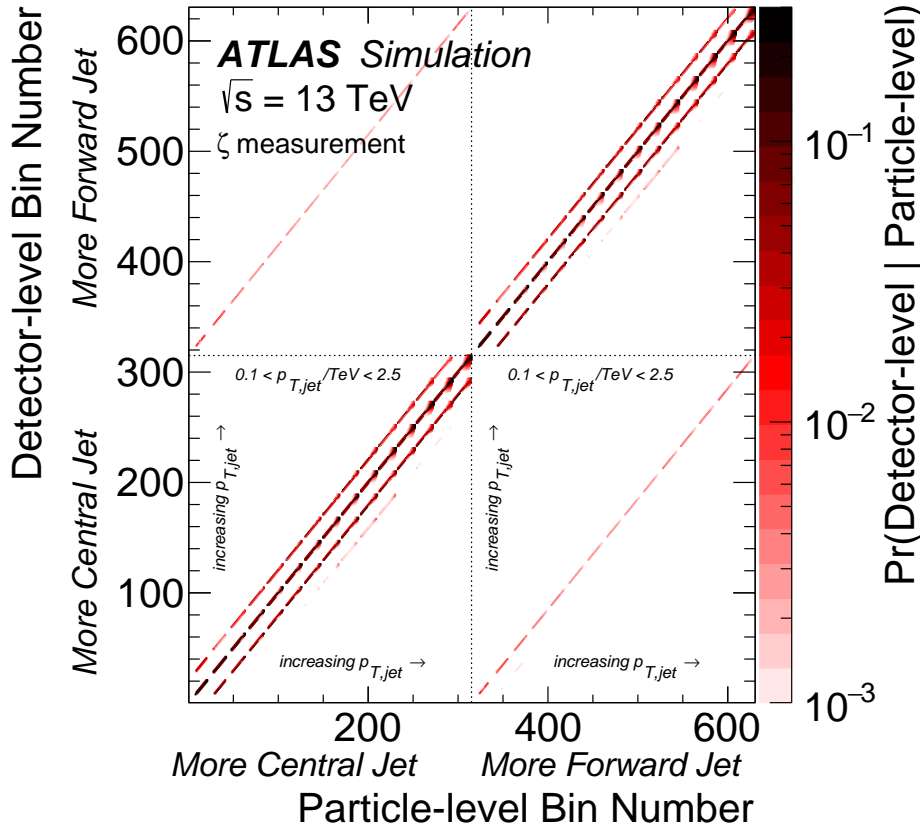


Figure 4: The probability distribution for the detector-level combined transverse momentum fraction ζ and jet transverse momentum p_T distribution normalized in bins of the particle-level variable using the PYTHIA simulation. The ζ distribution is concatenated with the jet p_T so that every 21 bins is a different jet- p_T bin. The first 315 bins represent the more central of the two jets and the second 315 bins correspond to the more forward jet. The z -axis is truncated at 10^{-3} for visualization only, to aid readability.

7 Uncertainties

Systematic and statistical uncertainties are assessed for each step of the analysis, including the acceptance correction factors, response matrix, and unfolding method. For each uncertainty, some component of the analysis chain is varied and then the entire unfolding procedure is repeated. Data and simulation statistical uncertainties are determined from pseudo-experiments using the bootstrap method [98]. The details of the experimental systematic uncertainties related to track and jet reconstruction are given in Section 7.1 and the uncertainties in the unfolding method and fragmentation modeling are described in Section 7.2. An additional source of uncertainty arising from binning effects is evaluated when computing the average value of an observable as a function of jet p_T . The average values are determined using the bin centers, so the correction described in Section 6 relies on the simulation for the distribution within a given bin. An uncertainty in the binning correction is estimated by comparing the correction factors derived from PYTHIA with those from SHERPA, where both simulations are reweighted to match the unfolded data distribution.

Figure 5 provides an overview of the systematic uncertainties for a selection of observables, using the average value versus p_T for illustration. The uncertainty in the rate of fake and secondary tracks is the leading experimental reconstruction uncertainty for $\langle n_{\text{ch}} \rangle$ and $\langle r \rangle$ except at low jet p_T where the uncertainties from the inclusive tracking efficiency and the unfolding procedure are larger. The jet energy uncertainties are the most important for ζ , with the tracking uncertainties matching in size in the highest jet- p_T bins. The tracking and jet energy uncertainties are about the same size for $\langle p_T^{\text{rel}} \rangle$. Fragmentation modeling uncertainties are large for $\langle n_{\text{ch}} \rangle$ at low jet p_T and for $\langle \zeta \rangle$ at high jet p_T . While the size of the binning correction uncertainty is less than 2% for $\langle p_T^{\text{rel}} \rangle$ and $\langle r \rangle$, it is still the dominant uncertainty for these observables. Further details about each uncertainty source are given below and the full covariance matrices, including all correlation information, are made available in Ref. [99].

7.1 Track and jet reconstruction

Except for ζ , the jet energy is only used to determine the p_T bin. Since the fragmentation properties vary slowly with jet p_T , the resulting impact of jet energy scale and resolution uncertainties on the analysis is often less important than other sources of uncertainty. Nonetheless, the impact of a 19-parameter decomposition of the jet energy scale uncertainty was evaluated [93]. Six of these 19 components are due to in situ constraints on the jet energy scale from various multi-object balance studies, such as Z+jets. Additional sources of uncertainty are related to pileup, jet flavor, and extrapolations to high p_T . The total uncertainty in the jet energy scale is about 1% for jets with p_T between 100 and 1000 GeV and the impact on this measurement is much less than 1% except at high ζ , where it can reach as high as 2%. The impact of the jet energy resolution is determined from an ensemble of event samples with jet energies smeared within the uncertainty.

The most important experimental uncertainties are related to track reconstruction and cover the track reconstruction efficiency, the rate of fake and secondary tracks, the momentum scale, and density effects from pixel and strip cluster merging. In the PYTHIA simulation, approximately 60% of the charged particles / tracks inside jets are charged pions that are well matched,³ 10% are well-matched kaons, 5% are

³ Reconstructed tracks are matched to charged particles by examining the pattern of sensors where energy was deposited. If over 50% of the weighted number of measurements on a track are due to one charged particle, it is declared matched to the track. The weights are chosen to reflect the amount of information present in each detector and are ten for the pixel detector, five for the strip detector, and one for the straw tube tracker.

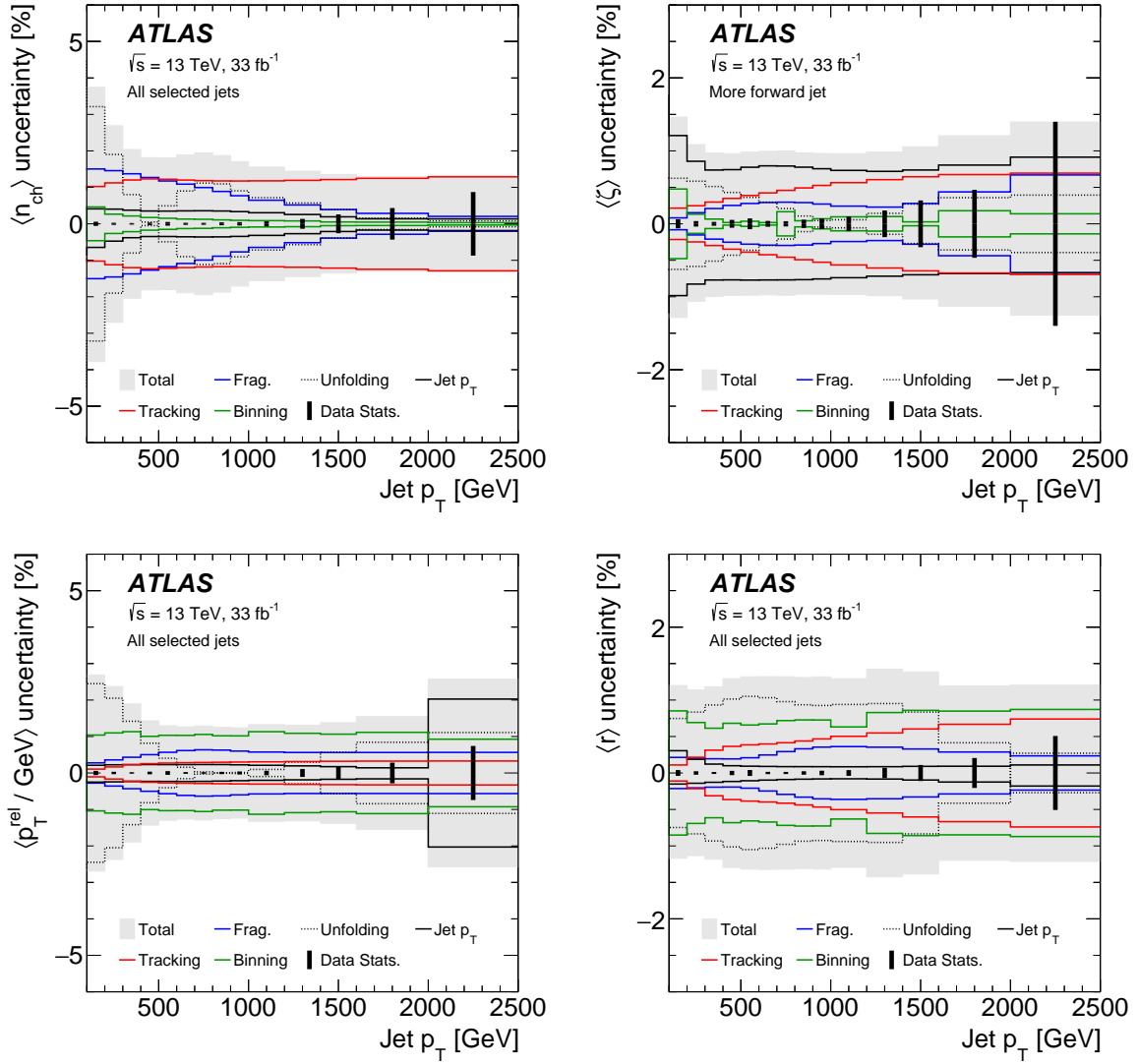


Figure 5: An overview of the statistical and systematic uncertainties for the average value of (top left) charged-particle multiplicity n_{ch} , (top right) transverse momentum fraction ζ , (bottom left) transverse momentum p_T^{rel} , and (bottom right) radial profile as a function of jet transverse momentum p_T . The MC statistical uncertainties are negligible and are not shown. When the uncertainties go through zero (as for the unfolding uncertainty in the top left), the signed uncertainty has changed from positive to negative or vice versa. Most of the lines are the sum in quadrature of individual sources of uncertainty in each category, such as the various sources of tracking uncertainties as described in Sec. 7.1.

well-matched protons, 15% are charged particles that are not matched to reconstructed tracks (inefficiency), 5% are secondaries (split equally between photon conversions and nuclear interactions), 1% are not well-matched tracks (fake tracks), and about $\mathcal{O}(0.1\%)$ are pileup tracks wrongly matched to the primary hard-scattering vertex. The pileup contribution decreases with jet p_T and momentum fraction, but increases with jet cone size (reaching 1% at $\Delta = 0.4$). In contrast, the fake-track rate increases slightly with jet p_T and has a contribution at high-momentum fraction of a few percent from kinked tracks reconstructed with a very high p_T . The reconstruction inefficiency grows with jet p_T , and is peaked at both low and high radial distance from the center of the jet and is reduced at high momentum fraction. This is because tracks with a larger radial distance from the jet axis tend to have lower p_T (larger material effects and thus lower efficiency), while tracks in the core of the jet suffer from an inefficiency in the pattern recognition in the dense environment.

The uncertainty in the inclusive track reconstruction efficiency is dominated by the uncertainty in the amount of material in the inner detector. Variations in the amount of material that are consistent with detector construction knowledge and measurements from secondary vertices [100] result in an uncertainty of 0.5% for $|\eta| < 0.1$, which grows to 2.7% for $2.3 < |\eta| < 2.5$. This uncertainty is applied in the simulation by randomly removing tracks with a p_T - and $|\eta|$ -dependent probability. This uncertainty dominates the n_{ch} measurement for jet $p_T \lesssim 1$ TeV.

Since the ATLAS pixel detector measures the charge collected from ionization, it is possible to constrain the inefficiency from density effects by looking for single tracks with pixel charge consistent with two minimum-ionizing particles [67]. The resulting uncertainty is about 0.4% for tracks with $\Delta R < 0.1$ and is validated with additional studies related to the charged-to-neutral ratio in the jet as well as the geometric orientation of pixel clusters [68]. This uncertainty is most important for the radial energy measurement at small radii from the jet axis and for the n_{ch} measurement in the highest jet- p_T bins.

The rate of fake tracks is studied inside jets by inverting some of the track quality criteria such as the fit χ^2/NDF and is found to agree between data and simulation at the 30% level [68]. A related source of uncertainty is due to the rate of secondary tracks. These tracks originate from real charged particles, but are the result of interactions in detector material and not direct fragmentation processes. The rate of secondaries is estimated by fitting the track d_0 distribution and is found to agree with simulation within about 30%. These rates are then varied to determine an uncertainty in the measurement. The fake-track rate is the leading source of uncertainty for n_{ch} when $p_T \gtrsim 1$ TeV and when $\zeta \sim 1$ or $r \lesssim 0.05$ for all jet- p_T bins. Uncertainties related to the modeling of pileup have a negligible impact.

The leading source of uncertainty in the track parameters is in the q/p_T (q is the electric charge) from a potential sagitta distortion due to detector misalignment weak modes [94]. This bias is corrected and the uncertainty in the correction is about 0.1/TeV except at $\phi \approx 0$ and $|\eta| \sim 2.5$ where the correction can reach 1/TeV. The impact on the measurement is smaller than the other tracking uncertainties.

7.2 Unfolding method and fragmentation modeling

An uncertainty resulting from the unfolding method described in Section 6 is determined by unfolding the prediction from a reweighted simulation with the nominal procedure. The reweighted simulation is constructed by modifying the nominal PYTHIA 8 particle-level spectrum so that the simulated detector-level spectrum, from propagating the reweighted particle-level spectrum through the response matrix, has significantly improved agreement with the data. The modified detector-level distribution is unfolded with the nominal response matrix and the difference between this and the reweighted particle-level spectrum is

an indication of the bias due to the unfolding method (in particular, the choice of prior) [101]. The weights are chosen by comparing the PYTHIA 8 particle-level spectrum with the unfolded data. After applying the reweighting, the χ^2/NDF calculated using only the statistical uncertainties improves significantly in each jet p_T bin. The resulting systematic uncertainties are generally much smaller than the detector-level differences between the data and simulation, as desired.

The unfolded result depends on the modeling of jet fragmentation through the prior, the response matrix, and the correction factors. Variations in the prior are already accounted for in the data-driven non-closure uncertainty described above. The other contributions are evaluated by comparing the result using PYTHIA 8 with the result using the alternative Herwig++ sample described in Section 4. A similar uncertainty is obtained when using Herwig++ or SHERPA as the alternative model. This comparison is decomposed into components corresponding to varying only the response matrix or only the initial/final correction factors, $\epsilon_{\text{reco not true}}$ and $\epsilon_{\text{true not reco}}$ in Eq. (2). All three components are added in quadrature to determine the total uncertainty due to fragmentation modeling. Even though these sources of uncertainty are correlated, they were treated as independent because the level of correlation is unknown given that there are only two alternative models. The resulting uncertainty is much smaller than the difference between PYTHIA 8 and Herwig++ at particle level. For n_{ch} , the response matrix is the dominant contribution to this uncertainty, except in the first jet- p_T bin where the correction factors and their uncertainty are also important. For the per-particle observables (ζ , r , p_T^{rel}), the correction factors dominate the uncertainty because acceptance effects are much more important.

8 Results

The unfolded data are presented in two ways. Section 8.1 focuses on the inclusive spectra for both jets together, while Section 8.2 uses the differences between forward and central jets to determine the unique features of quark-initiated and gluon-initiated jets, some of which can be compared with perturbative QCD calculations. These sections show a selection of jet p_T bins; a complete set of results can be found in Ref. [99].

8.1 Inclusive distributions

The unfolded averages of the measured observables are presented as a function of the jet p_T in Figure 6 for the more forward and more central jets separately and then combined in Figure 7. All other figures in this section combine measurements of both jets. The more central jets show properties that are more gluon-like than the more forward jets: they have a larger charged-particle multiplicity and a softer momentum-fraction spectrum. The modeling of the all-jet spectra is very similar to that of the more forward/backward jets and is described in detail for the all-jet spectra only.

As the jet p_T increases, the average charged-particle multiplicity increases, the average momentum fraction decreases, the average p_T^{rel} increases, and the average multiplicity-weighted radius decreases. Charged-particle multiplicity increases from about 10 at jet p_T of 100 GeV to just over 20 at 2.5 TeV. In most cases, PYTHIA 8 and SHERPA bracket the data, and are accurate to better than 10%; Herwig++ is often between these two and closer to the data. As the distribution of n_{ch} is almost Poissonian, nearly all of the information about the distribution is encoded in the mean value. In contrast, the distribution of ζ is

more complicated.⁴ The average momentum fraction is about 5% at jet p_T of 100 GeV and decreases to about 2.5% at 2.5 TeV (the most probable value, shown below, is lower). The distributions of p_T^{rel} and the radial profiles fall steeply (nearly exponentially) away from zero and the average values in Figure 7 give a sense of how fast they fall (exponential distributions are uniquely specified by their mean). The average p_T^{rel} at $p_T^{\text{jet}} = 100$ GeV is about 0.35 GeV and increases to about 0.55 GeV at $p_T^{\text{jet}} = 2.5$ TeV. If the angular distribution about the jet axis is independent of p_T , the average value of p_T^{rel} should be proportional to $\langle \zeta \rangle (p_T^{\text{jet}}) \times p_T^{\text{jet}}$. This would suggest an increase by a factor of $(2.5\%/5\%) \times (2500/100) \sim 12.5$ across the measured range; instead it only increases by a factor of about 1.5. This means that the angular distribution is not independent of p_T and in particular, the jets become more collimated. This is also consistent with direct measurement of the radial profile, where the average value drops from about 0.06 at $p_T^{\text{jet}} = 100$ GeV to about 0.03 at $p_T^{\text{jet}} = 2.5$ TeV. While PYTHIA 8, SHERPA, and Herwig++ agree well with the data for p_T^{rel} , SHERPA provides a poorer model of the average radial profile as a function of the jet p_T .

As noted above, the distribution of ζ cannot be described simply by its average value, in contrast to n_{ch} , p_T^{rel} and r , which are nearly Poisson or exponentially distributed. Therefore, it is useful to summarize the p_T^{jet} dependence of other aspects of the ζ distribution. Figure 8 shows partial integrals of the ζ distribution and Figure 9 shows the average values of $\zeta^{1/2}$, ζ^2 , $\sum_{i \in \text{jet}} \zeta^{1/2}$ and $\sum_{i \in \text{jet}} \zeta^2$. Figure 8 illustrates how the average fraction of charged particles with a given momentum fraction evolves with p_T^{jet} . There is no correction for binning effects, as the measured ζ distribution has bin edges which nearly align with 0.1%, 1%, and 10%. In particular, the ζ bins are $1/1.5^n$, for $n = 0, \dots, 21$, and the fractions in Figure 8 are estimated as $0.1\% \approx 1/1.5^{17}$, $1\% \approx 1/1.5^{11}$, and $10\% \approx 1/1.5^5$. The fraction of particles carrying 10% or less of the momentum changes very little across the entire p_T^{jet} range and is also near unity ($> 90\%$ for all p_T^{jet}). A strong p_T^{jet} dependence is introduced when the ζ threshold is lowered to 1% and to 0.1%. Since charged particles are required to have $p_T > 500$ MeV, only jets with $p_T^{\text{jet}} > 500$ GeV can have particles with $\zeta < 0.1\%$. The fraction of particles with $\zeta < 1\%$ has a logarithmic increase while the fraction of particles with $\zeta < 0.1\%$ appears to increase faster than linearly with p_T^{jet} . Both of these general trends are reproduced by PYTHIA 8, SHERPA, and Herwig++, although for example, PYTHIA 8 disagrees with the exact value at low p_T^{jet} for $\zeta < 1\%$ and all p_T^{jet} for $\zeta < 0.1\%$. For the $\zeta < 0.1\%$ case, SHERPA and PYTHIA 8 bracket the data, with SHERPA predicting more particles with a lower ζ fraction, while Herwig++ is much closer to the data. The average values of $\sqrt{\zeta}$ and ζ^2 for individual particles as a function of jet p_T^{jet} in the top panel of Figure 9 show a decreasing trend that is qualitatively similar to the trend for the average ζ in Figure 7. For $\sqrt{\zeta}$, PYTHIA 8/Herwig++ and SHERPA bracket the data, although PYTHIA 8 agrees with the data within the uncertainty. SHERPA predicts a significantly higher average ζ^2 than is present in the data. As with $\langle n_{\text{ch}} \rangle$, the average value of $\sum_{i \in \text{jet}} \zeta^{1/2}$ increases with the jet p_T , while the p_T dependence of $\langle \sum_{i \in \text{jet}} \zeta^2 \rangle$ is more complicated as it first decreases and then slowly increases with jet p_T . This trend is well reproduced by PYTHIA and Herwig++, but not by SHERPA.

To present more differential information, the full unfolded distributions for n_{ch} , ζ , p_T^{rel} , and r are shown in Figures 10, 11, 12, and 13, respectively, for representative p_T^{jet} bins. Many of the relevant trends are captured in the above discussion about the p_T^{jet} dependence of the moments. However, finer information that may be useful for generator tuning is provided by the differential distributions.

⁴ The distribution is nearly Gaussian in $\log \zeta$, so it is well specified by two parameters instead of one [73].

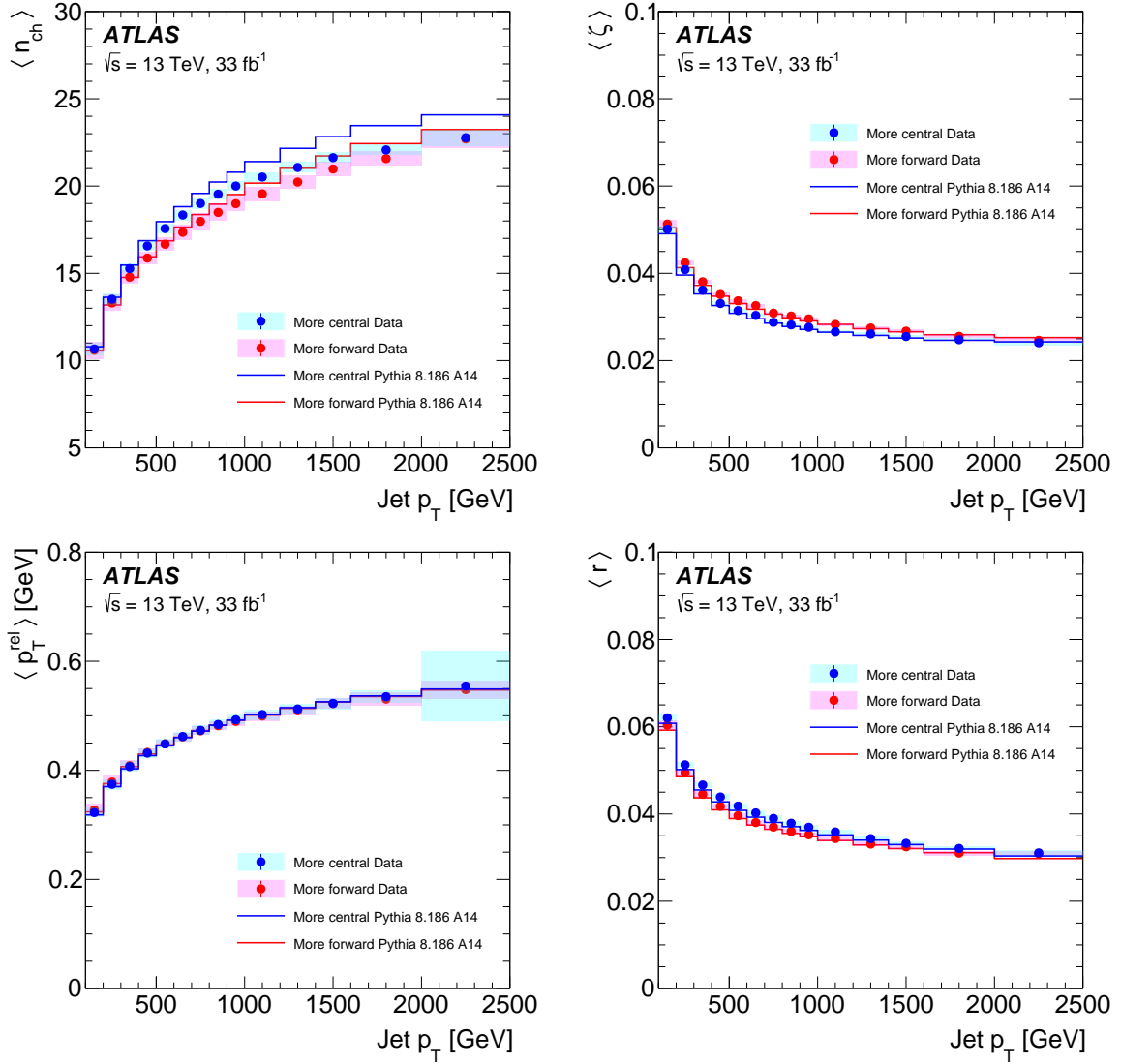


Figure 6: The unfolded measured averages for the (top left) charged-particle multiplicity n_{ch} , (top right) transverse momentum fraction ζ , (bottom left) transverse momentum $p_{\text{T}}^{\text{rel}}$, and (bottom right) radial profile as a function of the jet transverse momentum p_{T} for the more forward and more central of the two jets, separately. The uncertainty bands show the combined statistical and systematic uncertainty.

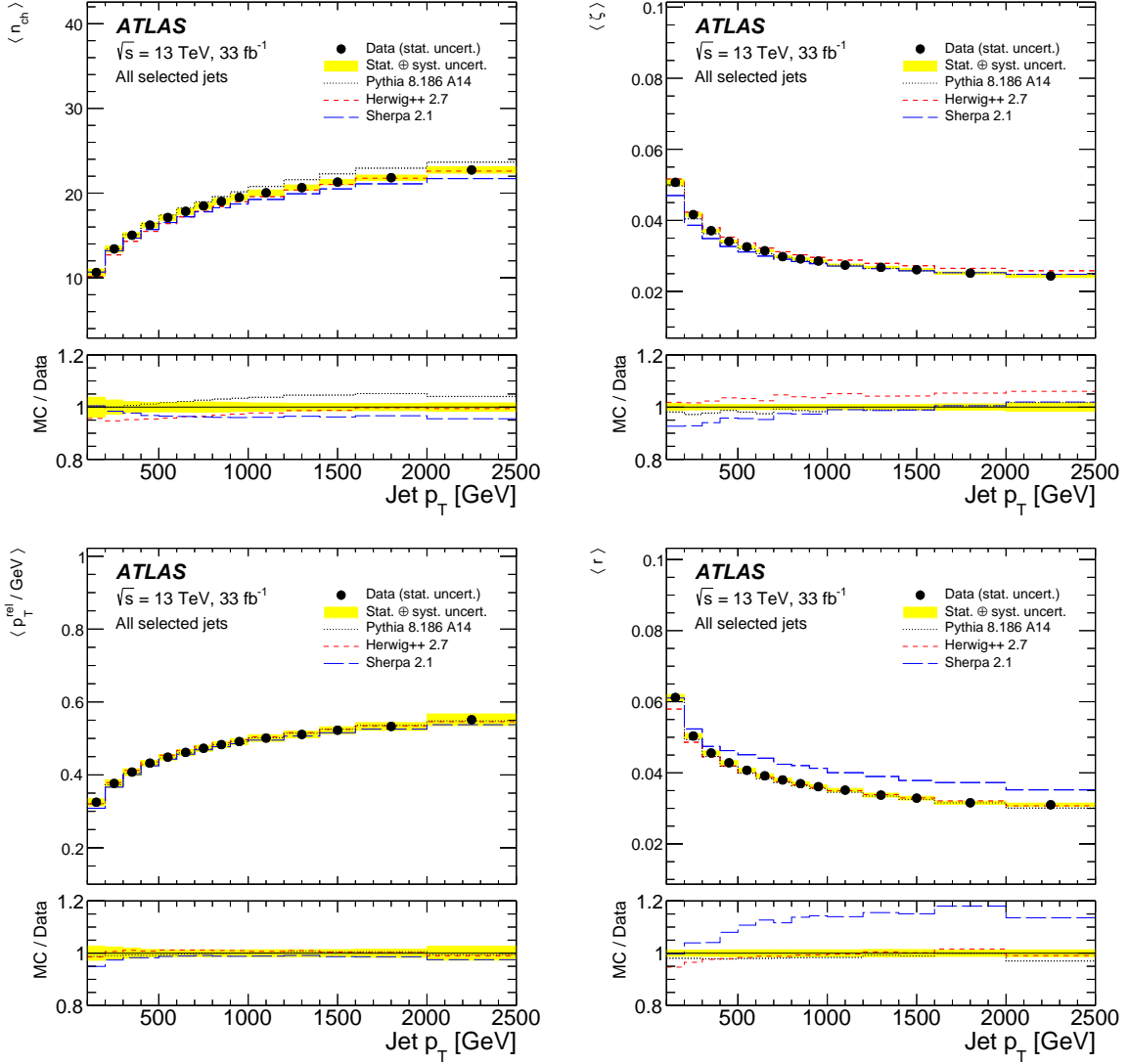


Figure 7: The unfolded measured averages (top left) charged-particle multiplicity n_{ch} , (top right) transverse momentum fraction ζ , (bottom left) transverse momentum p_T^{rel} , and (bottom right) radial profile as a function of the jet transverse momentum p_T . The lower panel shows the ratio of various MC predictions to the data, with the total uncertainty band centered on the data at unity.

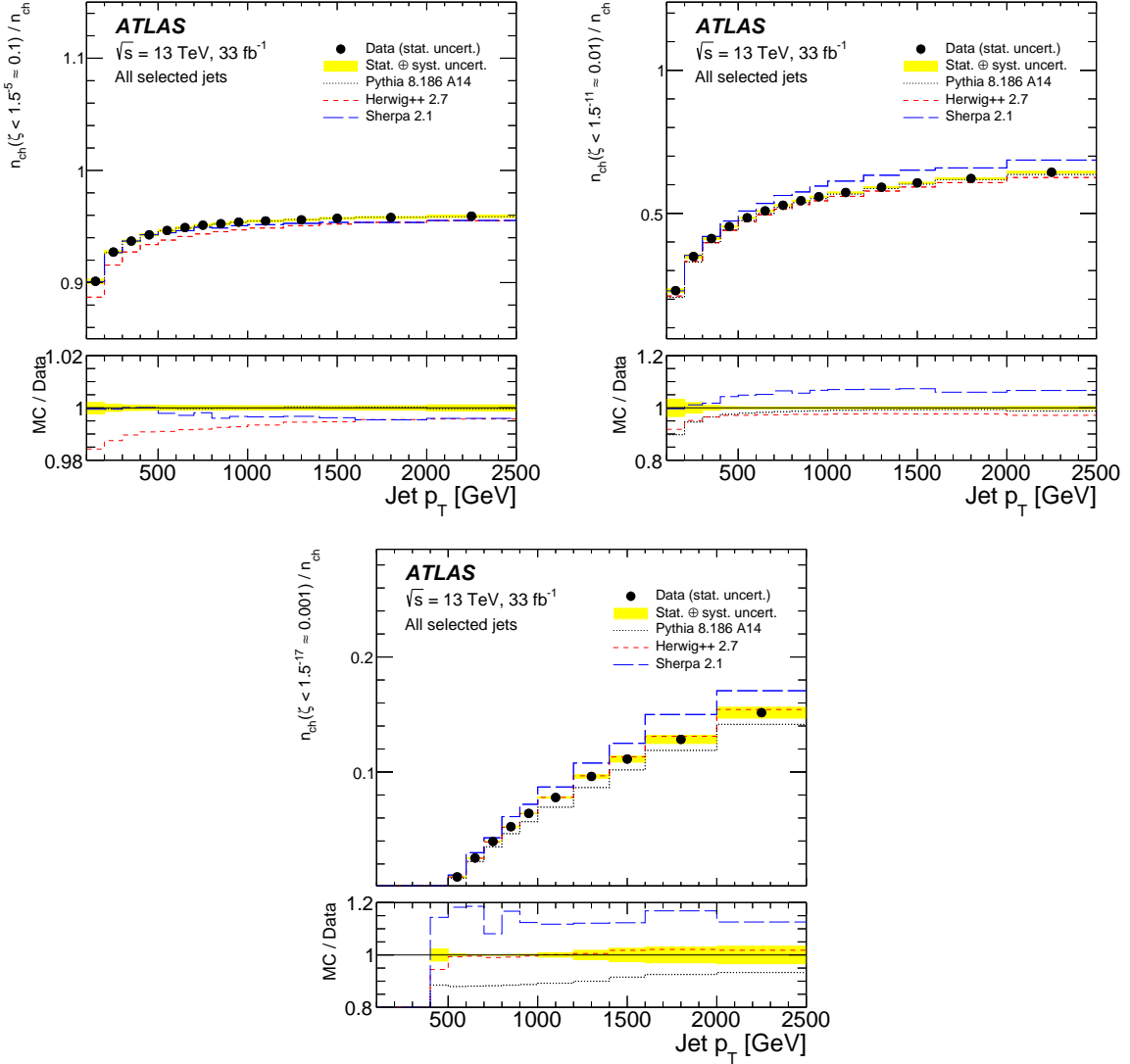


Figure 8: The unfolded fraction of charged particles carrying a fraction $\zeta \lesssim 10\%$ (top left), 1% (top right), and 0.1% (bottom) of the jet transverse momentum p_T . The exact fractions are given in the figures and correspond to powers of 1.5 so that the values align precisely with bin edges and thus no binning correction is required. The lower panels show the ratio of various MC predictions to the data, with the total uncertainty band centered on the data at unity.

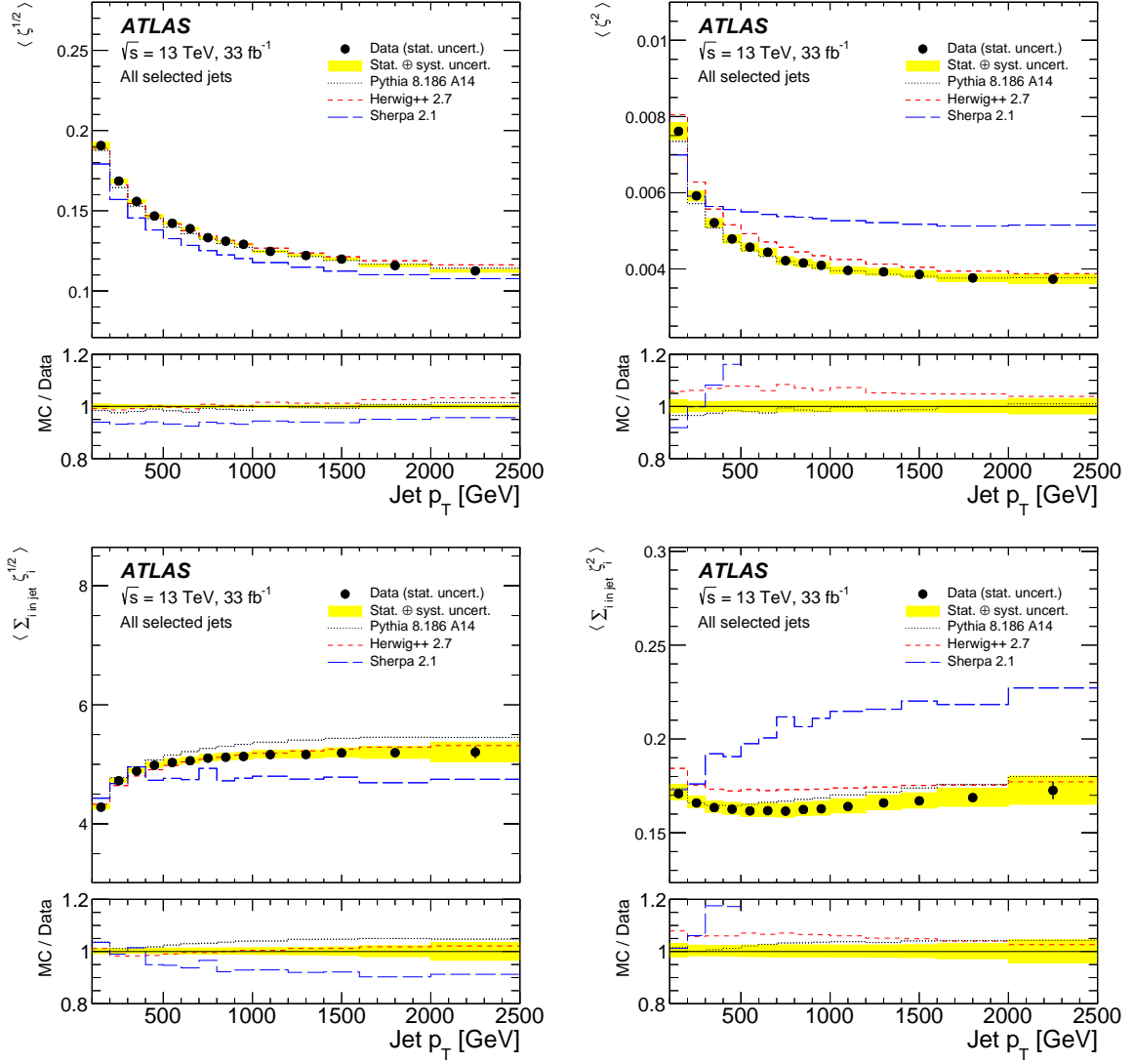


Figure 9: Top: The unfolded (left) 1/2 and (right) 2nd moments of the transverse momentum fraction, ζ , distribution as a function of the jet transverse momentum p_T . Bottom: The unfolded moment of (left) $\sum_{i \in \text{jet}} \zeta^{1/2}$ and (right) $\sum_{i \in \text{jet}} \zeta^2$ as a function of the jet p_T . Section 2 presents the definitions of both classes of observables. The lower panels show the ratio of various MC predictions to the data, with the total uncertainty band centered on the data at unity. The values are computed from the moments of the unfolded distributions in each jet- p_T bin, with a small correction added to account for binning effects.

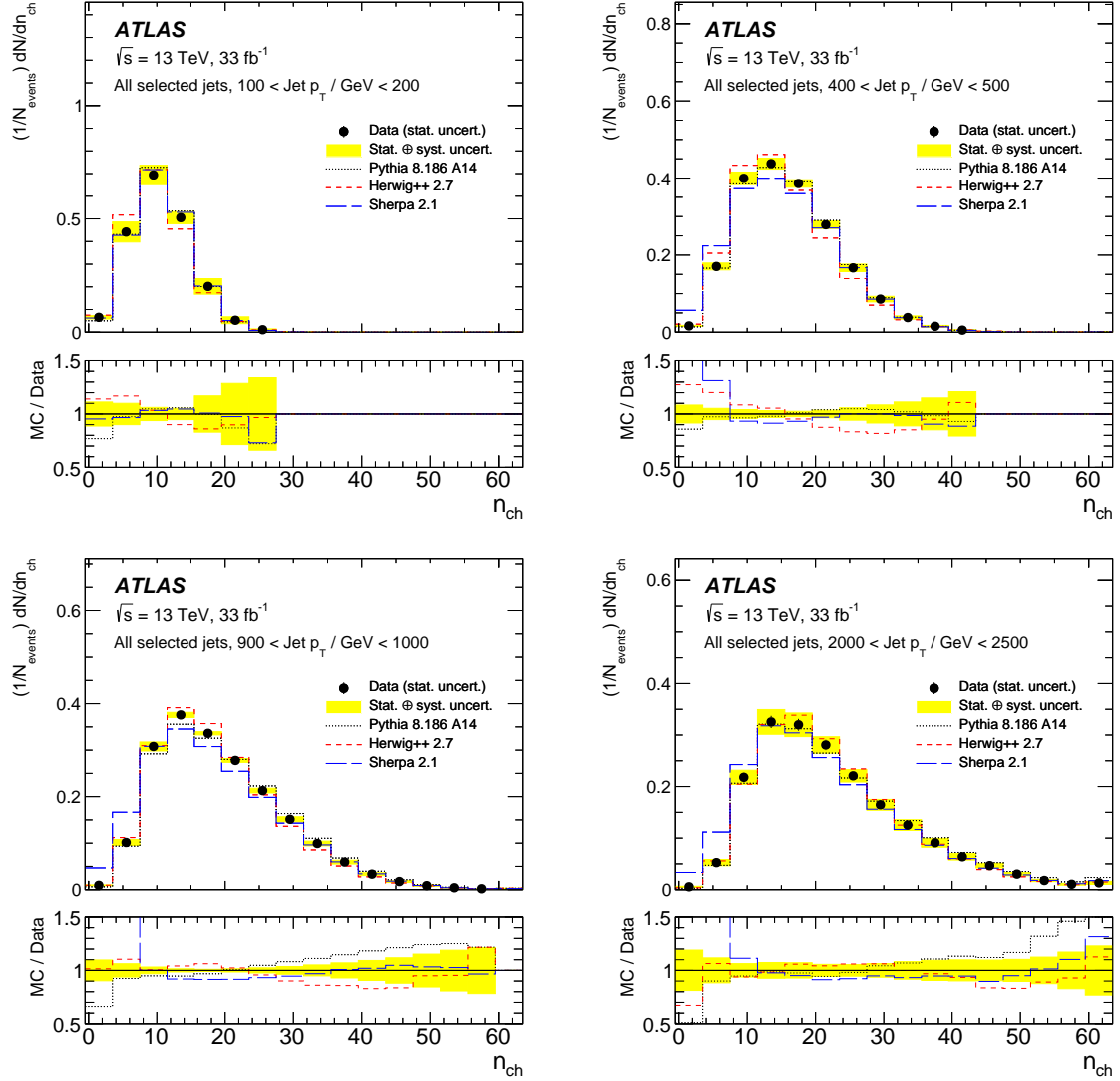


Figure 10: The distribution of charged-particle multiplicity n_{ch} in four bins of jet transverse momentum: (top left) $100 \text{ GeV} < p_{\text{T}}^{\text{jet}} < 200 \text{ GeV}$, (top right) $400 \text{ GeV} < p_{\text{T}}^{\text{jet}} < 500 \text{ GeV}$, (bottom left) $900 \text{ GeV} < p_{\text{T}}^{\text{jet}} < 1000 \text{ GeV}$, and (bottom right) $2000 \text{ GeV} < p_{\text{T}}^{\text{jet}} < 2500 \text{ GeV}$. The lower panels show the ratio of various MC predictions to the data, with the total uncertainty band centered on the data at unity. Additional $p_{\text{T}}^{\text{jet}}$ bins can be found in Ref. [99].

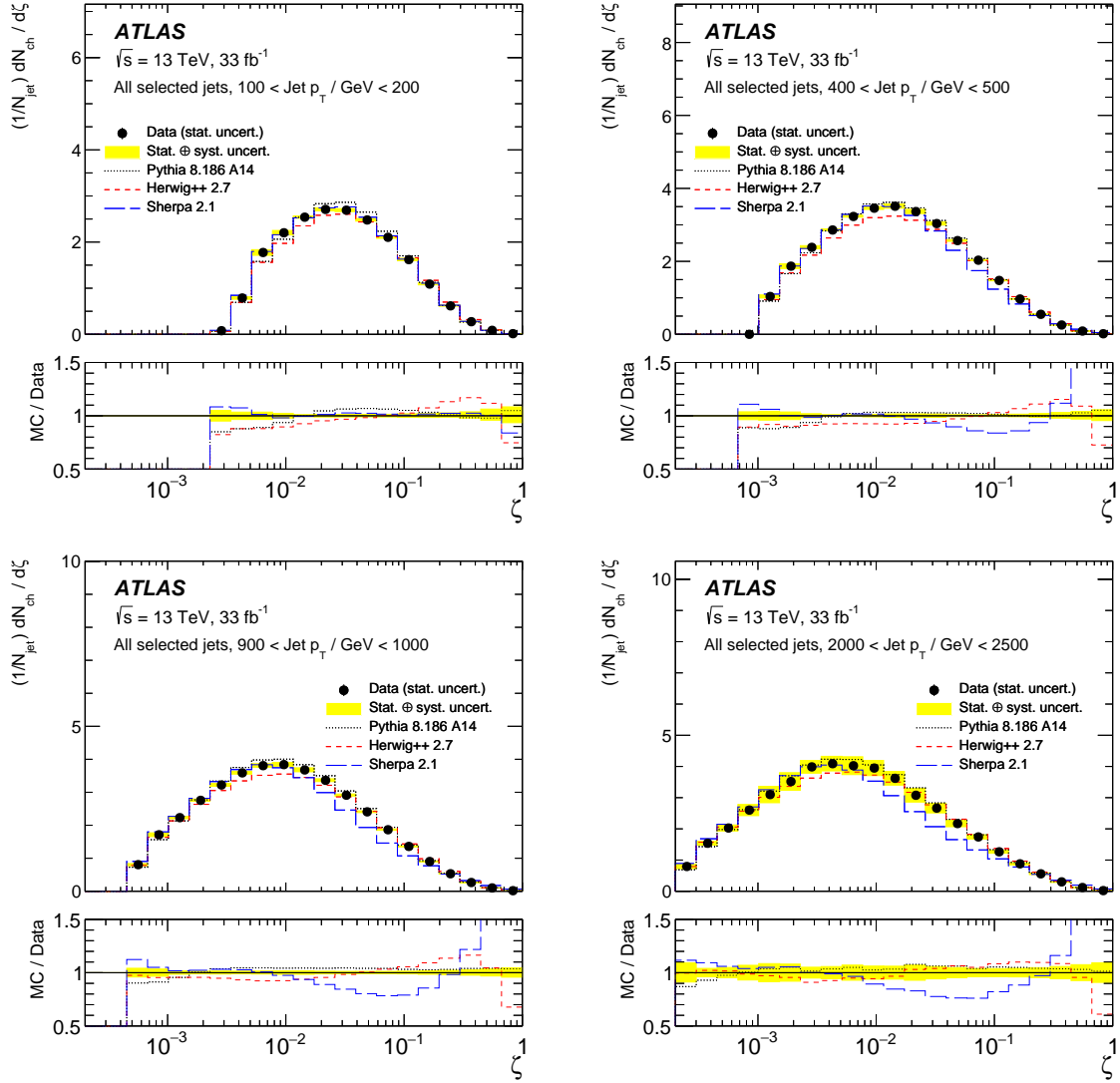


Figure 11: The transverse momentum fraction ζ distribution in four bins of jet transverse momentum: (top left) $100 \text{ GeV} < p_T^{\text{jet}} < 200 \text{ GeV}$, (top right) $400 \text{ GeV} < p_T^{\text{jet}} < 500 \text{ GeV}$, (bottom left) $900 \text{ GeV} < p_T^{\text{jet}} < 1000 \text{ GeV}$, and (bottom right) $2000 \text{ GeV} < p_T^{\text{jet}} < 2500 \text{ GeV}$. The lower panels show the ratio of various MC predictions to the data, with the total uncertainty band centered on the data at unity. Additional p_T^{jet} bins can be found in Ref. [99].

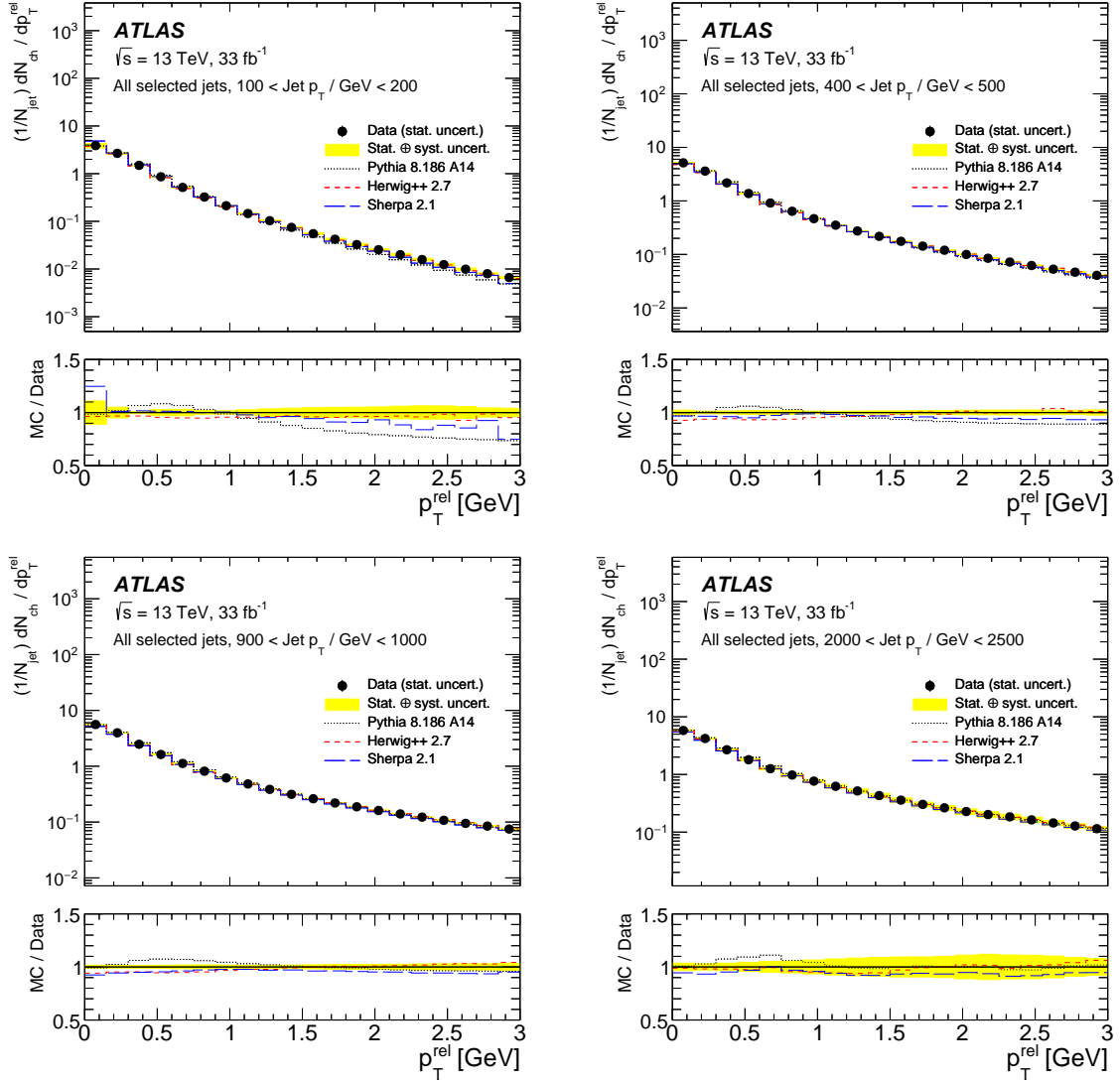


Figure 12: The transverse momentum p_T^{rel} distribution in four bins of jet transverse momentum: (top left) $100 \text{ GeV} < p_T^{\text{jet}} < 200 \text{ GeV}$, (top right) $400 \text{ GeV} < p_T^{\text{jet}} < 500 \text{ GeV}$, (bottom left) $900 \text{ GeV} < p_T^{\text{jet}} < 1000 \text{ GeV}$, and (bottom right) $2000 \text{ GeV} < p_T^{\text{jet}} < 2500 \text{ GeV}$. The lower panels show the ratio of various MC predictions to the data, with the total uncertainty band centered on the data at unity. Additional p_T^{jet} bins can be found in Ref. [99].

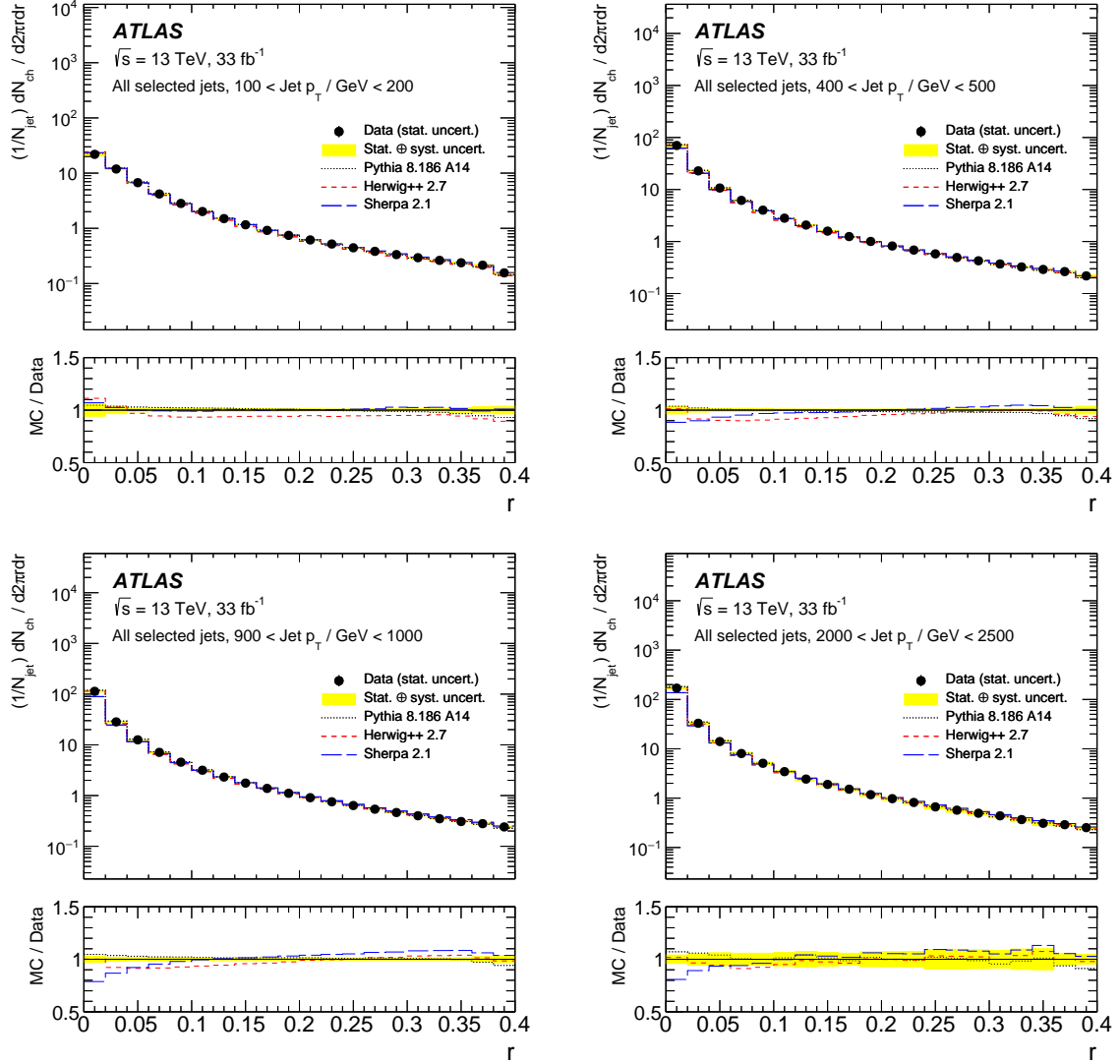


Figure 13: Distribution of track radial profile in bins of the radial distance r from the jet axis in four bins of jet transverse momentum: (top left) $100 \text{ GeV} < p_T^{\text{jet}} < 200 \text{ GeV}$, (top right) $400 \text{ GeV} < p_T^{\text{jet}} < 500 \text{ GeV}$, (bottom left) $900 \text{ GeV} < p_T^{\text{jet}} < 1000 \text{ GeV}$, and (bottom right) $2000 \text{ GeV} < p_T^{\text{jet}} < 2500 \text{ GeV}$. The lower panels show the ratio of various MC predictions to the data, with the total uncertainty band centered on the data at unity. Additional p_T^{jet} bins can be found in Ref. [99].

8.2 Quark and gluon distributions

As discussed in Section 5.2, the more forward and the more central of the two selected jets can be separated to study differences between the radiation patterns within quark and gluon jets. Using the fraction of quark jets f_q in the two jet samples (forward f and central c), one can extract the quark (h_i^q) and gluon (h_i^g) jet fragmentation properties separately by solving a system of equations per bin i of an observable:

$$\begin{aligned} h_i^f &= f_q^f h_i^q + (1 - f_q^f) h_i^g, \\ h_i^c &= f_q^c h_i^q + (1 - f_q^c) h_i^g, \end{aligned} \quad (4)$$

where f_q^x is the fraction of quark jets in sample x (see Figure 3 for the gluon fraction) and the nominal fractions are taken from the default PYTHIA simulation described in Section 4. The flavor of a jet is defined as the type of the highest-energy parton from the event record (all partons prior to hadronization) matched to the jet via ghost association. This definition is not unique because quark and gluon labels are not universal due to color connections with other partons in the event.⁵ In addition to the uncertainty in h_i^f and h_i^c from the unfolding method, uncertainties in the extracted h_i^g and h_i^q distributions arise from the PDF choice, from the matrix elements, from the fragmentation model (due to flavor changing), and from the method non-closure. The determination of the uncertainty from the choice of PDF uses the NNPDF uncertainty set (NNPDF 2.3 at LO in QCD and QED with $\alpha_S(m_Z) = 0.119$) and the matrix-element uncertainty is estimated by comparing the nominal fractions from PYTHIA with those from HERWIG.⁶ The non-closure uncertainty is due to the small (sub-percent level) differences between forward and central quark jets, as well as forward and central gluon jets, resulting from an η dependence in the jet fragmentation at a fixed jet p_T [102]. When presenting the average properties in bins of jet p_T , the binning correction described in Section 6 is also applied and the corresponding uncertainty contributes to the total uncertainty (though it is smaller than other sources of uncertainty).

The matrix-element uncertainty dominates the total uncertainty in the extraction procedure, resulting in an uncertainty that is about 1% at high jet p_T and about 5% at low to moderate jet p_T for quark jets, with the inverse trend for gluon jets (low uncertainty at low jet p_T and large uncertainty at high jet p_T). The extractions presented here use leading-order matrix elements and leading-logarithm parton shower programs; higher-order effects that modify the fractions f are not included in this leading-order extraction. Figure 14 shows the extracted quark and gluon distributions for jets with $1000 \text{ GeV} < p_T^{\text{jet}} < 1200 \text{ GeV}$. To reinforce the simulation dependence of these extractions, the data distributions are referred to as ‘extracted quark-like’ and ‘extracted gluon-like’.

⁵ However, for isolated jets, the topology dependence is predicted to be much smaller than the difference between quark and gluon jets [102].

⁶ These two generators also use different PDF sets, so this uncertainty is double-counted in the overall uncertainty.

A key challenge with the extraction based on Eqs. (4) and (5) is that it strongly depends on simulation for the fractions f_q and f_g . A new approach that does not require the input of any fractions is topic modeling [103, 104], which holds great promise for learning about quark- and gluon-like jets with less input from theory. In this approach, one can extract distributions of ‘topics’ T_1 and T_2 :

$$h_i^{T_1} = \frac{h_i^f - \left(\min_j \{h_j^f/h_j^c\}\right) \times h_i^c}{1 - \min_j h_j^f/h_j^c},$$

$$h_i^{T_2} = \frac{h_i^c - \left(\min_j \{h_j^c/h_j^f\}\right) \times h_i^f}{1 - \min_j h_j^c/h_j^f}.$$

In the limit that $\min_j \{h_j^g/h_j^q\} = \min_j \{h_j^q/h_j^g\} = 0$, $h^{T_1} = h^q$ and $h^{T_2} = h^g$. When this is not exactly the case, the topics are universal but not pure combinations of quarks and gluons. The extracted topics using n_{ch} in two jet p_T bins are shown in Figure 15. The very low n_{ch} region is dominated by quarks and the very high n_{ch} region is dominated by gluons and therefore n_{ch} nearly has the property that $\min_j \{h_j^g/h_j^q\} \approx \min_j \{h_j^q/h_j^g\} \approx 0$. Therefore, the first topic is well aligned with quarks and the second topic is more gluon-like. This alignment is better for quarks than for gluons, but the second topic does converge to the gluon distribution at high jet p_T . Other observables aside from n_{ch} are not considered for topic modeling because there are no bins where $h_j^g/h_j^q = 0$ or $h_j^q/h_j^g = 0$ is approximately true and therefore the topics do not align with quark- and gluon-like quantities.

While the full quark and gluon distributions presented in Figure 14 cannot be predicted from perturbative QCD, it is possible to model the p_T^{jet} dependence of the moments of the ζ distribution. Positive moments of the fragmentation function have a perturbative evolution with a proper α_S power series via DGLAP-like equations. In general, there are two terms that contribute to the right-hand side of Eq. (1) that prevent an analytic solution: one term proportional to D_g^h and one term proportional to D_q^h , where the coefficients for the κ sums are the Mellin transforms $\tilde{P}_{p' \leftarrow p}(\kappa) = \int_0^1 d\zeta \zeta^\kappa P_{p' \leftarrow p}(\zeta)$ for $p' = g$ and $p' = q$, respectively. For gluon jets ($p = g$), the $g \rightarrow qq'$ splitting function is finite,⁷ so $|\tilde{P}_{g \leftarrow g}| \gg |\tilde{P}_{q \leftarrow g}|$ for $\kappa \neq 0.8$ where $\tilde{P}_{g \leftarrow g}$ switches sign. Therefore, away from $\kappa \approx 0.8$ and in the modified leading-logarithm approximation (MLLA)⁸ [73, 108, 109],

$$\left\langle \sum_{i \in \text{jet}} \zeta_i^\kappa \right\rangle_{\text{gluons}}(p_T) \approx \log(p_T^2/\Lambda^2)^{2P_{g \leftarrow g}(\kappa)/\beta_0}, \quad (6)$$

where β_0 is the first term in the QCD β -function and Λ is a non-perturbative parameter (of order Λ_{QCD}). The predictions are scaled to match the data in the sixth jet p_T bin (referred to as the ‘anchor bin’). There is no a priori reason to select any particular bin as the anchor bin so one of the first bins after

⁷ The splitting function $\tilde{P}_{q \leftarrow q}$ is also finite, but is not numerically small compared with $\tilde{P}_{g \leftarrow q}$ except when κ is very small so this case is not considered further.

⁸ This means resummation that includes the leading-order splitting functions and the first-order running of the strong coupling. A more refined calculation [18, 19] using SCET [13–16] and fragmenting jet functions [105–107] is possible. However, the deviations from this simple approach are higher-order corrections and do not qualitatively change the comparisons in this section.

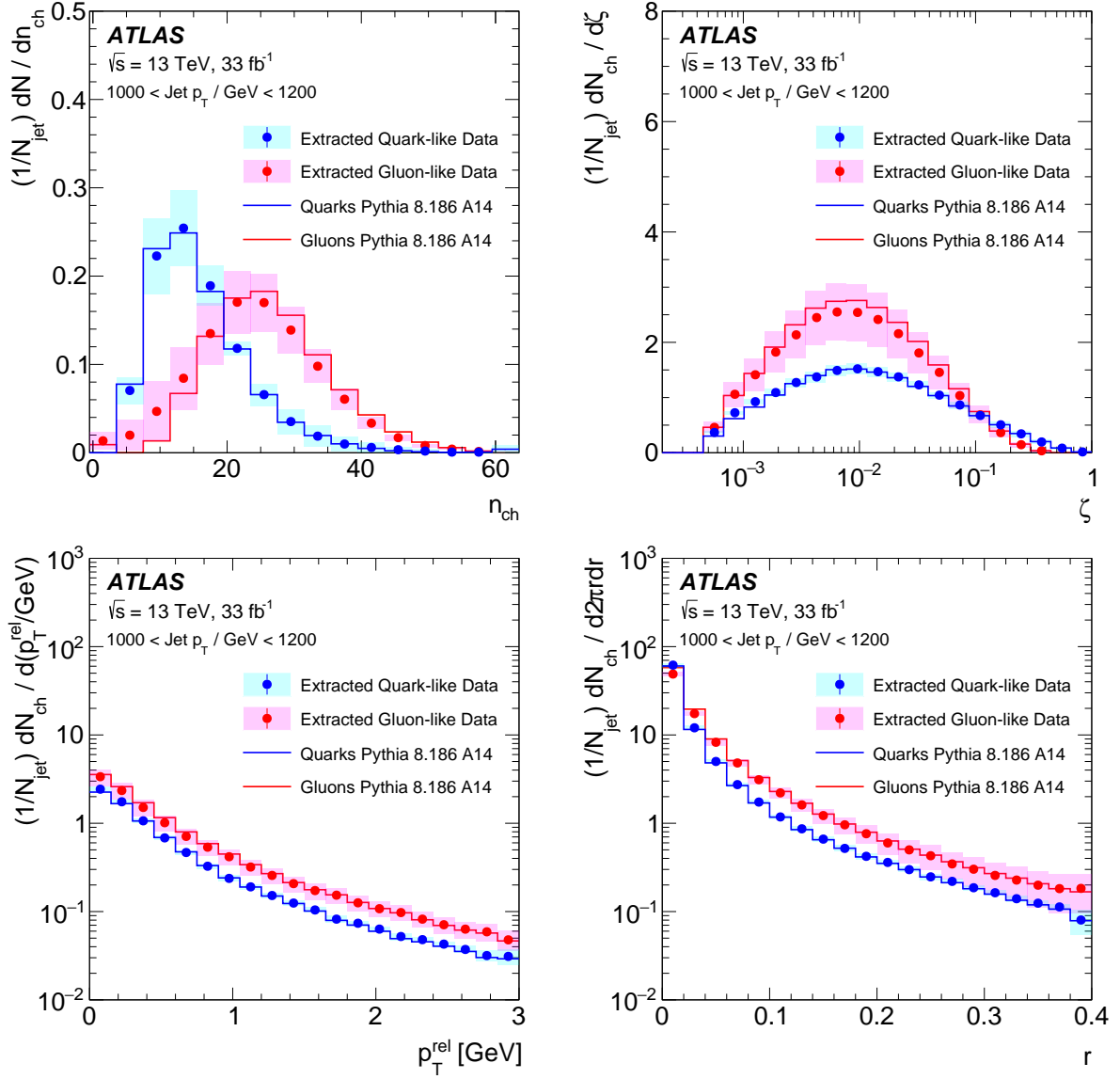


Figure 14: The extracted quark- and gluon-like distributions of (top left) charged-particle multiplicity n_{ch} , (top right) transverse momentum fraction ζ , (bottom left) transverse momentum p_T^{rel} , and (bottom right) the radial profile in bins of the radial distance r from the jet axis for jets with transverse momentum $1000 \text{ GeV} < p_T^{\text{jet}} < 1200 \text{ GeV}$. The quark- and gluon-jet distributions from PYTHIA are also shown for comparison. The uncertainty bands on the data include both statistical and systematic uncertainties while the error bars are due to statistical uncertainties only.

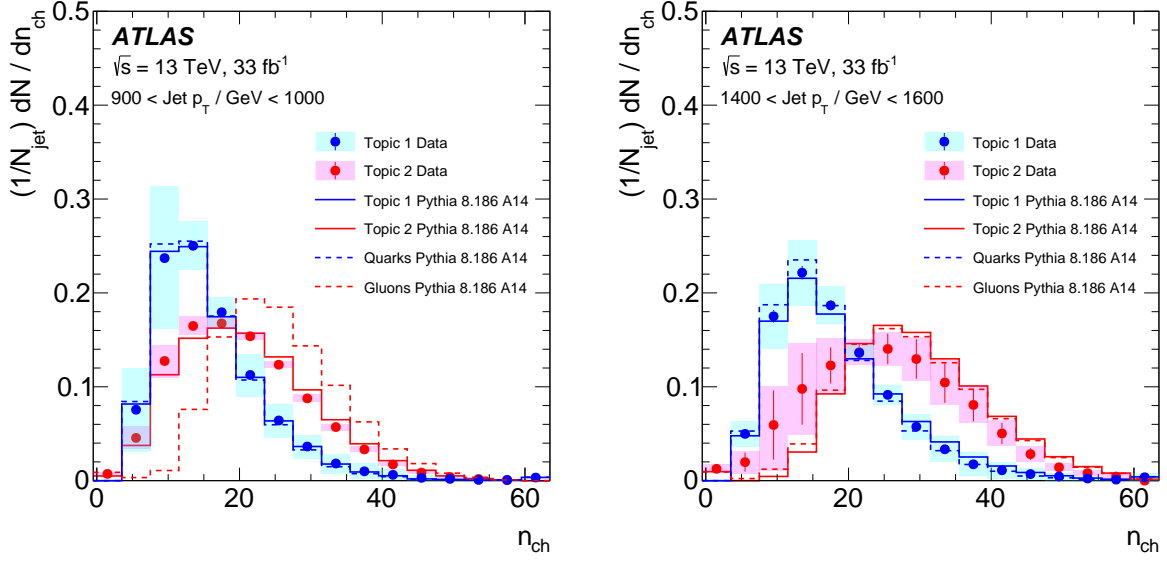


Figure 15: The jet topics extracted using charged-particle multiplicity n_{ch} for jets in two transverse momentum, p_{T} , bins together with the topics and quark and gluon distributions from PYTHIA. The uncertainty bands on the data include both statistical and systematic uncertainties while the error bars are due to statistical uncertainties only.

the lowest-threshold unrescaled jet trigger is selected. Figure 16 shows the distributions of the average $\sum_{i \in \text{jet}} \zeta_i^K$ for $\kappa = 0.5, 1.0$, and 2.0 for gluon jets. As mentioned above, $\tilde{P}_{g \leftarrow g}$ is predicted to change sign at $\kappa = 0.8$, a trend which is supported by the data: for low κ , the average value increases with p_{T} and when κ is large, the average decreases with p_{T} . For $\kappa = 1$, momentum conservation and isospin symmetry predict that the average value of $\sum_{i \in \text{jet}} \zeta_i$ should be constant and approximately $2/3$, the ratio of charged pions to all pions⁹. The leading-logarithm (LL) calculation predicts $\tilde{P}_{g \leftarrow g}(1) \approx 0$ so the p_{T} dependence is already negligible compared with the $\kappa = 0.5$ and $\kappa = 2$ cases.

When $\kappa \rightarrow 0$, both the quark and gluon fragmentation-function Mellin transforms diverge and so the analysis with Eq. (6) is not accurate. The $\kappa \rightarrow 0$ limit is $\langle n_{\text{ch}} \rangle$ and there is no known series in α_{S} to describe its $p_{\text{T}}^{\text{jet}}$ dependence. Despite this, the anomalous dimension for the $p_{\text{T}}^{\text{jet}}$ dependence of $\langle n_{\text{ch}} \rangle$ has been calculated to ‘N³LO’ where the series is in $\sqrt{\alpha_{\text{S}}}$ instead of α_{S} [22, 23]. Figure 17 shows $\langle n_{\text{ch}} \rangle$ as a function of $p_{\text{T}}^{\text{jet}}$ for both extracted quark-like and gluon-like jets as well as the topic extraction along with the prediction for the pure quark/gluon case. Gluon jets from data deviate significantly from simulation and from the calculation at high jet p_{T} ; this is also true to a lesser extent for quark jets, which seem to have a different slope that is most prominent at low jet p_{T} . A similar trend was first observed in Ref. [7], albeit with lower precision in the highest p_{T} bins. There are several possibilities for this discrepancy, such as an unaccounted for potential source of bias in the quark/gluon jet fractions. The data in the right panel of Figure 17 do not yet conclusively support or reject this hypothesis; with more data, it may be possible to determine if the data match topic 2 in PYTHIA or deviate as is the case for gluons in the left panel of Figure 17.

The p_{T} dependence of the average ζ , $p_{\text{T}}^{\text{rel}}$, and r are shown in Figure 18. Gluon jets have more constituents than quark jets on average so their average ζ is lower. For both quark and gluon jets, $\langle \zeta \rangle$ decreases with the jet p_{T} in part because constituent multiplicity increases with p_{T} . Gluon jets are wider than quark jets on

⁹ The measured value is not exactly $2/3$ because a jet’s energy is only about 60% due to pions.

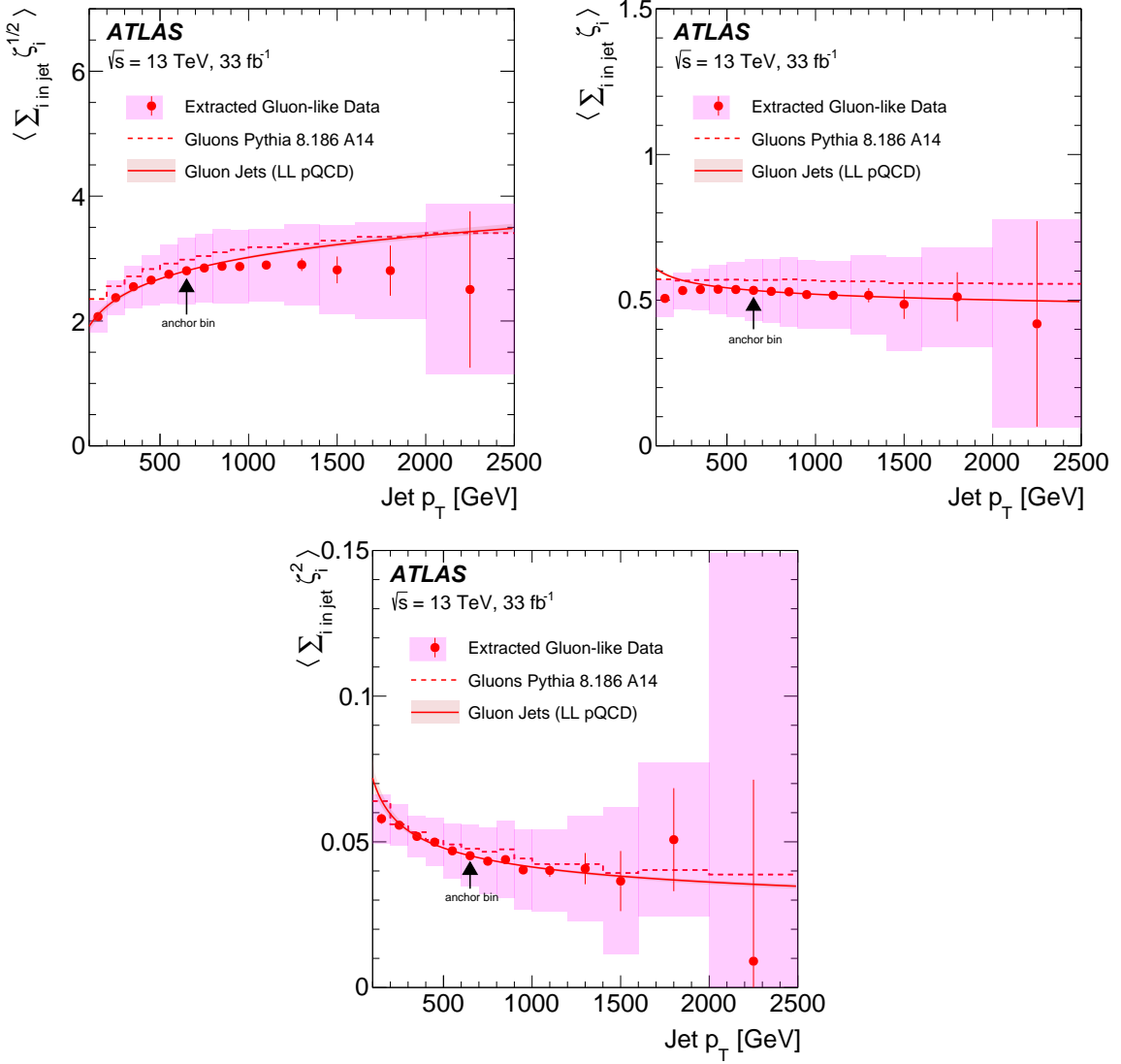


Figure 16: The dependence on transverse momentum p_T of the average extracted gluon-like transverse-momentum-fraction weighted sum $\sum_{i \in \text{jet}} \zeta_i^{\kappa}$ for (top left) $\kappa = 0.5$, (top right) $\kappa = 1.0$, and $\kappa = 2.0$ (bottom). For comparison, the results from PYTHIA and a simple leading-logarithm (LL) calculation are also presented. The prediction is normalized to the data in the sixth jet p_T bin, called the anchor bin and indicated by an arrow. The uncertainty band on the calculation is from varying Λ in Eq. (6) up and down by a factor of two from its nominal value of 400 MeV (in most regions, this band is not much wider than the line width and thus not visible). The uncertainty bands on the data include both statistical and systematic uncertainties while the error bars are due to statistical uncertainties only.

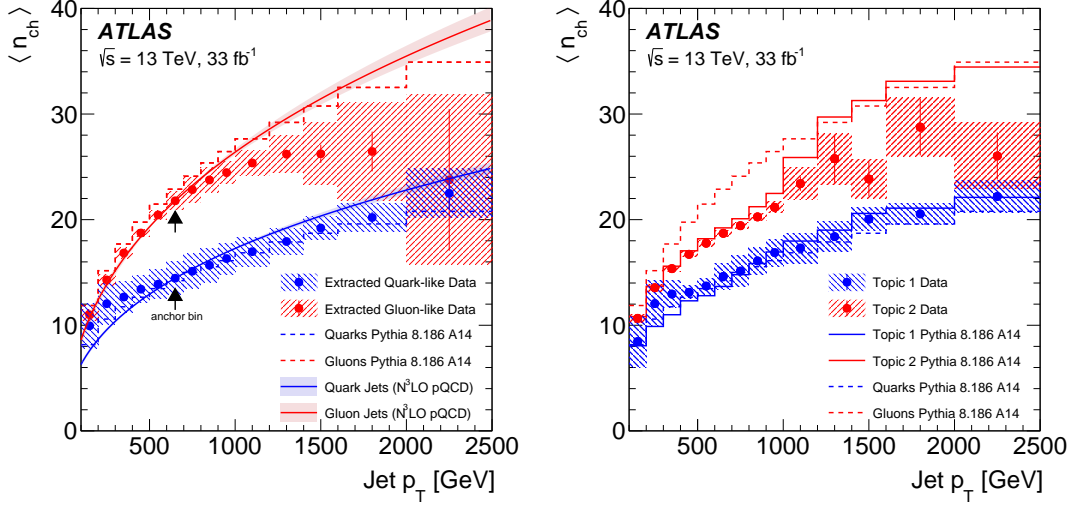


Figure 17: Left (right): The dependence on jet transverse momentum p_T of the mean charged-particle multiplicity $\langle n_{ch} \rangle$ for quark and gluon jets (topic 1 and topic 2) in data and in PYTHIA as well as from a calculation using perturbative QCD. The calculation cannot predict the overall normalization and therefore the prediction is normalized to the data in the sixth p_T bin, called the anchor bin and indicated by an arrow. The binning correction is not applied to the average topics, as this correction is very sensitive to fluctuations due to the limited number of simulated events. The uncertainty bands on the data include both statistical and systematic uncertainties while the error bars are due to statistical uncertainties only.

average, but both quark and gluon jets become denser with increasing jet p_T . The data show nearly the same trends as PYTHIA in all cases.

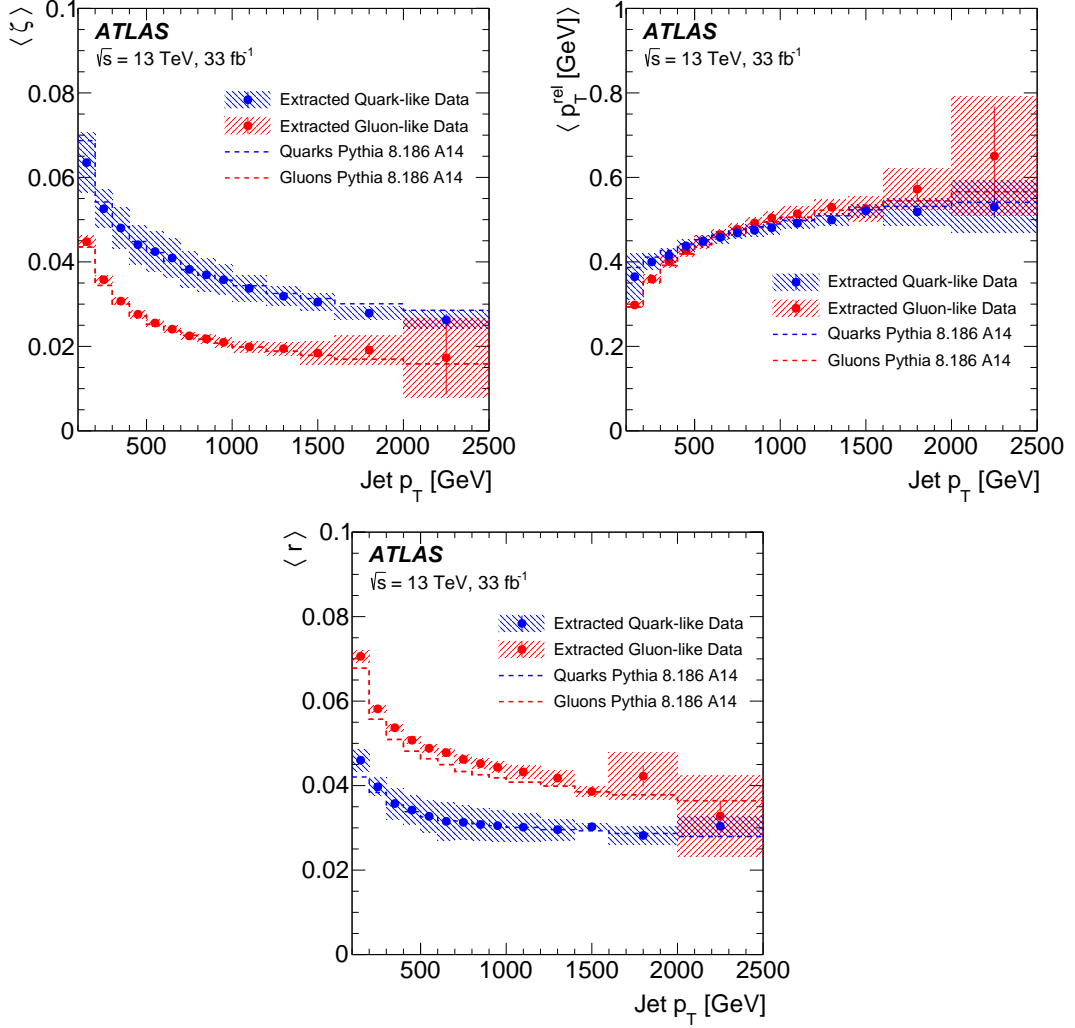


Figure 18: The dependence on jet transverse momentum p_T of the average extracted quark and gluon (top left) transverse momentum fraction ζ , (top right) transverse momentum p_T^{rel} , and (bottom) radial profile (per particle and not per jet). The uncertainty bands on the data include both statistical and systematic uncertainties while the error bars are due to statistical uncertainties only.

9 Conclusion

This paper documents a measurement of track-based jet fragmentation functions in pp collisions at $\sqrt{s} = 13$ TeV. The analysis uses a dataset corresponding to an integrated luminosity of 33 fb $^{-1}$ recorded by the ATLAS detector at the LHC. Multiple jet properties, including the charged-particle multiplicity, the momentum fraction carried by charged particles, and angular properties of the radiation pattern inside jets are studied. There are key areas where there are significant disagreements between the ATLAS default MC simulation (PYTHIA 8.2 with the A14 tune, Herwig++, and SHERPA) and the data, especially for the radial profiles and momentum distributions in SHERPA. The radial profile is systematically broader in data than in simulation, but the momentum transverse to the jet axis and the momentum fraction are well modeled within the precision of this measurement. Near 1 TeV in jet p_T , these measurements have achieved percent-level uncertainties for a variety of observables. In addition to measuring the forward, central, and

combined jet distributions, the forward and central jet spectra are considered separately to study quark- and gluon-like distributions. A first measurement of topic modeling for the charged-particle multiplicity provides a promising alternative to traditional methods of extracting quark- and gluon-jet distributions that use input from simulation. The simulations provide a reasonable description of the quark-like data across the jet p_T range presented in this measurement, but the gluon-like data have systematically fewer charged particles than the simulations by about 10%.

The unfolded data are made public through HepData to provide input to help improve both perturbative and non-perturbative aspects of fragmentation modeling in the future.

Acknowledgments

We thank CERN for the very successful operation of the LHC, as well as the support staff from our institutions without whom ATLAS could not be operated efficiently.

We acknowledge the support of ANPCyT, Argentina; YerPhI, Armenia; ARC, Australia; BMWFW and FWF, Austria; ANAS, Azerbaijan; SSTC, Belarus; CNPq and FAPESP, Brazil; NSERC, NRC and CFI, Canada; CERN; CONICYT, Chile; CAS, MOST and NSFC, China; COLCIENCIAS, Colombia; MSMT CR, MPO CR and VSC CR, Czech Republic; DNRF and DNSRC, Denmark; IN2P3-CNRS, CEA-DRF/IRFU, France; SRNSFG, Georgia; BMBF, HGF, and MPG, Germany; GSRT, Greece; RGC, Hong Kong SAR, China; ISF and Benozziyo Center, Israel; INFN, Italy; MEXT and JSPS, Japan; CNRST, Morocco; NWO, Netherlands; RCN, Norway; MNiSW and NCN, Poland; FCT, Portugal; MNE/IFA, Romania; MES of Russia and NRC KI, Russian Federation; JINR; MESTD, Serbia; MSSR, Slovakia; ARRS and MIZŠ, Slovenia; DST/NRF, South Africa; MINECO, Spain; SRC and Wallenberg Foundation, Sweden; SERI, SNSF and Cantons of Bern and Geneva, Switzerland; MOST, Taiwan; TAEK, Turkey; STFC, United Kingdom; DOE and NSF, United States of America. In addition, individual groups and members have received support from BCKDF, CANARIE, CRC and Compute Canada, Canada; COST, ERC, ERDF, Horizon 2020, and Marie Skłodowska-Curie Actions, European Union; Investissements d’Avenir Labex and Idex, ANR, France; DFG and AvH Foundation, Germany; Herakleitos, Thales and Aristeia programmes co-financed by EU-ESF and the Greek NSRF, Greece; BSF-NSF and GIF, Israel; CERCA Programme Generalitat de Catalunya, Spain; The Royal Society and Leverhulme Trust, United Kingdom.

The crucial computing support from all WLCG partners is acknowledged gratefully, in particular from CERN, the ATLAS Tier-1 facilities at TRIUMF (Canada), NDGF (Denmark, Norway, Sweden), CC-IN2P3 (France), KIT/GridKA (Germany), INFN-CNAF (Italy), NL-T1 (Netherlands), PIC (Spain), ASGC (Taiwan), RAL (UK) and BNL (USA), the Tier-2 facilities worldwide and large non-WLCG resource providers. Major contributors of computing resources are listed in Ref. [110].

References

- [1] A. Buckley et al., *General-purpose event generators for LHC physics*, *Phys. Rept.* **504** (2011) 145, arXiv: [1101.2599](https://arxiv.org/abs/1101.2599) [[hep-ph](https://arxiv.org/abs/1101.2599)].

- [2] ATLAS Collaboration, *Properties of jets measured from tracks in proton-proton collisions at center-of-mass energy $\sqrt{s} = 7$ TeV with the ATLAS detector*, *Phys. Rev. D* **84** (2011) 054001, arXiv: [1107.3311 \[hep-ex\]](#).
- [3] ATLAS Collaboration, *Study of jet shapes in inclusive jet production in pp collisions at $\sqrt{s} = 7$ TeV using the ATLAS detector*, *Phys. Rev. D* **83** (2011) 052003, arXiv: [1101.0070 \[hep-ex\]](#).
- [4] ATLAS Collaboration, *Measurement of jet shapes in top-quark pair events at $\sqrt{s} = 7$ TeV using the ATLAS detector*, *Eur. Phys. J. C* **73** (2013) 2676, arXiv: [1307.5749 \[hep-ex\]](#).
- [5] ATLAS Collaboration, *Jet mass and substructure of inclusive jets in $\sqrt{s} = 7$ TeV pp collisions with the ATLAS experiment*, *JHEP* **05** (2012) 128, arXiv: [1203.4606 \[hep-ex\]](#).
- [6] ATLAS Collaboration, *ATLAS Pythia 8 tunes to 7 TeV data*, ATL-PHYS-PUB-2014-021, 2014, URL: <https://cds.cern.ch/record/1966419>.
- [7] ATLAS Collaboration, *Measurement of the charged-particle multiplicity inside jets from $\sqrt{s} = 8$ TeV pp collisions with the ATLAS detector*, *Eur. Phys. J. C* **76** (2016) 322, arXiv: [1602.00988 \[hep-ex\]](#).
- [8] D. Reichelt, P. Richardson and A. Siodmok, *Improving the simulation of quark and gluon jets with Herwig 7*, *Eur. Phys. J. C* **77** (2017) 876, arXiv: [1708.01491 \[hep-ph\]](#).
- [9] J. Gallicchio and M. D. Schwartz, *Quark and gluon jet substructure*, *JHEP* **04** (2013) 090, arXiv: [1211.7038 \[hep-ph\]](#).
- [10] L. Asquith et al., *Jet Substructure at the Large Hadron Collider : Experimental Review*, (2018), arXiv: [1803.06991 \[hep-ex\]](#).
- [11] A. J. Larkoski, I. Moult and B. Nachman, *Jet Substructure at the Large Hadron Collider: A Review of Recent Advances in Theory and Machine Learning*, (2017), arXiv: [1709.04464 \[hep-ph\]](#).
- [12] ATLAS Collaboration, *Quark versus Gluon Jet Tagging Using Charged-Particle Constituent Multiplicity with the ATLAS Detector*, ATL-PHYS-PUB-2017-009, 2017, URL: <https://cds.cern.ch/record/2263679>.
- [13] C. W. Bauer, S. Fleming and M. Luke, *Summing Sudakov logarithms in $B \rightarrow X_s \gamma$ in effective field theory*, *Phys. Rev. D* **63** (2000) 014006, arXiv: [hep-ph/0005275](#).
- [14] C. W. Bauer, S. Fleming, D. Pirjol and I. W. Stewart, *An effective field theory for collinear and soft gluons: Heavy to light decays*, *Phys. Rev. D* **63** (2001) 114020, arXiv: [hep-ph/0011336](#).
- [15] C. W. Bauer and I. W. Stewart, *Invariant operators in collinear effective theory*, *Phys. Lett. B* **516** (2001) 134, arXiv: [hep-ph/0107001](#).
- [16] C. W. Bauer, D. Pirjol and I. W. Stewart, *Soft-collinear factorization in effective field theory*, *Phys. Rev. D* **65** (2002) 054022, arXiv: [hep-ph/0109045](#).
- [17] H.-M. Chang, M. Procura, J. Thaler and W. J. Waalewijn, *Calculating Track-Based Observables for the LHC*, *Phys. Rev. Lett.* **111** (2013) 102002, arXiv: [1303.6637 \[hep-ph\]](#).
- [18] W. J. Waalewijn, *Calculating the charge of a jet*, *Phys. Rev. D* **86** (2012) 094030, arXiv: [1209.3019 \[hep-ph\]](#).
- [19] D. Krohn, M. D. Schwartz, T. Lin and W. J. Waalewijn, *Jet Charge at the LHC*, *Phys. Rev. Lett.* **110** (2013) 212001, arXiv: [1209.2421 \[hep-ph\]](#).
- [20] B. T. Elder, M. Procura, J. Thaler, W. J. Waalewijn and K. Zhou, *Generalized fragmentation functions for fractal jet observables*, *JHEP* **06** (2017) 085, arXiv: [1704.05456 \[hep-ph\]](#).

- [21] ATLAS Collaboration, *Measurement of jet charge in dijet events from $\sqrt{s}=8$ TeV pp collisions with the ATLAS detector*, *Phys. Rev. D* **93** (2016) 052003, arXiv: [1509.05190 \[hep-ex\]](#).
- [22] A. Capella, I. M. Dremin, J. W. Gary, V. A. Nechitailo and J. Tran Thanh Van, *Evolution of average multiplicities of quark and gluon jets*, *Phys. Rev. D* **61** (2000) 074009, arXiv: [hep-ph/9910226](#).
- [23] I. M. Dremin and J. W. Gary, *Energy dependence of mean multiplicities in gluon and quark jets at the next-to-next-to-next-to leading order*, *Phys. Lett. B* **459** (1999) 341, [Erratum: *Phys. Lett. B* **463** (1999) 346], arXiv: [hep-ph/9905477](#).
- [24] A. J. Larkoski, S. Marzani and J. Thaler, *Sudakov safety in perturbative QCD*, *Phys. Rev. D* **91** (2015) 111501, arXiv: [1502.01719 \[hep-ph\]](#).
- [25] UA1 Collaboration, *Analysis of the fragmentation properties of quark and gluon jets at the CERN SPS $p\bar{p}$ collider*, *Nucl. Phys. B* **276** (1986) 253.
- [26] UA2 Collaboration, *Measurement of jet fragmentation properties at the CERN $p\bar{p}$ Collider*, *Phys. Lett. B* **144** (1984) 291.
- [27] UA2 Collaboration, *Measurement of production and properties of jets at the CERN $p\bar{p}$ collider*, *Z. Phys. C* **20** (1983) 117.
- [28] JADE Collaboration., *Experimental evidence for differences in $\langle p_{\perp} \rangle$ between quark jets and gluon jets*, *Phys. Lett. B* **123** (1983) 460.
- [29] TASSO Collaboration, *Charged multiplicity distributions and correlations in e^+e^- annihilation at PETRA energies*, *Z. Phys. C* **45** (1989) 193.
- [30] HRS Collaboration, *Comparison of charged particle multiplicities in quark and gluon jets produced in e^+e^- annihilation at 29 GeV*, *Phys. Lett. B* **165** (1985) 449.
- [31] MARK II Collaboration, *Inclusive Charged-Particle Distribution in Nearly Threefold-Symmetric Three-Jet Events at $E_{c.m.} = 29$ GeV*, *Phys. Rev. Lett.* **55** (1985) 1954.
- [32] SLD Collaboration, *Measurement of the charged multiplicity of $Z^0 \rightarrow b\bar{b}$ events*, *Phys. Rev. Lett.* **72** (1994) 3145, arXiv: [hep-ex/9405004](#).
- [33] SLD Collaboration, *Measurement of the charged multiplicities in b, c and light quark events from Z^0 decays*, *Phys. Lett. B* **386** (1996) 475, arXiv: [hep-ex/9608008](#).
- [34] AMY Collaboration, *Comparison of Quark and Gluon Jets Produced in High-Energy e^+e^- Annihilations*, *Phys. Rev. Lett.* **63** (1989) 1772.
- [35] CLEO Collaboration, *Study of gluon versus quark fragmentation in $\Upsilon \rightarrow gg\gamma$ and $e^+e^- \rightarrow q\bar{q}\gamma$ events at $\sqrt{s}=10$ GeV*, *Phys. Rev. D* **56** (1997) 17, arXiv: [hep-ex/9701006](#).
- [36] OPAL Collaboration, *A direct observation of quark-gluon jet differences at LEP*, *Phys. Lett. B* **265** (1991) 462.
- [37] OPAL Collaboration, *A study of differences between quark and gluon jets using vertex tagging of quark jets*, *Z. Phys. C* **58** (1993) 387.
- [38] OPAL Collaboration, *A model independent measurement of quark and gluon jet properties and differences*, *Z. Phys. C* **68** (1995) 179.
- [39] ALEPH Collaboration, *Study of the subjet structure of quark and gluon jets*, *Phys. Lett. B* **346** (1995) 389.
- [40] OPAL Collaboration, *Test of QCD analytic predictions for the multiplicity ratio between gluon and quark jets*, *Phys. Lett. B* **388** (1996) 659.

- [41] ALEPH Collaboration, *Quark and gluon jet properties in symmetric three-jet events*, *Phys. Lett. B* **384** (1996) 353.
- [42] DELPHI Collaboration, *Energy dependence of the differences between the quark and gluon jet fragmentation*, *Z. Phys. C* **70** (1996) 179.
- [43] OPAL Collaboration, *Multiplicity distributions of gluon and quark jets and tests of QCD analytic predictions*, *Eur. Phys. J. C* **1** (1998) 479, arXiv: [hep-ex/9708029](#).
- [44] DELPHI Collaboration, *The scale dependence of the hadron multiplicity in quark and gluon jets and a precise determination of C_A/C_F* , *Phys. Lett. B* **449** (1999) 383, arXiv: [hep-ex/9903073](#).
- [45] OPAL Collaboration, *Experimental properties of gluon and quark jets from a point source*, *Eur. Phys. J. C* **11** (1999) 217, arXiv: [hep-ex/9903027](#).
- [46] OPAL Collaboration, *A study of coherence of soft gluons in hadron jets*, *Phys. Lett. B* **247** (1990) 617.
- [47] OPAL Collaboration, *Scaling violations of quark and gluon jet fragmentation functions in e^+e^- annihilations at $\sqrt{s} = 91.2$ and $183 - 209$ GeV*, *Eur. Phys. J. C* **37** (2004) 25, arXiv: [hep-ex/0404026](#).
- [48] H1 Collaboration, *A Study of the fragmentation of quarks in e^-p collisions at HERA*, *Nucl. Phys. B* **445** (1995) 3, arXiv: [hep-ex/9505003](#).
- [49] ZEUS Collaboration, *Measurement of multiplicity and momentum spectra in the current fragmentation region of the Breit frame at HERA*, *Z. Phys. C* **67** (1995) 93, arXiv: [hep-ex/9501012](#).
- [50] CDF Collaboration, *Charged-Particle Multiplicity in $p\bar{p}$ Collisions at $\sqrt{s} = 1.8$ TeV*, *Phys. Rev. Lett.* **87** (2001) 211804.
- [51] CDF Collaboration, *Momentum distribution of charged particles in jets in dijet events in $p\bar{p}$ collisions at $\sqrt{s} = 1.8$ TeV and comparisons to perturbative QCD predictions*, *Phys. Rev. D* **68** (2003) 012003.
- [52] CDF Collaboration, *Two-particle momentum correlations in jets produced in $p\bar{p}$ collisions at $\sqrt{s} = 1.96$ TeV*, *Phys. Rev. D* **77** (2008) 092001, arXiv: [0802.3182 \[hep-ex\]](#).
- [53] CDF Collaboration, *Measurement of the k_T Distribution of Particles in Jets Produced in $p\bar{p}$ Collisions at $\sqrt{s} = 1.96$ TeV*, *Phys. Rev. Lett.* **102** (2009) 232002.
- [54] ATLAS Collaboration, *Measurement of jet fragmentation in Pb+Pb and pp collisions at $\sqrt{s_{NN}} = 2.76$ TeV with the ATLAS detector at the LHC*, *Eur. Phys. J. C* **77** (2017) 379, arXiv: [1702.00674 \[hep-ex\]](#).
- [55] CMS Collaboration, *Measurement of jet fragmentation into charged particles in pp and PbPb collisions at $\sqrt{s_{NN}} = 2.76$ TeV*, *JHEP* **10** (2012) 087, arXiv: [1205.5872 \[nucl-ex\]](#).
- [56] ATLAS Collaboration, *Measurement of jet fragmentation in 5.02 TeV proton-lead and proton-proton collisions with the ATLAS detector*, *Nucl. Phys. A* **978** (2018) 65, arXiv: [1706.02859 \[hep-ex\]](#).
- [57] ATLAS Collaboration, *Measurement of jet fragmentation in Pb+Pb and pp collisions at $\sqrt{s_{NN}} = 5.02$ TeV with the ATLAS detector*, *Phys. Rev. C* **98** (2018) 024908, arXiv: [1805.05424 \[nucl-ex\]](#).
- [58] ATLAS Collaboration, *Comparison of fragmentation functions for light-quark- and gluon-dominated jets from pp and Pb+Pb collisions in ATLAS*, (2019), arXiv: [1902.10007 \[nucl-ex\]](#).
- [59] ATLAS Collaboration, *Measurement of the jet fragmentation function and transverse profile in proton-proton collisions at a center-of-mass energy of 7 TeV with the ATLAS detector*, *Eur. Phys. J. C* **71** (2011) 1795, arXiv: [1109.5816 \[hep-ex\]](#).

- [60] CMS Collaboration, *Shape, transverse size, and charged hadron multiplicity of jets in pp Collisions at 7 TeV*, *JHEP* **06** (2012) 160, arXiv: [1204.3170 \[hep-ex\]](#).
- [61] CMS Collaboration, *Measurements of jet charge with dijet events in pp collisions at $\sqrt{s} = 8$ TeV*, *JHEP* **10** (2017) 131, arXiv: [1706.05868 \[hep-ex\]](#).
- [62] CMS Collaboration, *Measurement of jet fragmentation in PbPb and pp collisions at $\sqrt{s_{NN}} = 2.76$ TeV*, *Phys. Rev. C* **90** (2014) 024908, arXiv: [1406.0932 \[nucl-ex\]](#).
- [63] ATLAS Collaboration, *Measurement of inclusive jet charged-particle fragmentation functions in Pb+Pb collisions at $\sqrt{s_{NN}} = 2.76$ TeV with the ATLAS detector*, *Phys. Lett. B* **739** (2014) 320, arXiv: [1406.2979 \[hep-ex\]](#).
- [64] ATLAS Collaboration, *ATLAS Insertable B-Layer Technical Design Report*, ATLAS-TDR-19, 2010, URL: <https://cds.cern.ch/record/1291633>, Addendum: ATLAS-TDR-19-ADD-1, 2012, URL: <https://cds.cern.ch/record/1451888>.
- [65] B. Abbott et al., *Production and integration of the ATLAS Insertable B-Layer*, *JINST* **13** (2018) T05008, arXiv: [1803.00844 \[physics.ins-det\]](#).
- [66] ATLAS Collaboration, *A neural network clustering algorithm for the ATLAS silicon pixel detector*, *JINST* **9** (2014) P09009, arXiv: [1406.7690 \[hep-ex\]](#).
- [67] ATLAS Collaboration, *Performance of the ATLAS track reconstruction algorithms in dense environments in LHC Run 2*, *Eur. Phys. J. C* **77** (2017) 673, arXiv: [1704.07983 \[hep-ex\]](#).
- [68] ATLAS Collaboration, *Modelling of Track Reconstruction Inside Jets with the 2016 ATLAS $\sqrt{s} = 13$ TeV pp Dataset*, ATL-PHYS-PUB-2017-016 (2017), URL: <https://cds.cern.ch/record/2275639>.
- [69] ATLAS Collaboration, *Measurement of track reconstruction inefficiencies in the core of jets via pixel dE/dx with the ATLAS experiment using $\sqrt{s} = 13$ TeV pp collision data*, ATL-PHYS-PUB-2016-007, 2016, URL: <https://cds.cern.ch/record/2140460>.
- [70] G. Altarelli and G. Parisi, *Asymptotic freedom in parton language*, *Nucl. Phys. B* **126** (1977) 298.
- [71] Y. L. Dokshitzer, *Calculation of the Structure Functions for Deep Inelastic Scattering and e^+e^- Annihilation by Perturbation Theory in Quantum Chromodynamics.*, *Sov. Phys. JETP* **46** (1977) 641.
- [72] V. N. Gribov and L. N. Lipatov, *Deep inelastic $e p$ scattering in perturbation theory*, *Sov. J. Nucl. Phys.* **15** (1972) 438, [*Yad. Fiz.*15,781(1972)].
- [73] R. Ellis, W. Stirling and B. Webber, *QCD and Collider Physics*, Cambridge University Press, 2003, ISBN: 0521545897.
- [74] CMS Collaboration, *Search for a Higgs boson in the decay channel $H \rightarrow ZZ^{(*)} \rightarrow q\bar{q}\ell^-\ell^+$ in pp collisions at $\sqrt{s} = 7$ TeV*, *JHEP* **04** (2012) 036, arXiv: [1202.1416 \[hep-ex\]](#).
- [75] ATLAS Collaboration, *The ATLAS Experiment at the CERN Large Hadron Collider*, *JINST* **3** (2008) S08003.
- [76] ATLAS Collaboration, *Performance of the ATLAS trigger system in 2015*, *Eur. Phys. J. C* **77** (2017) 317, arXiv: [1611.09661 \[hep-ex\]](#).
- [77] T. Sjöstrand, S. Mrenna and P. Z. Skands, *A brief introduction to PYTHIA 8.1*, *Comput. Phys. Commun.* **178** (2008) 852, arXiv: [0710.3820 \[hep-ph\]](#).
- [78] R. D. Ball et al., *Parton distributions with LHC data*, *Nucl. Phys. B* **867** (2013) 244, arXiv: [1207.1303 \[hep-ph\]](#).

- [79] T. Gleisberg et al., *Event generation with SHERPA 1.1*, *JHEP* **02** (2009) 007, arXiv: [0811.4622 \[hep-ph\]](#).
- [80] S. Catani, F. Krauss, B. R. Webber and R. Kuhn, *QCD matrix elements + parton showers*, *JHEP* **11** (2001) 063, arXiv: [hep-ph/0109231](#).
- [81] H.-L. Lai et al., *New parton distributions for collider physics*, *Phys. Rev. D* **82** (2010) 074024, arXiv: [1007.2241 \[hep-ph\]](#).
- [82] M. Bähr et al., *Herwig++ physics and manual*, *Eur. Phys. J. C* **58** (2008) 639, arXiv: [0803.0883 \[hep-ph\]](#).
- [83] G. Corcella et al., *HERWIG 6: An event generator for hadron emission reactions with interfering gluons (including supersymmetric processes)*, *JHEP* **01** (2001) 010.
- [84] J. Pumplin et al., *New generation of parton distributions with uncertainties from global QCD analysis*, *JHEP* **07** (2002) 012, arXiv: [hep-ph/0201195](#).
- [85] M. H. Seymour and A. Siodmok, *Constraining MPI models using σ_{eff} and recent Tevatron and LHC Underlying Event data*, *JHEP* **10** (2013) 113, arXiv: [1307.5015 \[hep-ph\]](#).
- [86] ATLAS Collaboration, *The ATLAS Simulation Infrastructure*, *Eur. Phys. J. C* **70** (2010) 823, arXiv: [1005.4568 \[physics.ins-det\]](#).
- [87] S. Agostinelli et al., *GEANT4 – a simulation toolkit*, *Nucl. Instrum. Meth. A* **506** (2003) 250.
- [88] ATLAS Collaboration, *Summary of ATLAS Pythia 8 tunes*, ATL-PHYS-PUB-2012-003, 2012, URL: <https://cds.cern.ch/record/1474107>.
- [89] A. D. Martin, W. J. Stirling, R. S. Thorne and G. Watt, *Parton distributions for the LHC*, *Eur. Phys. J. C* **63** (2009) 189, arXiv: [0901.0002 \[hep-ph\]](#).
- [90] M. Cacciari, G. P. Salam and G. Soyez, *The anti- k_t jet clustering algorithm*, *JHEP* **04** (2008) 063, arXiv: [0802.1189 \[hep-ph\]](#).
- [91] M. Cacciari, G. P. Salam and G. Soyez, *FastJet user manual*, *Eur. Phys. J. C* **72** (2012) 1896, arXiv: [1111.6097 \[hep-ph\]](#).
- [92] ATLAS Collaboration, *Topological cell clustering in the ATLAS calorimeters and its performance in LHC Run 1*, *Eur. Phys. J. C* **77** (2017) 490, arXiv: [1603.02934 \[hep-ex\]](#).
- [93] ATLAS Collaboration, *Jet energy scale measurements and their systematic uncertainties in proton-proton collisions at $\sqrt{s} = 13$ TeV with the ATLAS detector*, *Phys. Rev. D* **96** (2017) 072002, arXiv: [1703.09665 \[hep-ex\]](#).
- [94] ATLAS Collaboration, *Early Inner Detector Tracking Performance in the 2015 Data at $\sqrt{s} = 13$ TeV*, ATL-PHYS-PUB-2015-051, 2015, URL: <https://cds.cern.ch/record/2110140>.
- [95] M. Cacciari, G. P. Salam and G. Soyez, *The catchment area of jets*, *JHEP* **04** (2008) 005, arXiv: [0802.1188 \[hep-ph\]](#).
- [96] G. D’Agostini, *A multidimensional unfolding method based on Bayes’ theorem*, *Nucl. Instrum. Meth. A* **362** (1995) 487.
- [97] T. Adye, *Unfolding algorithms and tests using RooUnfold*, (2011), arXiv: [1105.1160 \[physics.data-an\]](#).
- [98] B. Efron, *Bootstrap Methods: Another Look at the Jackknife*, *Ann. Statist.* **7** (1979) 1.
- [99] HepData, URL: <http://www.hepdata.net>.

- [100] ATLAS Collaboration, *Study of the material of the ATLAS inner detector for Run 2 of the LHC*, [JINST **12** \(2017\) P12009](#), arXiv: [1707.02826 \[hep-ex\]](#).
- [101] B. Malaescu, *An iterative, dynamically stabilized method of data unfolding*, (2009), arXiv: [0907.3791 \[physics.data-an\]](#).
- [102] S. Bright-Thonney and B. Nachman, *Investigating the topology dependence of quark and gluon jets*, [JHEP **03** \(2018\) 098](#), arXiv: [1810.05653 \[hep-ph\]](#).
- [103] E. M. Metodiev and J. Thaler, *Jet Topics: Disentangling Quarks and Gluons at Colliders*, [Phys. Rev. Lett. **120** \(2018\) 241602](#), arXiv: [1802.00008 \[hep-ph\]](#).
- [104] P. T. Komiske, E. M. Metodiev and J. Thaler, *An operational definition of quark and gluon jets*, [JHEP **11** \(2018\) 059](#), arXiv: [1809.01140 \[hep-ph\]](#).
- [105] M. Procura and W. J. Waalewijn, *Fragmentation in jets: Cone and threshold effects*, [Phys. Rev. D **85** \(2012\) 114041](#), arXiv: [arXiv:1111.6605 \[hep-ph\]](#).
- [106] A. Jain, M. Procura and W. J. Waalewijn, *Parton fragmentation within an identified jet at NNLL*, [JHEP **05** \(2011\) 035](#), arXiv: [arXiv:1101.4953 \[hep-ph\]](#).
- [107] M. Procura and I. W. Stewart, *Quark fragmentation within an identified jet*, [Phys. Rev. D **81** \(2010\) 074009](#), [Erratum: [Phys. Rev. D **83** \(2011\) 039902](#)], arXiv: [0911.4980 \[hep-ph\]](#).
- [108] V. A. Khoze, W. Ochs and J. Wosiek, *Analytical QCD and multiparticle production*, [At the frontier of particle physics **2** \(2000\) 1101](#), arXiv: [hep-ph/0009298](#).
- [109] R. Perez-Ramos and B. Machet, *Inclusive hadronic distributions inside one jet at high energy colliders at ‘modified leading logarithm approximation’ of quantum chromodynamics*, [JHEP **04** \(2006\) 043](#), arXiv: [hep-ph/0512236](#).
- [110] ATLAS Collaboration, *ATLAS Computing Acknowledgements*, ATL-GEN-PUB-2016-002, URL: <https://cds.cern.ch/record/2202407>.

The ATLAS Collaboration

G. Aad¹⁰¹, B. Abbott¹²⁸, D.C. Abbott¹⁰², O. Abidinov^{13,*}, A. Abed Abud^{70a,70b}, K. Abeling⁵³, D.K. Abhayasinghe⁹³, S.H. Abidi¹⁶⁷, O.S. AbouZeid⁴⁰, N.L. Abraham¹⁵⁶, H. Abramowicz¹⁶¹, H. Abreu¹⁶⁰, Y. Abulaiti⁶, B.S. Acharya^{66a,66b,n}, B. Achkar⁵³, S. Adachi¹⁶³, L. Adam⁹⁹, C. Adam Bourdarios¹³², L. Adamczyk^{83a}, L. Adamek¹⁶⁷, J. Adelman¹²¹, M. Adersberger¹¹⁴, A. Adiguzel^{12c,ai}, S. Adorni⁵⁴, T. Adye¹⁴⁴, A.A. Affolder¹⁴⁶, Y. Afik¹⁶⁰, C. Agapopoulou¹³², M.N. Agaras³⁸, A. Aggarwal¹¹⁹, C. Agheorghiesei^{27c}, J.A. Aguilar-Saavedra^{140f,140a,ah}, F. Ahmadov⁷⁹, W.S. Ahmed¹⁰³, X. Ai^{15a}, G. Aielli^{73a,73b}, S. Akatsuka⁸⁵, T.P.A. Åkesson⁹⁶, E. Akilli⁵⁴, A.V. Akimov¹¹⁰, K. Al Khoury¹³², G.L. Alberghi^{23b,23a}, J. Albert¹⁷⁶, M.J. Alconada Verzini⁸⁸, S. Alderweireldt³⁶, M. Aleksa³⁶, I.N. Aleksandrov⁷⁹, C. Alexa^{27b}, D. Alexandre¹⁹, T. Alexopoulos¹⁰, A. Alfonsi¹²⁰, M. Alhroob¹²⁸, B. Ali¹⁴², G. Alimonti^{68a}, J. Alison³⁷, S.P. Alkire¹⁴⁸, C. Allaire¹³², B.M.M. Allbrooke¹⁵⁶, B.W. Allen¹³¹, P.P. Allport²¹, A. Aloisio^{69a,69b}, A. Alonso⁴⁰, F. Alonso⁸⁸, C. Alpigiani¹⁴⁸, A.A. Alshehri⁵⁷, M. Alvarez Estevez⁹⁸, D. Álvarez Piqueras¹⁷⁴, M.G. Alviggi^{69a,69b}, Y. Amaral Coutinho^{80b}, A. Ambler¹⁰³, L. Ambroz¹³⁵, C. Amelung²⁶, D. Amidei¹⁰⁵, S.P. Amor Dos Santos^{140a}, S. Amoroso⁴⁶, C.S. Amrouche⁵⁴, F. An⁷⁸, C. Anastopoulos¹⁴⁹, N. Andari¹⁴⁵, T. Andeen¹¹, C.F. Anders^{61b}, J.K. Anders²⁰, A. Andreazza^{68a,68b}, V. Andrei^{61a}, C.R. Anelli¹⁷⁶, S. Angelidakis³⁸, A. Angerami³⁹, A.V. Anisenkov^{122b,122a}, A. Annovi^{71a}, C. Antel^{61a}, M.T. Anthony¹⁴⁹, M. Antonelli⁵¹, D.J.A. Antrim¹⁷¹, F. Anulli^{72a}, M. Aoki⁸¹, J.A. Aparisi Pozo¹⁷⁴, L. Aperio Bella³⁶, G. Arabidze¹⁰⁶, J.P. Araque^{140a}, V. Araujo Ferraz^{80b}, R. Araujo Pereira^{80b}, C. Arcangeletti⁵¹, A.T.H. Arce⁴⁹, F.A. Arduh⁸⁸, J-F. Arguin¹⁰⁹, S. Argyropoulos⁷⁷, J.-H. Arling⁴⁶, A.J. Armbruster³⁶, A. Armstrong¹⁷¹, O. Arnaez¹⁶⁷, H. Arnold¹²⁰, A. Artamonov^{111,*}, G. Artoni¹³⁵, S. Artz⁹⁹, S. Asai¹⁶³, N. Asbah⁵⁹, E.M. Asimakopoulou¹⁷², L. Asquith¹⁵⁶, K. Assamagan²⁹, R. Astalos^{28a}, R.J. Atkin^{33a}, M. Atkinson¹⁷³, N.B. Atlay¹⁵¹, H. Atmani¹³², K. Augsten¹⁴², G. Avolio³⁶, R. Avramidou^{60a}, M.K. Ayoub^{15a}, A.M. Azoulay^{168b}, G. Azuelos^{109,ax}, M.J. Baca²¹, H. Bachacou¹⁴⁵, K. Bachas^{67a,67b}, M. Backes¹³⁵, F. Backman^{45a,45b}, P. Bagnaia^{72a,72b}, M. Bahmani⁸⁴, H. Bahrasemani¹⁵², A.J. Bailey¹⁷⁴, V.R. Bailey¹⁷³, J.T. Baines¹⁴⁴, M. Bajic⁴⁰, C. Bakalis¹⁰, O.K. Baker¹⁸³, P.J. Bakker¹²⁰, D. Bakshi Gupta⁸, S. Balaji¹⁵⁷, E.M. Baldin^{122b,122a}, P. Balek¹⁸⁰, F. Balli¹⁴⁵, W.K. Balunas¹³⁵, J. Balz⁹⁹, E. Banas⁸⁴, A. Bandyopadhyay²⁴, Sw. Banerjee^{181,i}, A.A.E. Bannoura¹⁸², L. Barak¹⁶¹, W.M. Barbe³⁸, E.L. Barberio¹⁰⁴, D. Barberis^{55b,55a}, M. Barbero¹⁰¹, T. Barillari¹¹⁵, M-S. Barisits³⁶, J. Barkeloo¹³¹, T. Barklow¹⁵³, R. Barnea¹⁶⁰, S.L. Barnes^{60c}, B.M. Barnett¹⁴⁴, R.M. Barnett¹⁸, Z. Barnovska-Blenessy^{60a}, A. Baroncelli^{60a}, G. Barone²⁹, A.J. Barr¹³⁵, L. Barranco Navarro^{45a,45b}, F. Barreiro⁹⁸, J. Barreiro Guimarães da Costa^{15a}, S. Barsov¹³⁸, R. Bartoldus¹⁵³, G. Bartolini¹⁰¹, A.E. Barton⁸⁹, P. Bartos^{28a}, A. Basalae⁴⁶, A. Bassalat^{132,aq}, R.L. Bates⁵⁷, S.J. Batista¹⁶⁷, S. Batlamous^{35e}, J.R. Batley³², B. Batool¹⁵¹, M. Battaglia¹⁴⁶, M. Baucé^{72a,72b}, F. Bauer¹⁴⁵, K.T. Bauer¹⁷¹, H.S. Bawa^{31,l}, J.B. Beacham⁴⁹, T. Beau¹³⁶, P.H. Beauchemin¹⁷⁰, F. Becherer⁵², P. Bechtel²⁴, H.C. Beck⁵³, H.P. Beck^{20,r}, K. Becker⁵², M. Becker⁹⁹, C. Becot⁴⁶, A. Beddall^{12d}, A.J. Beddall^{12a}, V.A. Bednyakov⁷⁹, M. Bedognetti¹²⁰, C.P. Bee¹⁵⁵, T.A. Beermann⁷⁶, M. Begalli^{80b}, M. Begel²⁹, A. Behera¹⁵⁵, J.K. Behr⁴⁶, F. Beisiegel²⁴, A.S. Bell⁹⁴, G. Bella¹⁶¹, L. Bellagamba^{23b}, A. Bellerive³⁴, P. Bellos⁹, K. Beloborodov^{122b,122a}, K. Belotskiy¹¹², N.L. Belyaev¹¹², D. Benchechroun^{35a}, N. Benekos¹⁰, Y. Benhammou¹⁶¹, D.P. Benjamin⁶, M. Benoit⁵⁴, J.R. Bensinger²⁶, S. Bentvelsen¹²⁰, L. Beresford¹³⁵, M. Beretta⁵¹, D. Berge⁴⁶, E. Bergeaas Kuutmann¹⁷², N. Berger⁵, B. Bergmann¹⁴², L.J. Bergsten²⁶, J. Beringer¹⁸, S. Berlendis⁷, N.R. Bernard¹⁰², G. Bernardi¹³⁶, C. Bernius¹⁵³, T. Berry⁹³, P. Berta⁹⁹, C. Bertella^{15a}, I.A. Bertram⁸⁹, G.J. Besjes⁴⁰, O. Bessidskaia Bylund¹⁸², N. Besson¹⁴⁵, A. Bethani¹⁰⁰, S. Bethke¹¹⁵, A. Betti²⁴, A.J. Bevan⁹², J. Beyer¹¹⁵, R. Bi¹³⁹, R.M. Bianchi¹³⁹, O. Biebel¹¹⁴, D. Biedermann¹⁹, R. Bielski³⁶, K. Bierwagen⁹⁹, N.V. Biesuz^{71a,71b}, M. Biglietti^{74a}, T.R.V. Billoud¹⁰⁹, M. Bindi⁵³, A. Bingul^{12d}, C. Bini^{72a,72b},

S. Biondi^{23b,23a}, M. Birman¹⁸⁰, T. Bisanz⁵³, J.P. Biswal¹⁶¹, A. Bitadze¹⁰⁰, C. Bittrich⁴⁸, K. Bjørke¹³⁴,
 K.M. Black²⁵, T. Blazek^{28a}, I. Bloch⁴⁶, C. Blocker²⁶, A. Blue⁵⁷, U. Blumenschein⁹², G.J. Bobbink¹²⁰,
 V.S. Bobrovnikov^{122b,122a}, S.S. Bocchetta⁹⁶, A. Bocci⁴⁹, D. Boerner⁴⁶, D. Bogavac¹⁴,
 A.G. Bogdanchikov^{122b,122a}, C. Bohm^{45a}, V. Boisvert⁹³, P. Bokan^{53,172}, T. Bold^{83a}, A.S. Boldyrev¹¹³,
 A.E. Bolz^{61b}, M. Bomben¹³⁶, M. Bona⁹², J.S. Bonilla¹³¹, M. Boonekamp¹⁴⁵, H.M. Borecka-Bielska⁹⁰,
 A. Borisov¹²³, G. Borisso⁸⁹, J. Bortfeldt³⁶, D. Bortoletto¹³⁵, V. Bortolotto^{73a,73b}, D. Boscherini^{23b},
 M. Bosman¹⁴, J.D. Bossio Sola¹⁰³, K. Bouaouda^{35a}, J. Boudreau¹³⁹, E.V. Bouhova-Thacker⁸⁹,
 D. Boumediene³⁸, S.K. Boutle⁵⁷, A. Boveia¹²⁶, J. Boyd³⁶, D. Boye^{33b,ar}, I.R. Boyko⁷⁹, A.J. Bozson⁹³,
 J. Bracinik²¹, N. Brahim¹⁰¹, G. Brandt¹⁸², O. Brandt^{61a}, F. Braren⁴⁶, B. Brau¹⁰², J.E. Brau¹³¹,
 W.D. Breaden Madden⁵⁷, K. Brendlinger⁴⁶, L. Brenner⁴⁶, R. Brenner¹⁷², S. Bressler¹⁸⁰, B. Brickwedde⁹⁹,
 D.L. Briglin²¹, D. Britton⁵⁷, D. Britzger¹¹⁵, I. Brock²⁴, R. Brock¹⁰⁶, G. Brooijmans³⁹, W.K. Brooks^{147b},
 E. Brost¹²¹, J.H. Broughton²¹, P.A. Bruckman de Renstrom⁸⁴, D. Bruncko^{28b}, A. Bruni^{23b}, G. Bruni^{23b},
 L.S. Bruni¹²⁰, S. Bruno^{73a,73b}, B.H. Brunt³², M. Bruschi^{23b}, N. Brusino¹³⁹, P. Bryant³⁷, L. Bryngemark⁹⁶,
 T. Buanes¹⁷, Q. Buat³⁶, P. Buchholz¹⁵¹, A.G. Buckley⁵⁷, I.A. Budagov⁷⁹, M.K. Bugge¹³⁴, F. Bühner⁵²,
 O. Bulekov¹¹², T.J. Burch¹²¹, S. Burdin⁹⁰, C.D. Burgard¹²⁰, A.M. Burger¹²⁹, B. Burghgrave⁸, K. Burka⁸⁴,
 J.T.P. Burr⁴⁶, J.C. Burzynski¹⁰², V. Büscher⁹⁹, E. Buschmann⁵³, P.J. Bussey⁵⁷, J.M. Butler²⁵,
 C.M. Buttar⁵⁷, J.M. Butterworth⁹⁴, P. Butti³⁶, W. Buttinger³⁶, A. Buzatu¹⁵⁸, A.R. Buzykaev^{122b,122a},
 G. Cabras^{23b,23a}, S. Cabrera Urbán¹⁷⁴, D. Caforio⁵⁶, H. Cai¹⁷³, V.M.M. Cairo¹⁵³, O. Cakir^{4a}, N. Calace³⁶,
 P. Calafiura¹⁸, A. Calandri¹⁰¹, G. Calderini¹³⁶, P. Calfayan⁶⁵, G. Callea⁵⁷, L.P. Caloba^{80b},
 S. Calvente Lopez⁹⁸, D. Calvet³⁸, S. Calvet³⁸, T.P. Calvet¹⁵⁵, M. Calvetti^{71a,71b}, R. Camacho Toro¹³⁶,
 S. Camarda³⁶, D. Camarero Munoz⁹⁸, P. Camarri^{73a,73b}, D. Cameron¹³⁴, R. Caminal Armadans¹⁰²,
 C. Camincher³⁶, S. Campana³⁶, M. Campanelli⁹⁴, A. Camplani⁴⁰, A. Campoverde¹⁵¹, V. Canale^{69a,69b},
 A. Canesse¹⁰³, M. Cano Bret^{60c}, J. Cantero¹²⁹, T. Cao¹⁶¹, Y. Cao¹⁷³, M.D.M. Capeans Garrido³⁶,
 M. Capua^{41b,41a}, R. Cardarelli^{73a}, F.C. Cardillo¹⁴⁹, G. Carducci^{41b,41a}, I. Carli¹⁴³, T. Carli³⁶, G. Carlino^{69a},
 B.T. Carlson¹³⁹, L. Carminati^{68a,68b}, R.M.D. Carney^{45a,45b}, S. Caron¹¹⁹, E. Carquin^{147b}, S. Carrá⁴⁶,
 J.W.S. Carter¹⁶⁷, M.P. Casado^{14,d}, A.F. Casha¹⁶⁷, D.W. Casper¹⁷¹, R. Castelijin¹²⁰, F.L. Castillo¹⁷⁴,
 V. Castillo Gimenez¹⁷⁴, N.F. Castro^{140a,140e}, A. Catinaccio³⁶, J.R. Catmore¹³⁴, A. Cattai³⁶, J. Caudron²⁴,
 V. Cavaliere²⁹, E. Cavallaro¹⁴, M. Cavalli-Sforza¹⁴, V. Cavasinni^{71a,71b}, E. Celebi^{12b}, F. Ceradini^{74a,74b},
 L. Cerda Alberich¹⁷⁴, K. Cerny¹³⁰, A.S. Cerqueira^{80a}, A. Cerri¹⁵⁶, L. Cerrito^{73a,73b}, F. Cerutti¹⁸,
 A. Cervelli^{23b,23a}, S.A. Cetin^{12b}, Z. Chadi^{35a}, D. Chakraborty¹²¹, S.K. Chan⁵⁹, W.S. Chan¹²⁰, W.Y. Chan⁹⁰,
 J.D. Chapman³², B. Chargeishvili^{159b}, D.G. Charlton²¹, T.P. Charman⁹², C.C. Chau³⁴, S. Che¹²⁶,
 A. Chegwidan¹⁰⁶, S. Chekanov⁶, S.V. Chekulaev^{168a}, G.A. Chelkov^{79,aw}, M.A. Chelstowska³⁶, B. Chen⁷⁸,
 C. Chen^{60a}, C.H. Chen⁷⁸, H. Chen²⁹, J. Chen^{60a}, J. Chen³⁹, S. Chen¹³⁷, S.J. Chen^{15c}, X. Chen^{15b,av},
 Y. Chen⁸², Y-H. Chen⁴⁶, H.C. Cheng^{63a}, H.J. Cheng^{15a,15d}, A. Cheplakov⁷⁹, E. Cheremushkina¹²³,
 R. Cherkaoui El Moursli^{35e}, E. Cheu⁷, K. Cheung⁶⁴, T.J.A. Chevalérias¹⁴⁵, L. Chevalier¹⁴⁵, V. Chiarella⁵¹,
 G. Chiarelli^{71a}, G. Chiodini^{67a}, A.S. Chisholm^{36,21}, A. Chitan^{27b}, I. Chiu¹⁶³, Y.H. Chiu¹⁷⁶,
 M.V. Chizhov⁷⁹, K. Choi⁶⁵, A.R. Chomont^{72a,72b}, S. Chouridou¹⁶², Y.S. Chow¹²⁰, M.C. Chu^{63a}, X. Chu^{15a},
 J. Chudoba¹⁴¹, A.J. Chuinard¹⁰³, J.J. Chwastowski⁸⁴, L. Chytka¹³⁰, K.M. Ciesla⁸⁴, D. Cinca⁴⁷,
 V. Cindro⁹¹, I.A. Cioară^{27b}, A. Ciocio¹⁸, F. Ciotto^{69a,69b}, Z.H. Citron¹⁸⁰, M. Citterio^{68a},
 D.A. Ciubotaru^{27b}, B.M. Ciungu¹⁶⁷, A. Clark⁵⁴, M.R. Clark³⁹, P.J. Clark⁵⁰, C. Clement^{45a,45b},
 Y. Coadou¹⁰¹, M. Cokal^{66a,66c}, A. Coccaro^{55b}, J. Cochran⁷⁸, H. Cohen¹⁶¹, A.E.C. Coimbra³⁶,
 L. Colasurdo¹¹⁹, B. Cole³⁹, A.P. Colijn¹²⁰, J. Collot⁵⁸, P. Conde Muiño^{140a,e}, E. Coniavitis⁵²,
 S.H. Connell^{33b}, I.A. Connelly⁵⁷, S. Constantinescu^{27b}, F. Conventi^{69a,ay}, A.M. Cooper-Sarkar¹³⁵,
 F. Cormier¹⁷⁵, K.J.R. Cormier¹⁶⁷, L.D. Corpe⁹⁴, M. Corradi^{72a,72b}, E.E. Corrigan⁹⁶, F. Corriveau^{103,ad},
 A. Cortes-Gonzalez³⁶, M.J. Costa¹⁷⁴, F. Costanza⁵, D. Costanzo¹⁴⁹, G. Cowan⁹³, J.W. Cowley³²,
 J. Crane¹⁰⁰, K. Cranmer¹²⁴, S.J. Crawley⁵⁷, R.A. Creager¹³⁷, S. Crépe-Renaudin⁵⁸, F. Crescioli¹³⁶,
 M. Cristinziani²⁴, V. Croft¹²⁰, G. Crosetti^{41b,41a}, A. Cueto⁵, T. Cuhadar Donszelmann¹⁴⁹,

A.R. Cukierman¹⁵³, S. Czekerda⁸⁴, P. Czodrowski³⁶, M.J. Da Cunha Sargedas De Sousa^{60b},
 J.V. Da Fonseca Pinto^{80b}, C. Da Via¹⁰⁰, W. Dabrowski^{83a}, T. Dado^{28a}, S. Dahbi^{35e}, T. Dai¹⁰⁵,
 C. Dallapiccola¹⁰², M. Dam⁴⁰, G. D'amen^{23b,23a}, V. D'Amico^{74a,74b}, J. Damp⁹⁹, J.R. Dandoy¹³⁷,
 M.F. Daneri³⁰, N.P. Dang¹⁸¹, N.D. Dann¹⁰⁰, M. Danninger¹⁷⁵, V. Dao³⁶, G. Darbo^{55b}, O. Dartsi⁵,
 A. Dattagupta¹³¹, T. Daubney⁴⁶, S. D'Auria^{68a,68b}, W. Davey²⁴, C. David⁴⁶, T. Davidek¹⁴³, D.R. Davis⁴⁹,
 I. Dawson¹⁴⁹, K. De⁸, R. De Asmundis^{69a}, M. De Beurs¹²⁰, S. De Castro^{23b,23a}, S. De Cecco^{72a,72b},
 N. De Groot¹¹⁹, P. de Jong¹²⁰, H. De la Torre¹⁰⁶, A. De Maria^{15c}, D. De Pedis^{72a}, A. De Salvo^{72a},
 U. De Sanctis^{73a,73b}, M. De Santis^{73a,73b}, A. De Santo¹⁵⁶, K. De Vasconcelos Corga¹⁰¹,
 J.B. De Vivie De Regie¹³², C. Debenedetti¹⁴⁶, D.V. Dedovich⁷⁹, A.M. Deiana⁴², M. Del Gaudio^{41b,41a},
 J. Del Peso⁹⁸, Y. Delabat Diaz⁴⁶, D. Delgove¹³², F. Deliot^{145,q}, C.M. Delitzsch⁷, M. Della Pietra^{69a,69b},
 D. Della Volpe⁵⁴, A. Dell'Acqua³⁶, L. Dell'Asta^{73a,73b}, M. Delmastro⁵, C. Delporte¹³², P.A. Delsart⁵⁸,
 D.A. DeMarco¹⁶⁷, S. Demers¹⁸³, M. Demichev⁷⁹, G. Demontigny¹⁰⁹, S.P. Denisov¹²³, D. Denysiuk¹²⁰,
 L. D'Eramo¹³⁶, D. Derendarz⁸⁴, J.E. Derkaoui^{35d}, F. Derue¹³⁶, P. Dervan⁹⁰, K. Desch²⁴, C. Deterre⁴⁶,
 K. Dette¹⁶⁷, C. Deutsch²⁴, M.R. Devesa³⁰, P.O. Deviveiros³⁶, A. Dewhurst¹⁴⁴, S. Dhaliwal²⁶,
 F.A. Di Bello⁵⁴, A. Di Ciaccio^{73a,73b}, L. Di Ciaccio⁵, W.K. Di Clemente¹³⁷, C. Di Donato^{69a,69b},
 A. Di Girolamo³⁶, G. Di Gregorio^{71a,71b}, B. Di Micco^{74a,74b}, R. Di Nardo¹⁰², K.F. Di Petrillo⁵⁹,
 R. Di Sipio¹⁶⁷, D. Di Valentino³⁴, C. Diaconu¹⁰¹, F.A. Dias⁴⁰, T. Dias Do Vale^{140a}, M.A. Diaz^{147a},
 J. Dickinson¹⁸, E.B. Diehl¹⁰⁵, J. Dietrich¹⁹, S. Díez Cornell⁴⁶, A. Dimitrievska¹⁸, W. Ding^{15b},
 J. Dingfelder²⁴, F. Dittus³⁶, F. Djama¹⁰¹, T. Djobava^{159b}, J.I. Djuvsland¹⁷, M.A.B. Do Vale^{80c},
 M. Dobre^{27b}, D. Dodsworth²⁶, C. Doglioni⁹⁶, J. Dolejsi¹⁴³, Z. Dolezal¹⁴³, M. Donadelli^{80d}, B. Dong^{60c},
 J. Donini³⁸, A. D'onofrio⁹², M. D'Onofrio⁹⁰, J. Dopke¹⁴⁴, A. Doria^{69a}, M.T. Dova⁸⁸, A.T. Doyle⁵⁷,
 E. Drechsler¹⁵², E. Dreyer¹⁵², T. Dreyer⁵³, A.S. Drobac¹⁷⁰, Y. Duan^{60b}, F. Dubinin¹¹⁰, M. Dubovsky^{28a},
 A. Dubreuil⁵⁴, E. Duchovni¹⁸⁰, G. Duckeck¹¹⁴, A. Ducourthial¹³⁶, O.A. Ducu¹⁰⁹, D. Duda¹¹⁵,
 A. Dudarev³⁶, A.C. Dudder⁹⁹, E.M. Duffield¹⁸, L. Duflot¹³², M. Dührssen³⁶, C. Dülsen¹⁸²,
 M. Dumancic¹⁸⁰, A.E. Dumitriu^{27b}, A.K. Duncan⁵⁷, M. Dunford^{61a}, A. Duperrin¹⁰¹, H. Duran Yildiz^{4a},
 M. Düren⁵⁶, A. Durglishvili^{159b}, D. Duschinger⁴⁸, B. Dutta⁴⁶, D. Duvnjak¹, G.I. Dyckes¹³⁷, M. Dyndal³⁶,
 S. Dysch¹⁰⁰, B.S. Dziedzic⁸⁴, K.M. Ecker¹¹⁵, R.C. Edgar¹⁰⁵, M.G. Eggleston⁴⁹, T. Eifert³⁶, G. Eigen¹⁷,
 K. Einsweiler¹⁸, T. Ekelof¹⁷², H. El Jarrari^{35e}, M. El Kacimi^{35c}, R. El Kosseifi¹⁰¹, V. Ellajosyula¹⁷²,
 M. Ellert¹⁷², F. Ellinghaus¹⁸², A.A. Elliot⁹², N. Ellis³⁶, J. Elmsheuser²⁹, M. Elsing³⁶, D. Emelianov¹⁴⁴,
 A. Emerman³⁹, Y. Enari¹⁶³, M.B. Epland⁴⁹, J. Erdmann⁴⁷, A. Ereditato²⁰, M. Errenst³⁶, M. Escalier¹³²,
 C. Escobar¹⁷⁴, O. Estrada Pastor¹⁷⁴, E. Etzion¹⁶¹, H. Evans⁶⁵, A. Ezhilov¹³⁸, F. Fabbri⁵⁷, L. Fabbri^{23b,23a},
 V. Fabiani¹¹⁹, G. Facini⁹⁴, R.M. Faisca Rodrigues Pereira^{140a}, R.M. Fakhruddinov¹²³, S. Falciano^{72a},
 P.J. Falke⁵, S. Falke⁵, J. Faltova¹⁴³, Y. Fang^{15a}, Y. Fang^{15a}, G. Fanourakis⁴⁴, M. Fanti^{68a,68b}, M. Faraj^{66a,66c},
 A. Farbin⁸, A. Farilla^{74a}, E.M. Farina^{70a,70b}, T. Farooque¹⁰⁶, S. Farrell¹⁸, S.M. Farrington⁵⁰, P. Farthouat³⁶,
 F. Fassi^{35e}, P. Fassnacht³⁶, D. Fassouliotis⁹, M. Fauci Giannelli⁵⁰, W.J. Fawcett³², L. Fayard¹³²,
 O.L. Fedin^{138,o}, W. Fedorko¹⁷⁵, M. Feickert⁴², S. Feigl¹³⁴, L. Feligioni¹⁰¹, A. Fell¹⁴⁹, C. Feng^{60b},
 E.J. Feng³⁶, M. Feng⁴⁹, M.J. Fenton⁵⁷, A.B. Fenyuk¹²³, J. Ferrando⁴⁶, A. Ferrante¹⁷³, A. Ferrari¹⁷²,
 P. Ferrari¹²⁰, R. Ferrari^{70a}, D.E. Ferreira de Lima^{61b}, A. Ferrer¹⁷⁴, D. Ferrere⁵⁴, C. Ferretti¹⁰⁵, F. Fiedler⁹⁹,
 A. Filipčić⁹¹, F. Filthaut¹¹⁹, K.D. Finelli²⁵, M.C.N. Fiolhais^{140a}, L. Fiorini¹⁷⁴, F. Fischer¹¹⁴, W.C. Fisher¹⁰⁶,
 I. Fleck¹⁵¹, P. Fleischmann¹⁰⁵, R.R.M. Fletcher¹³⁷, T. Flick¹⁸², B.M. Flierl¹¹⁴, L.F. Flores¹³⁷,
 L.R. Flores Castillo^{63a}, F.M. Follega^{75a,75b}, N. Fomin¹⁷, J.H. Foo¹⁶⁷, G.T. Forcolin^{75a,75b}, A. Formica¹⁴⁵,
 F.A. Förster¹⁴, A.C. Forti¹⁰⁰, A.G. Foster²¹, M.G. Foti¹³⁵, D. Fournier¹³², H. Fox⁸⁹, P. Francavilla^{71a,71b},
 S. Francescato^{72a,72b}, M. Franchini^{23b,23a}, S. Franchino^{61a}, D. Francis³⁶, L. Franconi²⁰, M. Franklin⁵⁹,
 A.N. Fray⁹², B. Freund¹⁰⁹, W.S. Freund^{80b}, E.M. Freundlich⁴⁷, D.C. Frizzell¹²⁸, D. Froidevaux³⁶,
 J.A. Frost¹³⁵, C. Fukunaga¹⁶⁴, E. Fullana Torregrosa¹⁷⁴, E. Fumagalli^{55b,55a}, T. Fusayasu¹¹⁶, J. Fuster¹⁷⁴,
 A. Gabrielli^{23b,23a}, A. Gabrielli¹⁸, G.P. Gach^{83a}, S. Gadatsch⁵⁴, P. Gadow¹¹⁵, G. Gagliardi^{55b,55a},
 L.G. Gagnon¹⁰⁹, C. Galea^{27b}, B. Galhardo^{140a}, G.E. Gallardo¹³⁵, E.J. Gallas¹³⁵, B.J. Gallop¹⁴⁴,

G. Galster⁴⁰, R. Gamboa Goni⁹², K.K. Gan¹²⁶, S. Ganguly¹⁸⁰, J. Gao^{60a}, Y. Gao⁵⁰, Y.S. Gao^{31,1}, C. García¹⁷⁴, J.E. García Navarro¹⁷⁴, J.A. García Pascual^{15a}, C. Garcia-Argos⁵², M. Garcia-Sciveres¹⁸, R.W. Gardner³⁷, N. Garelli¹⁵³, S. Gargiulo⁵², V. Garonne¹³⁴, A. Gaudiello^{55b,55a}, G. Gaudio^{70a}, I.L. Gavrilenko¹¹⁰, A. Gavriilyuk¹¹¹, C. Gay¹⁷⁵, G. Gaycken⁴⁶, E.N. Gazis¹⁰, A.A. Geanta^{27b}, C.N.P. Gee¹⁴⁴, J. Geisen⁵³, M. Geisen⁹⁹, M.P. Geisler^{61a}, C. Gemme^{55b}, M.H. Genest⁵⁸, C. Geng¹⁰⁵, S. Gentile^{72a,72b}, S. George⁹³, T. Geralis⁴⁴, L.O. Gerlach⁵³, P. Gessinger-Befurt⁹⁹, G. Gessner⁴⁷, S. Ghasemi¹⁵¹, M. Ghasemi Bostanabad¹⁷⁶, M. Ghneimat²⁴, A. Ghosh¹³², A. Ghosh⁷⁷, B. Giacobbe^{23b}, S. Giagu^{72a,72b}, N. Giangiacomi^{23b,23a}, P. Giannetti^{71a}, A. Giannini^{69a,69b}, S.M. Gibson⁹³, M. Gignac¹⁴⁶, D. Gillberg³⁴, G. Gilles¹⁸², D.M. Gingrich^{3,ax}, M.P. Giordani^{66a,66c}, F.M. Giorgi^{23b}, P.F. Giraud¹⁴⁵, G. Giugliarelli^{66a,66c}, D. Giugni^{68a}, F. Giuli^{73a,73b}, S. Gkaitatzis¹⁶², I. Gkialas^{9,g}, E.L. Gkoukousis¹⁴, P. Gkoutoumis¹⁰, L.K. Gladilin¹¹³, C. Glasman⁹⁸, J. Glatzer¹⁴, P.C.F. Glaysher⁴⁶, A. Glazov⁴⁶, M. Goblirsch-Kolb²⁶, S. Goldfarb¹⁰⁴, T. Golling⁵⁴, D. Golubkov¹²³, A. Gomes^{140a,140b}, R. Goncalves Gama⁵³, R. Gonçalo^{140a,140b}, G. Gonella⁵², L. Gonella²¹, A. Gongadze⁷⁹, F. Gonnella²¹, J.L. Gonski⁵⁹, S. González de la Hoz¹⁷⁴, S. Gonzalez-Sevilla⁵⁴, G.R. Gonzalvo Rodriguez¹⁷⁴, L. Goossens³⁶, P.A. Gorbounov¹¹¹, H.A. Gordon²⁹, B. Gorini³⁶, E. Gorini^{67a,67b}, A. Gorišek⁹¹, A.T. Goshaw⁴⁹, M.I. Gostkin⁷⁹, C.A. Gottardo¹¹⁹, M. Goughri^{35b}, D. Goujdami^{35c}, A.G. Goussiou¹⁴⁸, N. Govender^{33b}, C. Goy⁵, E. Gozani¹⁶⁰, I. Grabowska-Bold^{83a}, E.C. Graham⁹⁰, J. Gramling¹⁷¹, E. Gramstad¹³⁴, S. Grancagnolo¹⁹, M. Grandi¹⁵⁶, V. Gratchev¹³⁸, P.M. Gravila^{27f}, F.G. Gravili^{67a,67b}, C. Gray⁵⁷, H.M. Gray¹⁸, C. Grefe²⁴, K. Gregersen⁹⁶, I.M. Gregor⁴⁶, P. Grenier¹⁵³, K. Grevtsov⁴⁶, C. Grieco¹⁴, N.A. Grieser¹²⁸, J. Griffiths⁸, A.A. Grillo¹⁴⁶, K. Grimm^{31,k}, S. Grinstein^{14,x}, J.-F. Grivaz¹³², S. Groh⁹⁹, E. Gross¹⁸⁰, J. Grosse-Knetter⁵³, Z.J. Grout⁹⁴, C. Grud¹⁰⁵, A. Grummer¹¹⁸, L. Guan¹⁰⁵, W. Guan¹⁸¹, J. Guenther³⁶, A. Guerguichon¹³², J.G.R. Guerrero Rojas¹⁷⁴, F. Guescini¹¹⁵, D. Guest¹⁷¹, R. Gugel⁵², T. Guillemin⁵, S. Guindon³⁶, U. Gul⁵⁷, J. Guo^{60c}, W. Guo¹⁰⁵, Y. Guo^{60a,s}, Z. Guo¹⁰¹, R. Gupta⁴⁶, S. Gurbuz^{12c}, G. Gustavino¹²⁸, P. Gutierrez¹²⁸, C. Gutsche⁹⁴, C. Guyot¹⁴⁵, C. Gwenlan¹³⁵, C.B. Gwilliam⁹⁰, A. Haas¹²⁴, C. Haber¹⁸, H.K. Hadavand⁸, N. Haddad^{35e}, A. Hadei^{60a}, S. Hageböck³⁶, M. Hagihara¹⁶⁹, M. Haleem¹⁷⁷, J. Haley¹²⁹, G. Halladjian¹⁰⁶, G.D. Hallewell¹⁰¹, K. Hamacher¹⁸², P. Hamal¹³⁰, K. Hamano¹⁷⁶, H. Hamdaoui^{35e}, G.N. Hamity¹⁴⁹, K. Han^{60a,ak}, L. Han^{60a}, S. Han^{15a,15d}, K. Hanagaki^{81,v}, M. Hance¹⁴⁶, D.M. Handl¹¹⁴, B. Haney¹³⁷, R. Hankache¹³⁶, E. Hansen⁹⁶, J.B. Hansen⁴⁰, J.D. Hansen⁴⁰, M.C. Hansen²⁴, P.H. Hansen⁴⁰, E.C. Hanson¹⁰⁰, K. Hara¹⁶⁹, A.S. Hard¹⁸¹, T. Harenberg¹⁸², S. Harkusha¹⁰⁷, P.F. Harrison¹⁷⁸, N.M. Hartmann¹¹⁴, Y. Hasegawa¹⁵⁰, A. Hasib⁵⁰, S. Hassani¹⁴⁵, S. Haug²⁰, R. Hauser¹⁰⁶, L.B. Havener³⁹, M. Havranek¹⁴², C.M. Hawkes²¹, R.J. Hawkings³⁶, D. Hayden¹⁰⁶, C. Hayes¹⁵⁵, R.L. Hayes¹⁷⁵, C.P. Hays¹³⁵, J.M. Hays⁹², H.S. Hayward⁹⁰, S.J. Haywood¹⁴⁴, F. He^{60a}, M.P. Heath⁵⁰, V. Hedberg⁹⁶, L. Heelan⁸, S. Heer²⁴, K.K. Heidegger⁵², W.D. Heidorn⁷⁸, J. Heilman³⁴, S. Heim⁴⁶, T. Heim¹⁸, B. Heinemann^{46,as}, J.J. Heinrich¹³¹, L. Heinrich³⁶, C. Heinz⁵⁶, J. Hejbal¹⁴¹, L. Helary^{61b}, A. Held¹⁷⁵, S. Hellesund¹³⁴, C.M. Helling¹⁴⁶, S. Hellman^{45a,45b}, C. Helsen³⁶, R.C.W. Henderson⁸⁹, Y. Heng¹⁸¹, S. Henkelmann¹⁷⁵, A.M. Henriques Correia³⁶, G.H. Herbert¹⁹, H. Herde²⁶, V. Herget¹⁷⁷, Y. Hernández Jiménez^{33c}, H. Herr⁹⁹, M.G. Herrmann¹¹⁴, T. Herrmann⁴⁸, G. Herten⁵², R. Hertenberger¹¹⁴, L. Hervas³⁶, T.C. Herwig¹³⁷, G.G. Hesketh⁹⁴, N.P. Hessey^{168a}, A. Higashida¹⁶³, S. Higashino⁸¹, E. Higón-Rodríguez¹⁷⁴, K. Hildebrand³⁷, E. Hill¹⁷⁶, J.C. Hill³², K.K. Hill²⁹, K.H. Hiller⁴⁶, S.J. Hillier²¹, M. Hils⁴⁸, I. Hinchliffe¹⁸, F. Hinterkeuser²⁴, M. Hirose¹³³, S. Hirose⁵², D. Hirschbuehl¹⁸², B. Hiti⁹¹, O. Hladik¹⁴¹, D.R. Hlaluku^{33c}, X. Hoad⁵⁰, J. Hobbs¹⁵⁵, N. Hod¹⁸⁰, M.C. Hodgkinson¹⁴⁹, A. Hoecker³⁶, F. Hoenig¹¹⁴, D. Hohn⁵², D. Hohov¹³², T.R. Holmes³⁷, M. Holzbock¹¹⁴, L.B.A.H. Hommels³², S. Honda¹⁶⁹, T. Honda⁸¹, T.M. Hong¹³⁹, A. Hönle¹¹⁵, B.H. Hooberman¹⁷³, W.H. Hopkins⁶, Y. Horii¹¹⁷, P. Horn⁴⁸, L.A. Horyn³⁷, A. Hostiuc¹⁴⁸, S. Hou¹⁵⁸, A. Hoummada^{35a}, J. Howarth¹⁰⁰, J. Hoya⁸⁸, M. Hrabovsky¹³⁰, J. Hrdinka⁷⁶, I. Hristova¹⁹, J. Hrivnac¹³², A. Hrynevich¹⁰⁸, T. Hryn'ova⁵, P.J. Hsu⁶⁴, S.-C. Hsu¹⁴⁸, Q. Hu²⁹, S. Hu^{60c}, Y. Huang^{15a}, Z. Hubacek¹⁴², F. Hubaut¹⁰¹, M. Huebner²⁴, F. Huegging²⁴, T.B. Huffman¹³⁵, M. Huhtinen³⁶, R.F.H. Hunter³⁴, P. Huo¹⁵⁵,

A.M. Hupe³⁴, N. Huseynov^{79,af}, J. Huston¹⁰⁶, J. Huth⁵⁹, R. Hyneman¹⁰⁵, S. Hyrych^{28a}, G. Iacobucci⁵⁴,
 G. Iakovidis²⁹, I. Ibragimov¹⁵¹, L. Iconomidou-Fayard¹³², Z. Idrissi^{35e}, P.I. Iengo³⁶, R. Ignazzi⁴⁰,
 O. Igonkina^{120,z,*}, R. Iguchi¹⁶³, T. Iizawa⁵⁴, Y. Ikegami⁸¹, M. Ikeno⁸¹, D. Iliadis¹⁶², N. Ilic¹¹⁹,
 F. Iltzsche⁴⁸, G. Introzzi^{70a,70b}, M. Iodice^{74a}, K. Iordanidou^{168a}, V. Ippolito^{72a,72b}, M.F. Isacson¹⁷²,
 M. Ishino¹⁶³, M. Ishitsuka¹⁶⁵, W. Islam¹²⁹, C. Issever¹³⁵, S. Istin¹⁶⁰, F. Ito¹⁶⁹, J.M. Iturbe Ponce^{63a},
 R. Iuppa^{75a,75b}, A. Ivina¹⁸⁰, H. Iwasaki⁸¹, J.M. Izen⁴³, V. Izzo^{69a}, P. Jacka¹⁴¹, P. Jackson¹, R.M. Jacobs²⁴,
 B.P. Jaeger¹⁵², V. Jain², G. Jäkel¹⁸², K.B. Jakobi⁹⁹, K. Jakobs⁵², S. Jakobsen⁷⁶, T. Jakoubek¹⁴¹,
 J. Jamieson⁵⁷, K.W. Janas^{83a}, R. Jansky⁵⁴, J. Janssen²⁴, M. Janus⁵³, P.A. Janus^{83a}, G. Jarlskog⁹⁶,
 N. Javadov^{79,af}, T. Javůrek³⁶, M. Javurkova⁵², F. Jeanneau¹⁴⁵, L. Jeanty¹³¹, J. Jejelava^{159a,ag},
 A. Jelinskas¹⁷⁸, P. Jenni^{52,a}, J. Jeong⁴⁶, N. Jeong⁴⁶, S. Jézéquel⁵, H. Ji¹⁸¹, J. Jia¹⁵⁵, H. Jiang⁷⁸, Y. Jiang^{60a},
 Z. Jiang^{153,p}, S. Jiggins⁵², F.A. Jimenez Morales³⁸, J. Jimenez Pena¹¹⁵, S. Jin^{15c}, A. Jinaru^{27b},
 O. Jinnouchi¹⁶⁵, H. Jivan^{33c}, P. Johansson¹⁴⁹, K.A. Johns⁷, C.A. Johnson⁶⁵, K. Jon-And^{45a,45b},
 R.W.L. Jones⁸⁹, S.D. Jones¹⁵⁶, S. Jones⁷, T.J. Jones⁹⁰, J. Jongmanns^{61a}, P.M. Jorge^{140a}, J. Jovicevic³⁶,
 X. Ju¹⁸, J.J. Junggeburth¹¹⁵, A. Juste Rozas^{14,x}, A. Kaczmarzka⁸⁴, M. Kado^{72a,72b}, H. Kagan¹²⁶,
 M. Kagan¹⁵³, C. Kahra⁹⁹, T. Kaji¹⁷⁹, E. Kajomovitz¹⁶⁰, C.W. Kalderon⁹⁶, A. Kaluza⁹⁹,
 A. Kamenshchikov¹²³, L. Kanjir⁹¹, Y. Kano¹⁶³, V.A. Kantserov¹¹², J. Kanzaki⁸¹, L.S. Kaplan¹⁸¹,
 D. Kar^{33c}, M.J. Kareem^{168b}, S.N. Karpov⁷⁹, Z.M. Karpova⁷⁹, V. Kartvelishvili⁸⁹, A.N. Karyukhin¹²³,
 L. Kashif¹⁸¹, R.D. Kass¹²⁶, A. Kastanas^{45a,45b}, Y. Kataoka¹⁶³, C. Kato^{60d,60c}, J. Katzy⁴⁶, K. Kawade⁸²,
 K. Kawagoe⁸⁷, T. Kawaguchi¹¹⁷, T. Kawamoto¹⁶³, G. Kawamura⁵³, E.F. Kay¹⁷⁶, V.F. Kazanin^{122b,122a},
 R. Keeler¹⁷⁶, R. Kehoe⁴², J.S. Keller³⁴, E. Kellermann⁹⁶, D. Kelsey¹⁵⁶, J.J. Kempster²¹, J. Kendrick²¹,
 O. Kepka¹⁴¹, S. Kersten¹⁸², B.P. Kerševan⁹¹, S. Ketabchi Haghighat¹⁶⁷, M. Khader¹⁷³, F. Khalil-Zada¹³,
 M. Khandoga¹⁴⁵, A. Khanov¹²⁹, A.G. Kharlamov^{122b,122a}, T. Kharlamova^{122b,122a}, E.E. Khoda¹⁷⁵,
 A. Khodinov¹⁶⁶, T.J. Khoo⁵⁴, E. Khramov⁷⁹, J. Khubua^{159b}, S. Kido⁸², M. Kiehn⁵⁴, C.R. Kilby⁹³,
 Y.K. Kim³⁷, N. Kimura^{66a,66c}, O.M. Kind¹⁹, B.T. King^{90,*}, D. Kirchmeier⁴⁸, J. Kirk¹⁴⁴, A.E. Kiryunin¹¹⁵,
 T. Kishimoto¹⁶³, D.P. Kisliuk¹⁶⁷, V. Kitali⁴⁶, O. Kivernyk⁵, E. Kladiva^{28b,*}, T. Klapdor-Kleingrothaus⁵²,
 M. Klassen^{61a}, M.H. Klein¹⁰⁵, M. Klein⁹⁰, U. Klein⁹⁰, K. Kleinknecht⁹⁹, P. Klimek¹²¹, A. Klimentov²⁹,
 T. Klingl²⁴, T. Klioutchnikova³⁶, F.F. Klitzner¹¹⁴, P. Kluit¹²⁰, S. Kluth¹¹⁵, E. Kneringer⁷⁶,
 E.B.F.G. Knoop¹⁰¹, A. Knue⁵², D. Kobayashi⁸⁷, T. Kobayashi¹⁶³, M. Kobel⁴⁸, M. Kocian¹⁵³, P. Kodys¹⁴³,
 P.T. Koenig²⁴, T. Koffas³⁴, N.M. Köhler³⁶, T. Koi¹⁵³, M. Kolb^{61b}, I. Koletsou⁵, T. Komarek¹³⁰, T. Kondo⁸¹,
 N. Kondrashova^{60c}, K. Köneke⁵², A.C. König¹¹⁹, T. Kono¹²⁵, R. Konoplich^{124,an}, V. Konstantinides⁹⁴,
 N. Konstantinidis⁹⁴, B. Konya⁹⁶, R. Kopeliansky⁶⁵, S. Koperny^{83a}, K. Korcyl⁸⁴, K. Kordas¹⁶²,
 G. Koren¹⁶¹, A. Korn⁹⁴, I. Korolkov¹⁴, E.V. Korolkova¹⁴⁹, N. Korotkova¹¹³, O. Kortner¹¹⁵, S. Kortner¹¹⁵,
 T. Kosek¹⁴³, V.V. Kostyukhin²⁴, A. Kotwal⁴⁹, A. Koulouris¹⁰, A. Kourkoumeli-Charalampidi^{70a,70b},
 C. Kourkoumelis⁹, E. Kourlitis¹⁴⁹, V. Kouskoura²⁹, A.B. Kowalewska⁸⁴, R. Kowalewski¹⁷⁶, C. Kozakai¹⁶³,
 W. Kozanecki¹⁴⁵, A.S. Kozhin¹²³, V.A. Kramarenko¹¹³, G. Kramberger⁹¹, D. Krasnopevtsev^{60a},
 M.W. Krasny¹³⁶, A. Krasznahorkay³⁶, D. Krauss¹¹⁵, J.A. Kremer^{83a}, J. Kretzschmar⁹⁰, P. Krieger¹⁶⁷,
 F. Krieter¹¹⁴, A. Krishnan^{61b}, K. Krizka¹⁸, K. Kroeninger⁴⁷, H. Kroha¹¹⁵, J. Kroll¹⁴¹, J. Kroll¹³⁷,
 J. Krstic¹⁶, U. Kruchonak⁷⁹, H. Krüger²⁴, N. Krumnack⁷⁸, M.C. Kruse⁴⁹, J.A. Krzysiak⁸⁴, T. Kubota¹⁰⁴,
 O. Kuchinskaia¹⁶⁶, S. Kудay^{4b}, J.T. Kuechler⁴⁶, S. Kuehn³⁶, A. Kugel^{61a}, T. Kuhl⁴⁶, V. Kukhtin⁷⁹,
 R. Kukla¹⁰¹, Y. Kulchitsky^{107,aj}, S. Kuleshov^{147b}, Y.P. Kulinich¹⁷³, M. Kuna⁵⁸, T. Kunigo⁸⁵, A. Kupco¹⁴¹,
 T. Kupfer⁴⁷, O. Kuprash⁵², H. Kurashige⁸², L.L. Kurchaninov^{168a}, Y.A. Kurochkin¹⁰⁷, A. Kurova¹¹²,
 M.G. Kurth^{15a,15d}, E.S. Kuwertz³⁶, M. Kuze¹⁶⁵, A.K. Kvam¹⁴⁸, J. Kvita¹³⁰, T. Kwan¹⁰³, A. La Rosa¹¹⁵,
 L. La Rotonda^{41b,41a}, F. La Ruffa^{41b,41a}, C. Lacasta¹⁷⁴, F. Lacava^{72a,72b}, D.P.J. Lack¹⁰⁰, H. Lacker¹⁹,
 D. Lacour¹³⁶, E. Ladygin⁷⁹, R. Lafaye⁵, B. Laforge¹³⁶, T. Lagouri^{33c}, S. Lai⁵³, S. Lammers⁶⁵, W. Lampl⁷,
 C. Lampoudis¹⁶², E. Lançon²⁹, U. Landgraf⁵², M.P.J. Landon⁹², M.C. Lanfermann⁵⁴, V.S. Lang⁴⁶,
 J.C. Lange⁵³, R.J. Langenberg³⁶, A.J. Lankford¹⁷¹, F. Lanni²⁹, K. Lantzsche²⁴, A. Lanza^{70a},
 A. Lapertosa^{55b,55a}, S. Laplace¹³⁶, J.F. Laporte¹⁴⁵, T. Lari^{68a}, F. Lasagni Manghi^{23b,23a}, M. Lassnig³⁶,

T.S. Lau^{63a}, A. Laudrain¹³², A. Laurier³⁴, M. Lavorgna^{69a,69b}, M. Lazzaroni^{68a,68b}, B. Le¹⁰⁴, E. Le Guirriec¹⁰¹, M. LeBlanc⁷, T. LeCompte⁶, F. Ledroit-Guillon⁵⁸, C.A. Lee²⁹, G.R. Lee¹⁷, L. Lee⁵⁹, S.C. Lee¹⁵⁸, S.J. Lee³⁴, B. Lefebvre^{168a}, M. Lefebvre¹⁷⁶, F. Legger¹¹⁴, C. Leggett¹⁸, K. Lehmann¹⁵², N. Lehmann¹⁸², G. Lehmann Miotto³⁶, W.A. Leight⁴⁶, A. Leisos^{162,w}, M.A.L. Leite^{80d}, C.E. Leitgeb¹¹⁴, R. Leitner¹⁴³, D. Lellouch^{180,*}, K.J.C. Leney⁴², T. Lenz²⁴, B. Lenzi³⁶, R. Leone⁷, S. Leone^{71a}, C. Leonidopoulos⁵⁰, A. Leopold¹³⁶, G. Lerner¹⁵⁶, C. Leroy¹⁰⁹, R. Les¹⁶⁷, C.G. Lester³², M. Levchenko¹³⁸, J. Levêque⁵, D. Levin¹⁰⁵, L.J. Levinson¹⁸⁰, D.J. Lewis²¹, B. Li^{15b}, B. Li¹⁰⁵, C-Q. Li^{60a}, F. Li^{60c}, H. Li^{60a}, H. Li^{60b}, J. Li^{60c}, K. Li¹⁵³, L. Li^{60c}, M. Li^{15a}, Q. Li^{15a,15d}, Q.Y. Li^{60a}, S. Li^{60d,60c}, X. Li⁴⁶, Y. Li⁴⁶, Z. Li^{60b}, Z. Liang^{15a}, B. Liberti^{73a}, A. Liblong¹⁶⁷, K. Lie^{63c}, S. Liem¹²⁰, C.Y. Lin³², K. Lin¹⁰⁶, T.H. Lin⁹⁹, R.A. Linck⁶⁵, J.H. Lindon²¹, A.L. Lioni⁵⁴, E. Lipeles¹³⁷, A. Lipniacka¹⁷, M. Lisovyi^{61b}, T.M. Liss^{173,au}, A. Lister¹⁷⁵, A.M. Litke¹⁴⁶, J.D. Little⁸, B. Liu^{78,ac}, B.L. Liu⁶, H.B. Liu²⁹, H. Liu¹⁰⁵, J.B. Liu^{60a}, J.K.K. Liu¹³⁵, K. Liu¹³⁶, M. Liu^{60a}, P. Liu¹⁸, Y. Liu^{15a,15d}, Y.L. Liu¹⁰⁵, Y.W. Liu^{60a}, M. Livan^{70a,70b}, A. Lleres⁵⁸, J. Llorente Merino^{15a}, S.L. Lloyd⁹², C.Y. Lo^{63b}, F. Lo Sterzo⁴², E.M. Lobodzinska⁴⁶, P. Loch⁷, S. Loffredo^{73a,73b}, T. Lohse¹⁹, K. Lohwasser¹⁴⁹, M. Lokajicek¹⁴¹, J.D. Long¹⁷³, R.E. Long⁸⁹, L. Longo³⁶, K.A. Looper¹²⁶, J.A. Lopez^{147b}, I. Lopez Paz¹⁰⁰, A. Lopez Solis¹⁴⁹, J. Lorenz¹¹⁴, N. Lorenzo Martinez⁵, M. Losada²², P.J. Lösel¹¹⁴, A. Lösle⁵², X. Lou⁴⁶, X. Lou^{15a}, A. Lounis¹³², J. Love⁶, P.A. Love⁸⁹, J.J. Lozano Bahilo¹⁷⁴, M. Lu^{60a}, Y.J. Lu⁶⁴, H.J. Lubatti¹⁴⁸, C. Luci^{72a,72b}, A. Lucotte⁵⁸, C. Luedtke⁵², F. Luehring⁶⁵, I. Luise¹³⁶, L. Luminari^{72a}, B. Lund-Jensen¹⁵⁴, M.S. Lutz¹⁰², D. Lynn²⁹, R. Lysak¹⁴¹, E. Lytken⁹⁶, F. Lyu^{15a}, V. Lyubushkin⁷⁹, T. Lyubushkina⁷⁹, H. Ma²⁹, L.L. Ma^{60b}, Y. Ma^{60b}, G. Maccarrone⁵¹, A. Macchiolo¹¹⁵, C.M. Macdonald¹⁴⁹, J. Machado Miguens¹³⁷, D. Madaffari¹⁷⁴, R. Madar³⁸, W.F. Mader⁴⁸, N. Madysa⁴⁸, J. Maeda⁸², K. Maekawa¹⁶³, S. Maeland¹⁷, T. Maeno²⁹, M. Maerker⁴⁸, A.S. Maevskiy¹¹³, V. Mageri⁵², N. Magini⁷⁸, D.J. Mahon³⁹, C. Maidantchik^{80b}, T. Maier¹¹⁴, A. Maio^{140a,140b,140d}, O. Majersky^{28a}, S. Majewski¹³¹, Y. Makida⁸¹, N. Makovec¹³², B. Malaescu¹³⁶, Pa. Malecki⁸⁴, V.P. Maleev¹³⁸, F. Malek⁵⁸, U. Mallik⁷⁷, D. Malon⁶, C. Malone³², S. Maltezos¹⁰, S. Malyukov³⁶, J. Mamuzic¹⁷⁴, G. Mancini⁵¹, I. Mandić⁹¹, L. Manhaes de Andrade Filho^{80a}, I.M. Maniatis¹⁶², J. Manjarres Ramos⁴⁸, K.H. Mankinen⁹⁶, A. Mann¹¹⁴, A. Manousos⁷⁶, B. Mansoulie¹⁴⁵, I. Manthos¹⁶², S. Manzoni¹²⁰, A. Marantis¹⁶², G. Marceca³⁰, L. Marchese¹³⁵, G. Marchiori¹³⁶, M. Marcisovsky¹⁴¹, C. Marcon⁹⁶, C.A. Marin Tobon³⁶, M. Marjanovic³⁸, Z. Marshall¹⁸, M.U.F. Martensson¹⁷², S. Marti-Garcia¹⁷⁴, C.B. Martin¹²⁶, T.A. Martin¹⁷⁸, V.J. Martin⁵⁰, B. Martin dit Latour¹⁷, L. Martinelli^{74a,74b}, M. Martinez^{14,x}, V.I. Martinez Outschoorn¹⁰², S. Martin-Haugh¹⁴⁴, V.S. Martoiu^{27b}, A.C. Martyniuk⁹⁴, A. Marzin³⁶, S.R. Maschek¹¹⁵, L. Masetti⁹⁹, T. Mashimo¹⁶³, R. Mashinistov¹¹⁰, J. Masik¹⁰⁰, A.L. Maslennikov^{122b,122a}, L.H. Mason¹⁰⁴, L. Massa^{73a,73b}, P. Massarotti^{69a,69b}, P. Mastrandrea^{71a,71b}, A. Mastroberardino^{41b,41a}, T. Masubuchi¹⁶³, D. Matakias¹⁰, A. Matic¹¹⁴, P. Mättig²⁴, J. Maurer^{27b}, B. Maček⁹¹, D.A. Maximov^{122b,122a}, R. Mazini¹⁵⁸, I. Maznas¹⁶², S.M. Mazza¹⁴⁶, S.P. Mc Kee¹⁰⁵, T.G. McCarthy¹¹⁵, L.I. McClymont⁹⁴, W.P. McCormack¹⁸, E.F. McDonald¹⁰⁴, J.A. Mcfayden³⁶, M.A. McKay⁴², K.D. McLean¹⁷⁶, S.J. McMahan¹⁴⁴, P.C. McNamara¹⁰⁴, C.J. McNicol¹⁷⁸, R.A. McPherson^{176,ad}, J.E. Mdhluli^{33c}, Z.A. Meadows¹⁰², S. Meehan¹⁴⁸, T. Megy⁵², S. Mehlhase¹¹⁴, A. Mehta⁹⁰, T. Meideck⁵⁸, B. Meirose⁴³, D. Melini¹⁷⁴, B.R. Mellado Garcia^{33c}, J.D. Mellenthin⁵³, M. Melo^{28a}, F. Meloni⁴⁶, A. Melzer²⁴, S.B. Menary¹⁰⁰, E.D. Mendes Gouveia^{140a,140e}, L. Meng³⁶, X.T. Meng¹⁰⁵, S. Menke¹¹⁵, E. Meoni^{41b,41a}, S. Mergelmeyer¹⁹, S.A.M. Merkt¹³⁹, C. Merlassino²⁰, P. Mermod⁵⁴, L. Merola^{69a,69b}, C. Meroni^{68a}, O. Meshkov^{113,110}, J.K.R. Meshreki¹⁵¹, A. Messina^{72a,72b}, J. Metcalfe⁶, A.S. Mete¹⁷¹, C. Meyer⁶⁵, J. Meyer¹⁶⁰, J-P. Meyer¹⁴⁵, H. Meyer Zu Theenhausen^{61a}, F. Miano¹⁵⁶, M. Michetti¹⁹, R.P. Middleton¹⁴⁴, L. Mijović⁵⁰, G. Mikenberg¹⁸⁰, M. Mikesstikova¹⁴¹, M. Mikuž⁹¹, H. Mildner¹⁴⁹, M. Milesi¹⁰⁴, A. Milic¹⁶⁷, D.A. Millar⁹², D.W. Miller³⁷, A. Milov¹⁸⁰, D.A. Milstead^{45a,45b}, R.A. Mina^{153,p}, A.A. Minaenko¹²³, M. Miñano Moya¹⁷⁴, I.A. Minashvili^{159b}, A.I. Mincer¹²⁴, B. Mindur^{83a}, M. Mineev⁷⁹, Y. Minegishi¹⁶³, Y. Ming¹⁸¹, L.M. Mir¹⁴, A. Mirto^{67a,67b}, K.P. Mistry¹³⁷, T. Mitani¹⁷⁹, J. Mitrevski¹¹⁴, V.A. Mitsou¹⁷⁴,

M. Mittal^{60c}, A. Miucci²⁰, P.S. Miyagawa¹⁴⁹, A. Mizukami⁸¹, J.U. Mjörnmark⁹⁶, T. Mkrtchyan¹⁸⁴,
M. Mlynarikova¹⁴³, T. Moa^{45a,45b}, K. Mochizuki¹⁰⁹, P. Mogg⁵², S. Mohapatra³⁹, R. Moles-Valls²⁴,
M.C. Mondragon¹⁰⁶, K. Mönig⁴⁶, J. Monk⁴⁰, E. Monnier¹⁰¹, A. Montalbano¹⁵², J. Montejo Berlingen³⁶,
M. Montella⁹⁴, F. Monticelli⁸⁸, S. Monzani^{68a}, N. Morange¹³², D. Moreno²², M. Moreno Llácer³⁶,
C. Moreno Martinez¹⁴, P. Morettini^{55b}, M. Morgenstern¹²⁰, S. Morgenstern⁴⁸, D. Mori¹⁵², M. Morii⁵⁹,
M. Morinaga¹⁷⁹, V. Morisbak¹³⁴, A.K. Morley³⁶, G. Mornacchi³⁶, A.P. Morris⁹⁴, L. Morvaj¹⁵⁵,
P. Moschovakos³⁶, B. Moser¹²⁰, M. Mosidze^{159b}, T. Moskalets¹⁴⁵, H.J. Moss¹⁴⁹, J. Moss^{31,m},
K. Motohashi¹⁶⁵, E. Mountricha³⁶, E.J.W. Moyse¹⁰², S. Muanza¹⁰¹, J. Mueller¹³⁹, R.S.P. Mueller¹¹⁴,
D. Muenstermann⁸⁹, G.A. Mullier⁹⁶, J.L. Munoz Martinez¹⁴, F.J. Munoz Sanchez¹⁰⁰, P. Murin^{28b},
W.J. Murray^{178,144}, A. Murrone^{68a,68b}, M. Muškinja¹⁸, C. Mwewa^{33a}, A.G. Myagkov^{123,ao}, J. Myers¹³¹,
M. Myska¹⁴², B.P. Nachman¹⁸, O. Nackenhorst⁴⁷, A.Nag Nag⁴⁸, K. Nagai¹³⁵, K. Nagano⁸¹, Y. Nagasaka⁶²,
M. Nagel⁵², E. Nagy¹⁰¹, A.M. Nairz³⁶, Y. Nakahama¹¹⁷, K. Nakamura⁸¹, T. Nakamura¹⁶³, I. Nakano¹²⁷,
H. Nanjo¹³³, F. Napolitano^{61a}, R.F. Naranjo Garcia⁴⁶, R. Narayan⁴², I. Naryshkin¹³⁸, T. Naumann⁴⁶,
G. Navarro²², H.A. Neal^{105,*}, P.Y. Nechaeva¹¹⁰, F. Nechansky⁴⁶, T.J. Neep²¹, A. Negri^{70a,70b},
M. Negrini^{23b}, C. Nellist⁵³, M.E. Nelson¹³⁵, S. Nemecek¹⁴¹, P. Nemethy¹²⁴, M. Nessi^{36,c},
M.S. Neubauer¹⁷³, M. Neumann¹⁸², P.R. Newman²¹, Y.S. Ng¹⁹, Y.W.Y. Ng¹⁷¹, H.D.N. Nguyen¹⁰¹,
T. Nguyen Manh¹⁰⁹, E. Nibigira³⁸, R.B. Nickerson¹³⁵, R. Nicolaidou¹⁴⁵, D.S. Nielsen⁴⁰, J. Nielsen¹⁴⁶,
N. Nikiforou¹¹, V. Nikolaenko^{123,ao}, I. Nikolic-Audit¹³⁶, K. Nikolopoulos²¹, P. Nilsson²⁹, H.R. Nindhito⁵⁴,
Y. Ninomiya⁸¹, A. Nisati^{72a}, N. Nishu^{60c}, R. Nisius¹¹⁵, I. Nitsche⁴⁷, T. Nitta¹⁷⁹, T. Nobe¹⁶³, Y. Noguchi⁸⁵,
I. Nomidis¹³⁶, M.A. Nomura²⁹, M. Nordberg³⁶, N. Norjoharuddeen¹³⁵, T. Novak⁹¹, O. Novgorodova⁴⁸,
R. Novotny¹⁴², L. Nozka¹³⁰, K. Ntekas¹⁷¹, E. Nurse⁹⁴, F.G. Oakham^{34,ax}, H. Oberlack¹¹⁵, J. Ocariz¹³⁶,
A. Ochi⁸², I. Ochoa³⁹, J.P. Ochoa-Ricoux^{147a}, K. O'Connor²⁶, S. Oda⁸⁷, S. Odaka⁸¹, S. Oerdek⁵³,
A. Ogrodnik^{83a}, A. Oh¹⁰⁰, S.H. Oh⁴⁹, C.C. Ohm¹⁵⁴, H. Oide^{55b,55a}, M.L. Ojeda¹⁶⁷, H. Okawa¹⁶⁹,
Y. Okazaki⁸⁵, Y. Okumura¹⁶³, T. Okuyama⁸¹, A. Olariu^{27b}, L.F. Oleiro Seabra^{140a}, S.A. Olivares Pino^{147a},
D. Oliveira Damazio²⁹, J.L. Oliver¹, M.J.R. Olsson¹⁷¹, A. Olszewski⁸⁴, J. Olszowska⁸⁴, D.C. O'Neil¹⁵²,
A. Onofre^{140a,140e}, K. Onogi¹¹⁷, P.U.E. Onyisi¹¹, H. Oppen¹³⁴, M.J. Oreglia³⁷, G.E. Orellana⁸⁸,
D. Orestano^{74a,74b}, N. Orlando¹⁴, R.S. Orr¹⁶⁷, V. O'Shea⁵⁷, R. Ospanov^{60a}, G. Otero y Garzon³⁰,
H. Otono⁸⁷, P.S. Ott^{61a}, M. Ouchrif^{35d}, J. Ouellette²⁹, F. Ould-Saada¹³⁴, A. Ouraou¹⁴⁵, Q. Ouyang^{15a},
M. Owen⁵⁷, R.E. Owen²¹, V.E. Ozcan^{12c}, N. Ozturk⁸, J. Pacalt¹³⁰, H.A. Pacey³², K. Pachal⁴⁹,
A. Pacheco Pages¹⁴, C. Padilla Aranda¹⁴, S. Pagan Griso¹⁸, M. Paganini¹⁸³, G. Palacino⁶⁵, S. Palazzo⁵⁰,
S. Palestini³⁶, M. Palka^{83b}, D. Pallin³⁸, I. Panagoulas¹⁰, C.E. Pandini³⁶, J.G. Panduro Vazquez⁹³,
P. Pani⁴⁶, G. Panizzo^{66a,66c}, L. Paolozzi⁵⁴, C. Papadatos¹⁰⁹, K. Papageorgiou^{9,g}, A. Paramonov⁶,
D. Paredes Hernandez^{63b}, S.R. Paredes Saenz¹³⁵, B. Parida¹⁶⁶, T.H. Park¹⁶⁷, A.J. Parker⁸⁹, M.A. Parker³²,
F. Parodi^{55b,55a}, E.W.P. Parrish¹²¹, J.A. Parsons³⁹, U. Parzefall⁵², L. Pascual Dominguez¹³⁶,
V.R. Pascuzzi¹⁶⁷, J.M.P. Pasner¹⁴⁶, E. Pasqualucci^{72a}, S. Passaggio^{55b}, F. Pastore⁹³, P. Pasuwan^{45a,45b},
S. Pataria⁹⁹, J.R. Pater¹⁰⁰, A. Pathak¹⁸¹, T. Pauly³⁶, B. Pearson¹¹⁵, M. Pedersen¹³⁴, L. Pedraza Diaz¹¹⁹,
R. Pedro^{140a}, T. Peiffer⁵³, S.V. Peleganchuk^{122b,122a}, O. Penc¹⁴¹, H. Peng^{60a}, B.S. Peralva^{80a},
M.M. Perego¹³², A.P. Pereira Peixoto^{140a}, D.V. Perepelitsa²⁹, F. Peri¹⁹, L. Perini^{68a,68b}, H. Pernegger³⁶,
S. Perrella^{69a,69b}, K. Peters⁴⁶, R.F.Y. Peters¹⁰⁰, B.A. Petersen³⁶, T.C. Petersen⁴⁰, E. Petit¹⁰¹, A. Petridis¹,
C. Petridou¹⁶², P. Petroff¹³², M. Petrov¹³⁵, F. Petrucci^{74a,74b}, M. Pettee¹⁸³, N.E. Pettersson¹⁰²,
K. Petukhova¹⁴³, A. Peyaud¹⁴⁵, R. Pezoa^{147b}, L. Pezzotti^{70a,70b}, T. Pham¹⁰⁴, F.H. Phillips¹⁰⁶,
P.W. Phillips¹⁴⁴, M.W. Phipps¹⁷³, G. Piacquadio¹⁵⁵, E. Pianori¹⁸, A. Picazio¹⁰², R.H. Pickles¹⁰⁰,
R. Piegaia³⁰, D. Pietreanu^{27b}, J.E. Pilcher³⁷, A.D. Pilkington¹⁰⁰, M. Pinamonti^{73a,73b}, J.L. Pinfold³,
M. Pitt¹⁸⁰, L. Pizzimento^{73a,73b}, M.-A. Pleier²⁹, V. Pleskot¹⁴³, E. Plotnikova⁷⁹, P. Podberczko^{122b,122a},
R. Poettgen⁹⁶, R. Poggi⁵⁴, L. Poggioli¹³², I. Pogrebnyak¹⁰⁶, D. Pohl²⁴, I. Pokharel⁵³, G. Polesello^{70a},
A. Poley¹⁸, A. Policicchio^{72a,72b}, R. Polifka¹⁴³, A. Polini^{23b}, C.S. Pollard⁴⁶, V. Polychronakos²⁹,
D. Ponomarenko¹¹², L. Pontecorvo³⁶, S. Popa^{27a}, G.A. Popeneciu^{27d}, D.M. Portillo Quintero⁵⁸,

S. Pospisil¹⁴², K. Potamianos⁴⁶, I.N. Potrap⁷⁹, C.J. Potter³², H. Potti¹¹, T. Poulsen⁹⁶, J. Poveda³⁶,
 T.D. Powell¹⁴⁹, G. Pownall⁴⁶, M.E. Pozo Astigarraga³⁶, P. Pralavorio¹⁰¹, S. Prell⁷⁸, D. Price¹⁰⁰,
 M. Primavera^{67a}, S. Prince¹⁰³, M.L. Proffitt¹⁴⁸, N. Proklova¹¹², K. Prokofiev^{63c}, F. Prokoshin⁷⁹,
 S. Protopopescu²⁹, J. Proudfoot⁶, M. Przybycien^{83a}, D. Pudzha¹³⁸, A. Puri¹⁷³, P. Puzo¹³², J. Qian¹⁰⁵,
 Y. Qin¹⁰⁰, A. Quadt⁵³, M. Queitsch-Maitland⁴⁶, A. Qureshi¹, P. Rados¹⁰⁴, F. Ragusa^{68a,68b}, G. Rahal⁹⁷,
 J.A. Raine⁵⁴, S. Rajagopalan²⁹, A. Ramirez Morales⁹², K. Ran^{15a,15d}, T. Rashid¹³², S. Raspopov⁵,
 D.M. Rauch⁴⁶, F. Rauscher¹¹⁴, S. Rave⁹⁹, B. Ravina¹⁴⁹, I. Ravinovich¹⁸⁰, J.H. Rawling¹⁰⁰, M. Raymond³⁶,
 A.L. Read¹³⁴, N.P. Readioff⁵⁸, M. Reale^{67a,67b}, D.M. Rebuffi^{70a,70b}, A. Redelbach¹⁷⁷, G. Redlinger²⁹,
 K. Reeves⁴³, L. Rehnisch¹⁹, J. Reichert¹³⁷, D. Reikher¹⁶¹, A. Reiss⁹⁹, A. Rej¹⁵¹, C. Rembser³⁶,
 M. Renda^{27b}, M. Rescigno^{72a}, S. Resconi^{68a}, E.D. Resseguie¹³⁷, S. Rettie¹⁷⁵, E. Reynolds²¹,
 O.L. Rezanova^{122b,122a}, P. Reznicek¹⁴³, E. Ricci^{75a,75b}, R. Richter¹¹⁵, S. Richter⁴⁶, E. Richter-Was^{83b},
 O. Ricken²⁴, M. Ridel¹³⁶, P. Rieck¹¹⁵, C.J. Riegel¹⁸², O. Rifki⁴⁶, M. Rijssenbeek¹⁵⁵, A. Rimoldi^{70a,70b},
 M. Rimoldi⁴⁶, L. Rinaldi^{23b}, G. Ripellino¹⁵⁴, B. Ristic⁸⁹, I. Riu¹⁴, J.C. Rivera Vergara¹⁷⁶,
 F. Rizatdinova¹²⁹, E. Rizvi⁹², C. Rizzi³⁶, R.T. Roberts¹⁰⁰, S.H. Robertson^{103,ad}, M. Robin⁴⁶,
 D. Robinson³², J.E.M. Robinson⁴⁶, C.M. Robles Gajardo^{147b}, A. Robson⁵⁷, E. Rocco⁹⁹, C. Roda^{71a,71b},
 S. Rodriguez Bosca¹⁷⁴, A. Rodriguez Perez¹⁴, D. Rodriguez Rodriguez¹⁷⁴, A.M. Rodríguez Vera^{168b},
 S. Roe³⁶, O. Røhne¹³⁴, R. Röhrig¹¹⁵, C.P.A. Roland⁶⁵, J. Roloff⁵⁹, A. Romaniouk¹¹², M. Romano^{23b,23a},
 N. Rompotis⁹⁰, M. Ronzani¹²⁴, L. Roos¹³⁶, S. Rosati^{72a}, K. Rosbach⁵², G. Rosin¹⁰², B.J. Rosser¹³⁷,
 E. Rossi⁴⁶, E. Rossi^{74a,74b}, E. Rossi^{69a,69b}, L.P. Rossi^{55b}, L. Rossini^{68a,68b}, R. Rosten¹⁴, M. Rotaru^{27b},
 J. Rothberg¹⁴⁸, D. Rousseau¹³², G. Rovelli^{70a,70b}, A. Roy¹¹, D. Roy^{33c}, A. Rozanov¹⁰¹, Y. Rozen¹⁶⁰,
 X. Ruan^{33c}, F. Rubbo¹⁵³, F. Rühr⁵², A. Ruiz-Martinez¹⁷⁴, A. Rummeler³⁶, Z. Rurikova⁵²,
 N.A. Rusakovich⁷⁹, H.L. Russell¹⁰³, L. Rustige^{38,47}, J.P. Rutherford⁷, E.M. Rüttinger^{46,j}, Y.F. Ryabov¹³⁸,
 M. Rybar³⁹, G. Rybkin¹³², E.B. Rye¹³⁴, A. Ryzhov¹²³, G.F. Rzehorz⁵³, P. Sabatini⁵³, G. Sabato¹²⁰,
 S. Sacerdoti¹³², H.F.W. Sadrozinski¹⁴⁶, R. Sadykov⁷⁹, F. Safai Tehrani^{72a}, B. Safarzadeh Samani¹⁵⁶,
 P. Saha¹²¹, S. Saha¹⁰³, M. Sahinsoy^{61a}, A. Sahu¹⁸², M. Saimpert⁴⁶, M. Saito¹⁶³, T. Saito¹⁶³,
 H. Sakamoto¹⁶³, A. Sakharov^{124,an}, D. Salamani⁵⁴, G. Salamanna^{74a,74b}, J.E. Salazar Loyola^{147b},
 P.H. Sales De Bruin¹⁷², A. Salnikov¹⁵³, J. Salt¹⁷⁴, D. Salvatore^{41b,41a}, F. Salvatore¹⁵⁶, A. Salvucci^{63a,63b,63c},
 A. Salzburger³⁶, J. Samarati³⁶, D. Sammel⁵², D. Sampsonidis¹⁶², D. Sampsonidou¹⁶², J. Sánchez¹⁷⁴,
 A. Sanchez Pineda^{66a,66c}, H. Sandaker¹³⁴, C.O. Sander⁴⁶, I.G. Sanderswood⁸⁹, M. Sandhoff¹⁸²,
 C. Sandoval²², D.P.C. Sankey¹⁴⁴, M. Sannino^{55b,55a}, Y. Sano¹¹⁷, A. Sansoni⁵¹, C. Santoni³⁸,
 H. Santos^{140a,140b}, S.N. Santpur¹⁸, A. Santra¹⁷⁴, A. Saponov⁷⁹, J.G. Saraiva^{140a,140d}, O. Sasaki⁸¹,
 K. Sato¹⁶⁹, E. Sauvan⁵, P. Savard^{167,ax}, N. Savic¹¹⁵, R. Sawada¹⁶³, C. Sawyer¹⁴⁴, L. Sawyer^{95,al},
 C. Sbarra^{23b}, A. Sbrizzi^{23a}, T. Scanlon⁹⁴, J. Schaarschmidt¹⁴⁸, P. Schacht¹¹⁵, B.M. Schachtner¹¹⁴,
 D. Schaefer³⁷, L. Schaefer¹³⁷, J. Schaeffer⁹⁹, S. Schaepe³⁶, U. Schäfer⁹⁹, A.C. Schaffer¹³², D. Schaile¹¹⁴,
 R.D. Schamberger¹⁵⁵, N. Scharmberg¹⁰⁰, V.A. Schegelsky¹³⁸, D. Scheirich¹⁴³, F. Schenck¹⁹,
 M. Schernau¹⁷¹, C. Schiavi^{55b,55a}, S. Schier¹⁴⁶, L.K. Schildgen²⁴, Z.M. Schillaci²⁶, E.J. Schioppa³⁶,
 M. Schioppa^{41b,41a}, K.E. Schleicher⁵², S. Schlenker³⁶, K.R. Schmidt-Sommerfeld¹¹⁵, K. Schmieden³⁶,
 C. Schmitt⁹⁹, S. Schmitt⁴⁶, S. Schmitz⁹⁹, J.C. Schmoedel⁴⁶, U. Schnoor⁵², L. Schoeffel¹⁴⁵,
 A. Schoening^{61b}, P.G. Scholer⁵², E. Schopf¹³⁵, M. Schott⁹⁹, J.F.P. Schouwenberg¹¹⁹, J. Schovancova³⁶,
 S. Schramm⁵⁴, F. Schroeder¹⁸², A. Schulte⁹⁹, H-C. Schultz-Coulon^{61a}, M. Schumacher⁵²,
 B.A. Schumm¹⁴⁶, Ph. Schune¹⁴⁵, A. Schwartzman¹⁵³, T.A. Schwarz¹⁰⁵, Ph. Schwemling¹⁴⁵,
 R. Schwienhorst¹⁰⁶, A. Sciandra¹⁴⁶, G. Sciolla²⁶, M. Scodreggio⁴⁶, M. Scornajenghi^{41b,41a}, F. Scuri^{71a},
 F. Scutti¹⁰⁴, L.M. Scyboz¹¹⁵, C.D. Sebastiani^{72a,72b}, P. Seema¹⁹, S.C. Seidel¹¹⁸, A. Seiden¹⁴⁶, T. Seiss³⁷,
 J.M. Seixas^{80b}, G. Sekhniaidze^{69a}, K. Sekhon¹⁰⁵, S.J. Sekula⁴², N. Semprini-Cesari^{23b,23a}, S. Sen⁴⁹,
 S. Senkin³⁸, C. Serfon⁷⁶, L. Serin¹³², L. Serkin^{66a,66b}, M. Sessa^{60a}, H. Severini¹²⁸, F. Sforza¹⁷⁰, A. Sfyrla⁵⁴,
 E. Shabalina⁵³, J.D. Shahinian¹⁴⁶, N.W. Shaikh^{45a,45b}, D. Shaked Renous¹⁸⁰, L.Y. Shan^{15a}, R. Shang¹⁷³,
 J.T. Shank²⁵, M. Shapiro¹⁸, A. Sharma¹³⁵, A.S. Sharma¹, P.B. Shatalov¹¹¹, K. Shaw¹⁵⁶, S.M. Shaw¹⁰⁰,

A. Shcherbakova¹³⁸, Y. Shen¹²⁸, N. Sherafati³⁴, A.D. Sherman²⁵, P. Sherwood⁹⁴, L. Shi^{158,at}, S. Shimizu⁸¹,
 C.O. Shimmin¹⁸³, Y. Shimogama¹⁷⁹, M. Shimojima¹¹⁶, I.P.J. Shipsey¹³⁵, S. Shirabe⁸⁷, M. Shiyakova^{79,aa},
 J. Shlomi¹⁸⁰, A. Shmeleva¹¹⁰, M.J. Shochet³⁷, S. Shojaii¹⁰⁴, D.R. Shope¹²⁸, S. Shrestha¹²⁶, E.M. Shrif^{33c},
 E. Shulga¹⁸⁰, P. Sicho¹⁴¹, A.M. Sickles¹⁷³, P.E. Sidebo¹⁵⁴, E. Sideras Haddad^{33c}, O. Sidiropoulou³⁶,
 A. Sidoti^{23b,23a}, F. Siegert⁴⁸, Dj. Sijacki¹⁶, M. Silva Jr.¹⁸¹, M.V. Silva Oliveira^{80a}, S.B. Silverstein^{45a},
 S. Simion¹³², E. Simioni⁹⁹, R. Simoniello⁹⁹, S. Simsek^{12b}, P. Sinervo¹⁶⁷, V. Sinetckii^{113,110}, N.B. Sinev¹³¹,
 M. Sioli^{23b,23a}, I. Siral¹⁰⁵, S.Yu. Sivoklov¹¹³, J. Sjölin^{45a,45b}, E. Skorda⁹⁶, P. Skubic¹²⁸, M. Slawinska⁸⁴,
 K. Sliwa¹⁷⁰, R. Slovak¹⁴³, V. Smakhtin¹⁸⁰, B.H. Smart¹⁴⁴, J. Smiesko^{28a}, N. Smirnov¹¹²,
 S.Yu. Smirnov¹¹², Y. Smirnov¹¹², L.N. Smirnova^{113,t}, O. Smirnova⁹⁶, J.W. Smith⁵³, M. Smizanska⁸⁹,
 K. Smolek¹⁴², A. Smykiewicz⁸⁴, A.A. Snesarev¹¹⁰, H.L. Snoek¹²⁰, I.M. Snyder¹³¹, S. Snyder²⁹,
 R. Sobie^{176,ad}, A.M. Soffa¹⁷¹, A. Soffer¹⁶¹, A. Søggaard⁵⁰, F. Sohns⁵³, C.A. Solans Sanchez³⁶,
 E.Yu. Soldatov¹¹², U. Soldevila¹⁷⁴, A.A. Solodkov¹²³, A. Soloshenko⁷⁹, O.V. Solovyanov¹²³,
 V. Solovyev¹³⁸, P. Sommer¹⁴⁹, H. Son¹⁷⁰, W. Song¹⁴⁴, W.Y. Song^{168b}, A. Sopczak¹⁴², F. Sopkova^{28b},
 C.L. Sotiropoulou^{71a,71b}, S. Sottocornola^{70a,70b}, R. Soualah^{66a,66c,f}, A.M. Soukharev^{122b,122a}, D. South⁴⁶,
 S. Spagnolo^{67a,67b}, M. Spalla¹¹⁵, M. Spangenberg¹⁷⁸, F. Spanò⁹³, D. Sperlich⁵², T.M. Spieker^{61a},
 R. Spighi^{23b}, G. Spigo³⁶, M. Spina¹⁵⁶, D.P. Spiteri⁵⁷, M. Spousta¹⁴³, A. Stabile^{68a,68b}, B.L. Stamas¹²¹,
 R. Stamen^{61a}, M. Stamenkovic¹²⁰, E. Stanecka⁸⁴, R.W. Stanek⁶, B. Stanislaus¹³⁵, M.M. Stanitzki⁴⁶,
 M. Stankaityte¹³⁵, B. Stapf¹²⁰, E.A. Starchenko¹²³, G.H. Stark¹⁴⁶, J. Stark⁵⁸, S.H. Stark⁴⁰, P. Staroba¹⁴¹,
 P. Starovoitov^{61a}, S. Stärz¹⁰³, R. Staszewski⁸⁴, G. Stavropoulos⁴⁴, M. Stegler⁴⁶, P. Steinberg²⁹,
 A.L. Steinhebel¹³¹, B. Stelzer¹⁵², H.J. Stelzer¹³⁹, O. Stelzer-Chilton^{168a}, H. Stenzel⁵⁶, T.J. Stevenson¹⁵⁶,
 G.A. Stewart³⁶, M.C. Stockton³⁶, G. Stoicea^{27b}, M. Stolarski^{140a}, P. Stolte⁵³, S. Stonjek¹¹⁵,
 A. Straessner⁴⁸, J. Strandberg¹⁵⁴, S. Strandberg^{45a,45b}, M. Strauss¹²⁸, P. Strizenec^{28b}, R. Ströhmer¹⁷⁷,
 D.M. Strom¹³¹, R. Stroynowski⁴², A. Strubig⁵⁰, S.A. Stucci²⁹, B. Stugu¹⁷, J. Stupak¹²⁸, N.A. Styles⁴⁶,
 D. Su¹⁵³, S. Sucheck^{61a}, V.V. Sulin¹¹⁰, M.J. Sullivan⁹⁰, D.M.S. Sultan⁵⁴, S. Sultansoy^{4c}, T. Sumida⁸⁵,
 S. Sun¹⁰⁵, X. Sun³, K. Suruliz¹⁵⁶, C.J.E. Suster¹⁵⁷, M.R. Sutton¹⁵⁶, S. Suzuki⁸¹, M. Svatos¹⁴¹,
 M. Swiatlowski³⁷, S.P. Swift², T. Swirski¹⁷⁷, A. Sydorenko⁹⁹, I. Sykora^{28a}, M. Sykora¹⁴³, T. Sykora¹⁴³,
 D. Ta⁹⁹, K. Tackmann^{46,y}, J. Taenzer¹⁶¹, A. Taffard¹⁷¹, R. Tafirout^{168a}, H. Takai²⁹, R. Takashima⁸⁶,
 K. Takeda⁸², T. Takeshita¹⁵⁰, E.P. Takeva⁵⁰, Y. Takubo⁸¹, M. Talby¹⁰¹, A.A. Talyshev^{122b,122a},
 N.M. Tamir¹⁶¹, J. Tanaka¹⁶³, M. Tanaka¹⁶⁵, R. Tanaka¹³², S. Tapia Araya¹⁷³, S. Tapprogge⁹⁹,
 A. Tarek Abouelfadl Mohamed¹³⁶, S. Tarem¹⁶⁰, G. Tarna^{27b,b}, G.F. Tartarelli^{68a}, P. Tas¹⁴³, M. Tasevsky¹⁴¹,
 T. Tashiro⁸⁵, E. Tassi^{41b,41a}, A. Tavares Delgado^{140a,140b}, Y. Tayalati^{35e}, A.J. Taylor⁵⁰, G.N. Taylor¹⁰⁴,
 W. Taylor^{168b}, A.S. Tee⁸⁹, R. Teixeira De Lima¹⁵³, P. Teixeira-Dias⁹³, H. Ten Kate³⁶, J.J. Teoh¹²⁰,
 S. Terada⁸¹, K. Terashi¹⁶³, J. Terron⁹⁸, S. Terzo¹⁴, M. Testa⁵¹, R.J. Teuscher^{167,ad}, S.J. Thais¹⁸³,
 T. Theveneaux-Pelzer⁴⁶, F. Thiele⁴⁰, D.W. Thomas⁹³, J.O. Thomas⁴², J.P. Thomas²¹, A.S. Thompson⁵⁷,
 P.D. Thompson²¹, L.A. Thomsen¹⁸³, E. Thomson¹³⁷, E.J. Thorpe⁹², Y. Tian³⁹, R.E. Ticse Torres⁵³,
 V.O. Tikhomirov^{110,ap}, Yu.A. Tikhonov^{122b,122a}, S. Timoshenko¹¹², P. Tipton¹⁸³, S. Tisserant¹⁰¹,
 K. Todome^{23b,23a}, S. Todorova-Nova⁵, S. Todt⁴⁸, J. Tojo⁸⁷, S. Tokár^{28a}, K. Tokushuku⁸¹, E. Tolley¹²⁶,
 K.G. Tomiwa^{33c}, M. Tomoto¹¹⁷, L. Tompkins^{153,p}, K. Toms¹¹⁸, B. Tong⁵⁹, P. Tornambe¹⁰², E. Torrence¹³¹,
 H. Torres⁴⁸, E. Torró Pastor¹⁴⁸, C. Tosciri¹³⁵, J. Toth^{101,ab}, D.R. Tovey¹⁴⁹, A. Traeet¹⁷, C.J. Treado¹²⁴,
 T. Trefzger¹⁷⁷, F. Tresoldi¹⁵⁶, A. Tricoli²⁹, I.M. Trigger^{168a}, S. Trincaz-Duvoid¹³⁶, W. Trischuk¹⁶⁷,
 B. Trocme⁵⁸, A. Trofymov¹³², C. Troncon^{68a}, M. Trovatelli¹⁷⁶, F. Trovato¹⁵⁶, L. Truong^{33b},
 M. Trzebinski⁸⁴, A. Trzupek⁸⁴, F. Tsai⁴⁶, J.C-L. Tseng¹³⁵, P.V. Tsiareshka^{107,aj}, A. Tsirigotis¹⁶²,
 N. Tsirintanis⁹, V. Tsiskaridze¹⁵⁵, E.G. Tskhadadze^{159a}, M. Tsopoulou¹⁶², I.I. Tsukerman¹¹¹, V. Tsulaia¹⁸,
 S. Tsuno⁸¹, D. Tsybychev¹⁵⁵, Y. Tu^{63b}, A. Tudorache^{27b}, V. Tudorache^{27b}, T.T. Tulbure^{27a}, A.N. Tuna⁵⁹,
 S. Turchikhin⁷⁹, D. Turgeman¹⁸⁰, I. Turk Cakir^{4b,u}, R.J. Turner²¹, R.T. Turra^{68a}, P.M. Tuts³⁹,
 S. Tzamarias¹⁶², E. Tzovara⁹⁹, G. Uccelli⁴⁷, K. Uchida¹⁶³, I. Ueda⁸¹, M. Ughetto^{45a,45b}, F. Ukegawa¹⁶⁹,
 G. Unal³⁶, A. Undrus²⁹, G. Unel¹⁷¹, F.C. Ungaro¹⁰⁴, Y. Unno⁸¹, K. Uno¹⁶³, J. Urban^{28b}, P. Urquijo¹⁰⁴,

G. Usai⁸, J. Usui⁸¹, Z. Uysal^{12d}, L. Vacavant¹⁰¹, V. Vacek¹⁴², B. Vachon¹⁰³, K.O.H. Vadla¹³⁴, A. Vaidya⁹⁴, C. Valderanis¹¹⁴, E. Valdes Santurio^{45a,45b}, M. Valente⁵⁴, S. Valentinetti^{23b,23a}, A. Valero¹⁷⁴, L. Valéry⁴⁶, R.A. Vallance²¹, A. Vallier³⁶, J.A. Valls Ferrer¹⁷⁴, T.R. Van Daalen¹⁴, P. Van Gemmeren⁶, I. Van Vulpen¹²⁰, M. Vanadia^{73a,73b}, W. Vandelli³⁶, A. Vaniachine¹⁶⁶, D. Vannicola^{72a,72b}, R. Vari^{72a}, E.W. Varnes⁷, C. Varni^{55b,55a}, T. Varol⁴², D. Varouchas¹³², K.E. Varvell¹⁵⁷, M.E. Vasile^{27b}, G.A. Vasquez¹⁷⁶, J.G. Vasquez¹⁸³, F. Vazeille³⁸, D. Vazquez Furelos¹⁴, T. Vazquez Schroeder³⁶, J. Veatch⁵³, V. Vecchio^{74a,74b}, M.J. Veen¹²⁰, L.M. Veloce¹⁶⁷, F. Veloso^{140a,140c}, S. Veneziano^{72a}, A. Ventura^{67a,67b}, N. Venturi³⁶, A. Verbytskyi¹¹⁵, V. Vercesi^{70a}, M. Verducci^{71a,71b}, C.M. Vergel Infante⁷⁸, C. Vergis²⁴, W. Verkerke¹²⁰, A.T. Vermeulen¹²⁰, J.C. Vermeulen¹²⁰, M.C. Vetterli^{152,ax}, N. Viaux Maira^{147b}, M. Vicente Barreto Pinto⁵⁴, T. Vickey¹⁴⁹, O.E. Vickey Boeriu¹⁴⁹, G.H.A. Viehhauser¹³⁵, L. Vigani^{61b}, M. Villa^{23b,23a}, M. Villaplana Perez^{68a,68b}, E. Vilucchi⁵¹, M.G. Vinciter³⁴, V.B. Vinogradov⁷⁹, A. Vishwakarma⁴⁶, C. Vittori^{23b,23a}, I. Vivarelli¹⁵⁶, M. Vogel¹⁸², P. Vokac¹⁴², S.E. von Buddenbrock^{33c}, E. Von Toerne²⁴, V. Vorobel¹⁴³, K. Vorobev¹¹², M. Vos¹⁷⁴, J.H. Vossebeld⁹⁰, M. Vozak¹⁰⁰, N. Vranjes¹⁶, M. Vranjes Milosavljevic¹⁶, V. Vrba¹⁴², M. Vreeswijk¹²⁰, T. Šfiligoj⁹¹, R. Vuillermet³⁶, I. Vukotic³⁷, T. Ženiš^{28a}, L. Živković¹⁶, P. Wagner²⁴, W. Wagner¹⁸², J. Wagner-Kuhr¹¹⁴, S. Wahdan¹⁸², H. Wahlberg⁸⁸, K. Wakamiya⁸², V.M. Walbrecht¹¹⁵, J. Walder⁸⁹, R. Walker¹¹⁴, S.D. Walker⁹³, W. Walkowiak¹⁵¹, V. Wallangen^{45a,45b}, A.M. Wang⁵⁹, C. Wang^{60c}, C. Wang^{60b}, F. Wang¹⁸¹, H. Wang¹⁸, H. Wang³, J. Wang¹⁵⁷, J. Wang^{61b}, P. Wang⁴², Q. Wang¹²⁸, R.-J. Wang⁹⁹, R. Wang^{60a}, R. Wang⁶, S.M. Wang¹⁵⁸, W.T. Wang^{60a}, W. Wang^{15c,ae}, W.X. Wang^{60a,ae}, Y. Wang^{60a,am}, Z. Wang^{60c}, C. Wanotayaroj⁴⁶, A. Warburton¹⁰³, C.P. Ward³², D.R. Wardrope⁹⁴, N. Warrack⁵⁷, A. Washbrook⁵⁰, A.T. Watson²¹, M.F. Watson²¹, G. Watts¹⁴⁸, B.M. Waugh⁹⁴, A.F. Webb¹¹, S. Webb⁹⁹, C. Weber¹⁸³, M.S. Weber²⁰, S.A. Weber³⁴, S.M. Weber^{61a}, A.R. Weidberg¹³⁵, J. Weingarten⁴⁷, M. Weirich⁹⁹, C. Weiser⁵², P.S. Wells³⁶, T. Wenaus²⁹, T. Wengler³⁶, S. Wenig³⁶, N. Wermes²⁴, M.D. Werner⁷⁸, M. Wessels^{61a}, T.D. Weston²⁰, K. Whalen¹³¹, N.L. Whallon¹⁴⁸, A.M. Wharton⁸⁹, A.S. White¹⁰⁵, A. White⁸, M.J. White¹, D. Whiteson¹⁷¹, B.W. Whitmore⁸⁹, W. Wiedenmann¹⁸¹, M. Wielers¹⁴⁴, N. Wieseotte⁹⁹, C. Wiglesworth⁴⁰, L.A.M. Wiik-Fuchs⁵², F. Wilk¹⁰⁰, H.G. Wilkens³⁶, L.J. Wilkins⁹³, H.H. Williams¹³⁷, S. Williams³², C. Willis¹⁰⁶, S. Willocq¹⁰², J.A. Wilson²¹, I. Wingerter-Seez⁵, E. Winkels¹⁵⁶, F. Winklmeier¹³¹, O.J. Winston¹⁵⁶, B.T. Winter⁵², M. Wittgen¹⁵³, M. Wobisch⁹⁵, A. Wolf⁹⁹, T.M.H. Wolf¹²⁰, R. Wolff¹⁰¹, R.W. Wölker¹³⁵, J. Wollrath⁵², M.W. Wolter⁸⁴, H. Wolters^{140a,140c}, V.W.S. Wong¹⁷⁵, N.L. Woods¹⁴⁶, S.D. Worm²¹, B.K. Wosiek⁸⁴, K.W. Woźniak⁸⁴, K. Wraight⁵⁷, S.L. Wu¹⁸¹, X. Wu⁵⁴, Y. Wu^{60a}, T.R. Wyatt¹⁰⁰, B.M. Wynne⁵⁰, S. Xella⁴⁰, Z. Xi¹⁰⁵, L. Xia¹⁷⁸, D. Xu^{15a}, H. Xu^{60a,b}, L. Xu²⁹, T. Xu¹⁴⁵, W. Xu¹⁰⁵, Z. Xu^{60b}, Z. Xu¹⁵³, B. Yabsley¹⁵⁷, S. Yacoub^{33a}, K. Yajima¹³³, D.P. Yallup⁹⁴, D. Yamaguchi¹⁶⁵, Y. Yamaguchi¹⁶⁵, A. Yamamoto⁸¹, F. Yamane⁸², M. Yamatani¹⁶³, T. Yamazaki¹⁶³, Y. Yamazaki⁸², Z. Yan²⁵, H.J. Yang^{60c,60d}, H.T. Yang¹⁸, S. Yang⁷⁷, X. Yang^{60b,58}, Y. Yang¹⁶³, W.-M. Yao¹⁸, Y.C. Yap⁴⁶, Y. Yasu⁸¹, E. Yatsenko^{60c,60d}, J. Ye⁴², S. Ye²⁹, I. Yeletskikh⁷⁹, M.R. Yexley⁸⁹, E. Yigitbasi²⁵, K. Yorita¹⁷⁹, K. Yoshihara¹³⁷, C.J.S. Young³⁶, C. Young¹⁵³, J. Yu⁷⁸, R. Yuan^{60b,h}, X. Yue^{61a}, S.P.Y. Yuen²⁴, B. Zabinski⁸⁴, G. Zacharis¹⁰, E. Zaffaroni⁵⁴, J. Zahreddine¹³⁶, A.M. Zaitsev^{123,ao}, T. Zakareishvili^{159b}, N. Zakharchuk³⁴, S. Zambito⁵⁹, D. Zanzi³⁶, D.R. Zaripovas⁵⁷, S.V. Zeiβner⁴⁷, C. Zeitnitz¹⁸², G. Zemaityte¹³⁵, J.C. Zeng¹⁷³, O. Zenin¹²³, D. Zerwas¹³², M. Zgubic¹³⁵, D.F. Zhang^{15b}, F. Zhang¹⁸¹, G. Zhang^{15b}, H. Zhang^{15c}, J. Zhang⁶, L. Zhang^{15c}, L. Zhang^{60a}, M. Zhang¹⁷³, R. Zhang²⁴, X. Zhang^{60b}, Y. Zhang^{15a,15d}, Z. Zhang^{63a}, Z. Zhang¹³², P. Zhao⁴⁹, Y. Zhao^{60b}, Z. Zhao^{60a}, A. Zhemchugov⁷⁹, Z. Zheng¹⁰⁵, D. Zhong¹⁷³, B. Zhou¹⁰⁵, C. Zhou¹⁸¹, M.S. Zhou^{15a,15d}, M. Zhou¹⁵⁵, N. Zhou^{60c}, Y. Zhou⁷, C.G. Zhu^{60b}, H.L. Zhu^{60a}, H. Zhu^{15a}, J. Zhu¹⁰⁵, Y. Zhu^{60a}, X. Zhuang^{15a}, K. Zhukov¹¹⁰, V. Zhulanov^{122b,122a}, D. Zieminska⁶⁵, N.I. Zimine⁷⁹, S. Zimmermann⁵², Z. Zinonos¹¹⁵, M. Ziolkowski¹⁵¹, G. Zobernig¹⁸¹, A. Zoccoli^{23b,23a}, K. Zoch⁵³, T.G. Zorbas¹⁴⁹, R. Zou³⁷, L. Zwalinski³⁶.

- ¹Department of Physics, University of Adelaide, Adelaide; Australia.
- ²Physics Department, SUNY Albany, Albany NY; United States of America.
- ³Department of Physics, University of Alberta, Edmonton AB; Canada.
- ^{4(a)}Department of Physics, Ankara University, Ankara;^(b)Istanbul Aydin University, Istanbul;^(c)Division of Physics, TOBB University of Economics and Technology, Ankara; Turkey.
- ⁵LAPP, Université Grenoble Alpes, Université Savoie Mont Blanc, CNRS/IN2P3, Annecy; France.
- ⁶High Energy Physics Division, Argonne National Laboratory, Argonne IL; United States of America.
- ⁷Department of Physics, University of Arizona, Tucson AZ; United States of America.
- ⁸Department of Physics, University of Texas at Arlington, Arlington TX; United States of America.
- ⁹Physics Department, National and Kapodistrian University of Athens, Athens; Greece.
- ¹⁰Physics Department, National Technical University of Athens, Zografou; Greece.
- ¹¹Department of Physics, University of Texas at Austin, Austin TX; United States of America.
- ^{12(a)}Bahcesehir University, Faculty of Engineering and Natural Sciences, Istanbul;^(b)Istanbul Bilgi University, Faculty of Engineering and Natural Sciences, Istanbul;^(c)Department of Physics, Bogazici University, Istanbul;^(d)Department of Physics Engineering, Gaziantep University, Gaziantep; Turkey.
- ¹³Institute of Physics, Azerbaijan Academy of Sciences, Baku; Azerbaijan.
- ¹⁴Institut de Física d'Altes Energies (IFAE), Barcelona Institute of Science and Technology, Barcelona; Spain.
- ^{15(a)}Institute of High Energy Physics, Chinese Academy of Sciences, Beijing;^(b)Physics Department, Tsinghua University, Beijing;^(c)Department of Physics, Nanjing University, Nanjing;^(d)University of Chinese Academy of Science (UCAS), Beijing; China.
- ¹⁶Institute of Physics, University of Belgrade, Belgrade; Serbia.
- ¹⁷Department for Physics and Technology, University of Bergen, Bergen; Norway.
- ¹⁸Physics Division, Lawrence Berkeley National Laboratory and University of California, Berkeley CA; United States of America.
- ¹⁹Institut für Physik, Humboldt Universität zu Berlin, Berlin; Germany.
- ²⁰Albert Einstein Center for Fundamental Physics and Laboratory for High Energy Physics, University of Bern, Bern; Switzerland.
- ²¹School of Physics and Astronomy, University of Birmingham, Birmingham; United Kingdom.
- ²²Facultad de Ciencias y Centro de Investigaciones, Universidad Antonio Nariño, Bogota; Colombia.
- ^{23(a)}INFN Bologna and Università di Bologna, Dipartimento di Fisica;^(b)INFN Sezione di Bologna; Italy.
- ²⁴Physikalisches Institut, Universität Bonn, Bonn; Germany.
- ²⁵Department of Physics, Boston University, Boston MA; United States of America.
- ²⁶Department of Physics, Brandeis University, Waltham MA; United States of America.
- ^{27(a)}Transilvania University of Brasov, Brasov;^(b)Horia Hulubei National Institute of Physics and Nuclear Engineering, Bucharest;^(c)Department of Physics, Alexandru Ioan Cuza University of Iasi, Iasi;^(d)National Institute for Research and Development of Isotopic and Molecular Technologies, Physics Department, Cluj-Napoca;^(e)University Politehnica Bucharest, Bucharest;^(f)West University in Timisoara, Timisoara; Romania.
- ^{28(a)}Faculty of Mathematics, Physics and Informatics, Comenius University, Bratislava;^(b)Department of Subnuclear Physics, Institute of Experimental Physics of the Slovak Academy of Sciences, Kosice; Slovak Republic.
- ²⁹Physics Department, Brookhaven National Laboratory, Upton NY; United States of America.
- ³⁰Departamento de Física, Universidad de Buenos Aires, Buenos Aires; Argentina.
- ³¹California State University, CA; United States of America.
- ³²Cavendish Laboratory, University of Cambridge, Cambridge; United Kingdom.
- ^{33(a)}Department of Physics, University of Cape Town, Cape Town;^(b)Department of Mechanical

Engineering Science, University of Johannesburg, Johannesburg;^(c)School of Physics, University of the Witwatersrand, Johannesburg; South Africa.

³⁴Department of Physics, Carleton University, Ottawa ON; Canada.

³⁵^(a)Faculté des Sciences Ain Chock, Réseau Universitaire de Physique des Hautes Energies - Université Hassan II, Casablanca;^(b)Faculté des Sciences, Université Ibn-Tofail, Kénitra;^(c)Faculté des Sciences Semlalia, Université Cadi Ayyad, LPHEA-Marrakech;^(d)Faculté des Sciences, Université Mohamed Premier and LPTPM, Oujda;^(e)Faculté des sciences, Université Mohammed V, Rabat; Morocco.

³⁶CERN, Geneva; Switzerland.

³⁷Enrico Fermi Institute, University of Chicago, Chicago IL; United States of America.

³⁸LPC, Université Clermont Auvergne, CNRS/IN2P3, Clermont-Ferrand; France.

³⁹Nevis Laboratory, Columbia University, Irvington NY; United States of America.

⁴⁰Niels Bohr Institute, University of Copenhagen, Copenhagen; Denmark.

⁴¹^(a)Dipartimento di Fisica, Università della Calabria, Rende;^(b)INFN Gruppo Collegato di Cosenza, Laboratori Nazionali di Frascati; Italy.

⁴²Physics Department, Southern Methodist University, Dallas TX; United States of America.

⁴³Physics Department, University of Texas at Dallas, Richardson TX; United States of America.

⁴⁴National Centre for Scientific Research "Demokritos", Agia Paraskevi; Greece.

⁴⁵^(a)Department of Physics, Stockholm University;^(b)Oskar Klein Centre, Stockholm; Sweden.

⁴⁶Deutsches Elektronen-Synchrotron DESY, Hamburg and Zeuthen; Germany.

⁴⁷Lehrstuhl für Experimentelle Physik IV, Technische Universität Dortmund, Dortmund; Germany.

⁴⁸Institut für Kern- und Teilchenphysik, Technische Universität Dresden, Dresden; Germany.

⁴⁹Department of Physics, Duke University, Durham NC; United States of America.

⁵⁰SUPA - School of Physics and Astronomy, University of Edinburgh, Edinburgh; United Kingdom.

⁵¹INFN e Laboratori Nazionali di Frascati, Frascati; Italy.

⁵²Physikalisches Institut, Albert-Ludwigs-Universität Freiburg, Freiburg; Germany.

⁵³II. Physikalisches Institut, Georg-August-Universität Göttingen, Göttingen; Germany.

⁵⁴Département de Physique Nucléaire et Corpusculaire, Université de Genève, Genève; Switzerland.

⁵⁵^(a)Dipartimento di Fisica, Università di Genova, Genova;^(b)INFN Sezione di Genova; Italy.

⁵⁶II. Physikalisches Institut, Justus-Liebig-Universität Giessen, Giessen; Germany.

⁵⁷SUPA - School of Physics and Astronomy, University of Glasgow, Glasgow; United Kingdom.

⁵⁸LPSC, Université Grenoble Alpes, CNRS/IN2P3, Grenoble INP, Grenoble; France.

⁵⁹Laboratory for Particle Physics and Cosmology, Harvard University, Cambridge MA; United States of America.

⁶⁰^(a)Department of Modern Physics and State Key Laboratory of Particle Detection and Electronics, University of Science and Technology of China, Hefei;^(b)Institute of Frontier and Interdisciplinary Science and Key Laboratory of Particle Physics and Particle Irradiation (MOE), Shandong University, Qingdao;^(c)School of Physics and Astronomy, Shanghai Jiao Tong University, KLPPAC-MoE, SKLPPC, Shanghai;^(d)Tsung-Dao Lee Institute, Shanghai; China.

⁶¹^(a)Kirchhoff-Institut für Physik, Ruprecht-Karls-Universität Heidelberg, Heidelberg;^(b)Physikalisches Institut, Ruprecht-Karls-Universität Heidelberg, Heidelberg; Germany.

⁶²Faculty of Applied Information Science, Hiroshima Institute of Technology, Hiroshima; Japan.

⁶³^(a)Department of Physics, Chinese University of Hong Kong, Shatin, N.T., Hong Kong;^(b)Department of Physics, University of Hong Kong, Hong Kong;^(c)Department of Physics and Institute for Advanced Study, Hong Kong University of Science and Technology, Clear Water Bay, Kowloon, Hong Kong; China.

⁶⁴Department of Physics, National Tsing Hua University, Hsinchu; Taiwan.

⁶⁵Department of Physics, Indiana University, Bloomington IN; United States of America.

⁶⁶^(a)INFN Gruppo Collegato di Udine, Sezione di Trieste, Udine;^(b)ICTP, Trieste;^(c)Dipartimento

- Politecnico di Ingegneria e Architettura, Università di Udine, Udine; Italy.
- ^{67(a)}INFN Sezione di Lecce;^(b)Dipartimento di Matematica e Fisica, Università del Salento, Lecce; Italy.
- ^{68(a)}INFN Sezione di Milano;^(b)Dipartimento di Fisica, Università di Milano, Milano; Italy.
- ^{69(a)}INFN Sezione di Napoli;^(b)Dipartimento di Fisica, Università di Napoli, Napoli; Italy.
- ^{70(a)}INFN Sezione di Pavia;^(b)Dipartimento di Fisica, Università di Pavia, Pavia; Italy.
- ^{71(a)}INFN Sezione di Pisa;^(b)Dipartimento di Fisica E. Fermi, Università di Pisa, Pisa; Italy.
- ^{72(a)}INFN Sezione di Roma;^(b)Dipartimento di Fisica, Sapienza Università di Roma, Roma; Italy.
- ^{73(a)}INFN Sezione di Roma Tor Vergata;^(b)Dipartimento di Fisica, Università di Roma Tor Vergata, Roma; Italy.
- ^{74(a)}INFN Sezione di Roma Tre;^(b)Dipartimento di Matematica e Fisica, Università Roma Tre, Roma; Italy.
- ^{75(a)}INFN-TIFPA;^(b)Università degli Studi di Trento, Trento; Italy.
- ⁷⁶Institut für Astro- und Teilchenphysik, Leopold-Franzens-Universität, Innsbruck; Austria.
- ⁷⁷University of Iowa, Iowa City IA; United States of America.
- ⁷⁸Department of Physics and Astronomy, Iowa State University, Ames IA; United States of America.
- ⁷⁹Joint Institute for Nuclear Research, Dubna; Russia.
- ^{80(a)}Departamento de Engenharia Elétrica, Universidade Federal de Juiz de Fora (UFJF), Juiz de Fora;^(b)Universidade Federal do Rio De Janeiro COPPE/EE/IF, Rio de Janeiro;^(c)Universidade Federal de São João del Rei (UFSJ), São João del Rei;^(d)Instituto de Física, Universidade de São Paulo, São Paulo; Brazil.
- ⁸¹KEK, High Energy Accelerator Research Organization, Tsukuba; Japan.
- ⁸²Graduate School of Science, Kobe University, Kobe; Japan.
- ^{83(a)}AGH University of Science and Technology, Faculty of Physics and Applied Computer Science, Krakow;^(b)Marian Smoluchowski Institute of Physics, Jagiellonian University, Krakow; Poland.
- ⁸⁴Institute of Nuclear Physics Polish Academy of Sciences, Krakow; Poland.
- ⁸⁵Faculty of Science, Kyoto University, Kyoto; Japan.
- ⁸⁶Kyoto University of Education, Kyoto; Japan.
- ⁸⁷Research Center for Advanced Particle Physics and Department of Physics, Kyushu University, Fukuoka ; Japan.
- ⁸⁸Instituto de Física La Plata, Universidad Nacional de La Plata and CONICET, La Plata; Argentina.
- ⁸⁹Physics Department, Lancaster University, Lancaster; United Kingdom.
- ⁹⁰Oliver Lodge Laboratory, University of Liverpool, Liverpool; United Kingdom.
- ⁹¹Department of Experimental Particle Physics, Jožef Stefan Institute and Department of Physics, University of Ljubljana, Ljubljana; Slovenia.
- ⁹²School of Physics and Astronomy, Queen Mary University of London, London; United Kingdom.
- ⁹³Department of Physics, Royal Holloway University of London, Egham; United Kingdom.
- ⁹⁴Department of Physics and Astronomy, University College London, London; United Kingdom.
- ⁹⁵Louisiana Tech University, Ruston LA; United States of America.
- ⁹⁶Fysiska institutionen, Lunds universitet, Lund; Sweden.
- ⁹⁷Centre de Calcul de l'Institut National de Physique Nucléaire et de Physique des Particules (IN2P3), Villeurbanne; France.
- ⁹⁸Departamento de Física Teórica C-15 and CIAFF, Universidad Autónoma de Madrid, Madrid; Spain.
- ⁹⁹Institut für Physik, Universität Mainz, Mainz; Germany.
- ¹⁰⁰School of Physics and Astronomy, University of Manchester, Manchester; United Kingdom.
- ¹⁰¹CPPM, Aix-Marseille Université, CNRS/IN2P3, Marseille; France.
- ¹⁰²Department of Physics, University of Massachusetts, Amherst MA; United States of America.
- ¹⁰³Department of Physics, McGill University, Montreal QC; Canada.
- ¹⁰⁴School of Physics, University of Melbourne, Victoria; Australia.

- ¹⁰⁵Department of Physics, University of Michigan, Ann Arbor MI; United States of America.
- ¹⁰⁶Department of Physics and Astronomy, Michigan State University, East Lansing MI; United States of America.
- ¹⁰⁷B.I. Stepanov Institute of Physics, National Academy of Sciences of Belarus, Minsk; Belarus.
- ¹⁰⁸Research Institute for Nuclear Problems of Byelorussian State University, Minsk; Belarus.
- ¹⁰⁹Group of Particle Physics, University of Montreal, Montreal QC; Canada.
- ¹¹⁰P.N. Lebedev Physical Institute of the Russian Academy of Sciences, Moscow; Russia.
- ¹¹¹Institute for Theoretical and Experimental Physics of the National Research Centre Kurchatov Institute, Moscow; Russia.
- ¹¹²National Research Nuclear University MEPhI, Moscow; Russia.
- ¹¹³D.V. Skobeltsyn Institute of Nuclear Physics, M.V. Lomonosov Moscow State University, Moscow; Russia.
- ¹¹⁴Fakultät für Physik, Ludwig-Maximilians-Universität München, München; Germany.
- ¹¹⁵Max-Planck-Institut für Physik (Werner-Heisenberg-Institut), München; Germany.
- ¹¹⁶Nagasaki Institute of Applied Science, Nagasaki; Japan.
- ¹¹⁷Graduate School of Science and Kobayashi-Maskawa Institute, Nagoya University, Nagoya; Japan.
- ¹¹⁸Department of Physics and Astronomy, University of New Mexico, Albuquerque NM; United States of America.
- ¹¹⁹Institute for Mathematics, Astrophysics and Particle Physics, Radboud University Nijmegen/Nikhef, Nijmegen; Netherlands.
- ¹²⁰Nikhef National Institute for Subatomic Physics and University of Amsterdam, Amsterdam; Netherlands.
- ¹²¹Department of Physics, Northern Illinois University, DeKalb IL; United States of America.
- ¹²²^(a)Budker Institute of Nuclear Physics and NSU, SB RAS, Novosibirsk; ^(b)Novosibirsk State University Novosibirsk; Russia.
- ¹²³Institute for High Energy Physics of the National Research Centre Kurchatov Institute, Protvino; Russia.
- ¹²⁴Department of Physics, New York University, New York NY; United States of America.
- ¹²⁵Ochanomizu University, Otsuka, Bunkyo-ku, Tokyo; Japan.
- ¹²⁶Ohio State University, Columbus OH; United States of America.
- ¹²⁷Faculty of Science, Okayama University, Okayama; Japan.
- ¹²⁸Homer L. Dodge Department of Physics and Astronomy, University of Oklahoma, Norman OK; United States of America.
- ¹²⁹Department of Physics, Oklahoma State University, Stillwater OK; United States of America.
- ¹³⁰Palacký University, RCPTM, Joint Laboratory of Optics, Olomouc; Czech Republic.
- ¹³¹Center for High Energy Physics, University of Oregon, Eugene OR; United States of America.
- ¹³²LAL, Université Paris-Sud, CNRS/IN2P3, Université Paris-Saclay, Orsay; France.
- ¹³³Graduate School of Science, Osaka University, Osaka; Japan.
- ¹³⁴Department of Physics, University of Oslo, Oslo; Norway.
- ¹³⁵Department of Physics, Oxford University, Oxford; United Kingdom.
- ¹³⁶LPNHE, Sorbonne Université, Paris Diderot Sorbonne Paris Cité, CNRS/IN2P3, Paris; France.
- ¹³⁷Department of Physics, University of Pennsylvania, Philadelphia PA; United States of America.
- ¹³⁸Konstantinov Nuclear Physics Institute of National Research Centre "Kurchatov Institute", PNPI, St. Petersburg; Russia.
- ¹³⁹Department of Physics and Astronomy, University of Pittsburgh, Pittsburgh PA; United States of America.
- ¹⁴⁰^(a)Laboratório de Instrumentação e Física Experimental de Partículas - LIP; ^(b)Departamento de Física, Faculdade de Ciências, Universidade de Lisboa, Lisboa; ^(c)Departamento de Física, Universidade de

- Coimbra, Coimbra;^(d)Centro de Física Nuclear da Universidade de Lisboa, Lisboa;^(e)Departamento de Física, Universidade do Minho, Braga;^(f)Universidad de Granada, Granada (Spain);^(g)Dep Física and CEFITEC of Faculdade de Ciências e Tecnologia, Universidade Nova de Lisboa, Caparica; Portugal.
- ¹⁴¹Institute of Physics of the Czech Academy of Sciences, Prague; Czech Republic.
- ¹⁴²Czech Technical University in Prague, Prague; Czech Republic.
- ¹⁴³Charles University, Faculty of Mathematics and Physics, Prague; Czech Republic.
- ¹⁴⁴Particle Physics Department, Rutherford Appleton Laboratory, Didcot; United Kingdom.
- ¹⁴⁵IRFU, CEA, Université Paris-Saclay, Gif-sur-Yvette; France.
- ¹⁴⁶Santa Cruz Institute for Particle Physics, University of California Santa Cruz, Santa Cruz CA; United States of America.
- ¹⁴⁷^(a)Departamento de Física, Pontificia Universidad Católica de Chile, Santiago;^(b)Departamento de Física, Universidad Técnica Federico Santa María, Valparaíso; Chile.
- ¹⁴⁸Department of Physics, University of Washington, Seattle WA; United States of America.
- ¹⁴⁹Department of Physics and Astronomy, University of Sheffield, Sheffield; United Kingdom.
- ¹⁵⁰Department of Physics, Shinshu University, Nagano; Japan.
- ¹⁵¹Department Physik, Universität Siegen, Siegen; Germany.
- ¹⁵²Department of Physics, Simon Fraser University, Burnaby BC; Canada.
- ¹⁵³SLAC National Accelerator Laboratory, Stanford CA; United States of America.
- ¹⁵⁴Physics Department, Royal Institute of Technology, Stockholm; Sweden.
- ¹⁵⁵Departments of Physics and Astronomy, Stony Brook University, Stony Brook NY; United States of America.
- ¹⁵⁶Department of Physics and Astronomy, University of Sussex, Brighton; United Kingdom.
- ¹⁵⁷School of Physics, University of Sydney, Sydney; Australia.
- ¹⁵⁸Institute of Physics, Academia Sinica, Taipei; Taiwan.
- ¹⁵⁹^(a)E. Andronikashvili Institute of Physics, Iv. Javakhishvili Tbilisi State University, Tbilisi;^(b)High Energy Physics Institute, Tbilisi State University, Tbilisi; Georgia.
- ¹⁶⁰Department of Physics, Technion, Israel Institute of Technology, Haifa; Israel.
- ¹⁶¹Raymond and Beverly Sackler School of Physics and Astronomy, Tel Aviv University, Tel Aviv; Israel.
- ¹⁶²Department of Physics, Aristotle University of Thessaloniki, Thessaloniki; Greece.
- ¹⁶³International Center for Elementary Particle Physics and Department of Physics, University of Tokyo, Tokyo; Japan.
- ¹⁶⁴Graduate School of Science and Technology, Tokyo Metropolitan University, Tokyo; Japan.
- ¹⁶⁵Department of Physics, Tokyo Institute of Technology, Tokyo; Japan.
- ¹⁶⁶Tomsk State University, Tomsk; Russia.
- ¹⁶⁷Department of Physics, University of Toronto, Toronto ON; Canada.
- ¹⁶⁸^(a)TRIUMF, Vancouver BC;^(b)Department of Physics and Astronomy, York University, Toronto ON; Canada.
- ¹⁶⁹Division of Physics and Tomonaga Center for the History of the Universe, Faculty of Pure and Applied Sciences, University of Tsukuba, Tsukuba; Japan.
- ¹⁷⁰Department of Physics and Astronomy, Tufts University, Medford MA; United States of America.
- ¹⁷¹Department of Physics and Astronomy, University of California Irvine, Irvine CA; United States of America.
- ¹⁷²Department of Physics and Astronomy, University of Uppsala, Uppsala; Sweden.
- ¹⁷³Department of Physics, University of Illinois, Urbana IL; United States of America.
- ¹⁷⁴Instituto de Física Corpuscular (IFIC), Centro Mixto Universidad de Valencia - CSIC, Valencia; Spain.
- ¹⁷⁵Department of Physics, University of British Columbia, Vancouver BC; Canada.
- ¹⁷⁶Department of Physics and Astronomy, University of Victoria, Victoria BC; Canada.

- ¹⁷⁷Fakultät für Physik und Astronomie, Julius-Maximilians-Universität Würzburg, Würzburg; Germany.
- ¹⁷⁸Department of Physics, University of Warwick, Coventry; United Kingdom.
- ¹⁷⁹Waseda University, Tokyo; Japan.
- ¹⁸⁰Department of Particle Physics, Weizmann Institute of Science, Rehovot; Israel.
- ¹⁸¹Department of Physics, University of Wisconsin, Madison WI; United States of America.
- ¹⁸²Fakultät für Mathematik und Naturwissenschaften, Fachgruppe Physik, Bergische Universität Wuppertal, Wuppertal; Germany.
- ¹⁸³Department of Physics, Yale University, New Haven CT; United States of America.
- ¹⁸⁴Yerevan Physics Institute, Yerevan; Armenia.
- ^a Also at CERN, Geneva; Switzerland.
- ^b Also at CPPM, Aix-Marseille Université, CNRS/IN2P3, Marseille; France.
- ^c Also at Département de Physique Nucléaire et Corpusculaire, Université de Genève, Genève; Switzerland.
- ^d Also at Departament de Física de la Universitat Autònoma de Barcelona, Barcelona; Spain.
- ^e Also at Departamento de Física, Instituto Superior Técnico, Universidade de Lisboa, Lisboa; Portugal.
- ^f Also at Department of Applied Physics and Astronomy, University of Sharjah, Sharjah; United Arab Emirates.
- ^g Also at Department of Financial and Management Engineering, University of the Aegean, Chios; Greece.
- ^h Also at Department of Physics and Astronomy, Michigan State University, East Lansing MI; United States of America.
- ⁱ Also at Department of Physics and Astronomy, University of Louisville, Louisville, KY; United States of America.
- ^j Also at Department of Physics and Astronomy, University of Sheffield, Sheffield; United Kingdom.
- ^k Also at Department of Physics, California State University, East Bay; United States of America.
- ^l Also at Department of Physics, California State University, Fresno; United States of America.
- ^m Also at Department of Physics, California State University, Sacramento; United States of America.
- ⁿ Also at Department of Physics, King's College London, London; United Kingdom.
- ^o Also at Department of Physics, St. Petersburg State Polytechnical University, St. Petersburg; Russia.
- ^p Also at Department of Physics, Stanford University, Stanford CA; United States of America.
- ^q Also at Department of Physics, University of Adelaide, Adelaide; Australia.
- ^r Also at Department of Physics, University of Fribourg, Fribourg; Switzerland.
- ^s Also at Department of Physics, University of Michigan, Ann Arbor MI; United States of America.
- ^t Also at Faculty of Physics, M.V. Lomonosov Moscow State University, Moscow; Russia.
- ^u Also at Giresun University, Faculty of Engineering, Giresun; Turkey.
- ^v Also at Graduate School of Science, Osaka University, Osaka; Japan.
- ^w Also at Hellenic Open University, Patras; Greece.
- ^x Also at Institutio Catalana de Recerca i Estudis Avancats, ICREA, Barcelona; Spain.
- ^y Also at Institut für Experimentalphysik, Universität Hamburg, Hamburg; Germany.
- ^z Also at Institute for Mathematics, Astrophysics and Particle Physics, Radboud University Nijmegen/Nikhef, Nijmegen; Netherlands.
- ^{aa} Also at Institute for Nuclear Research and Nuclear Energy (INRNE) of the Bulgarian Academy of Sciences, Sofia; Bulgaria.
- ^{ab} Also at Institute for Particle and Nuclear Physics, Wigner Research Centre for Physics, Budapest; Hungary.
- ^{ac} Also at Institute of High Energy Physics, Chinese Academy of Sciences, Beijing; China.
- ^{ad} Also at Institute of Particle Physics (IPP); Canada.
- ^{ae} Also at Institute of Physics, Academia Sinica, Taipei; Taiwan.

- af* Also at Institute of Physics, Azerbaijan Academy of Sciences, Baku; Azerbaijan.
- ag* Also at Institute of Theoretical Physics, Ilia State University, Tbilisi; Georgia.
- ah* Also at Instituto de Fisica Teorica, IFT-UAM/CSIC, Madrid; Spain.
- ai* Also at Istanbul University, Dept. of Physics, Istanbul; Turkey.
- aj* Also at Joint Institute for Nuclear Research, Dubna; Russia.
- ak* Also at LAL, Université Paris-Sud, CNRS/IN2P3, Université Paris-Saclay, Orsay; France.
- al* Also at Louisiana Tech University, Ruston LA; United States of America.
- am* Also at LPNHE, Sorbonne Université, Paris Diderot Sorbonne Paris Cité, CNRS/IN2P3, Paris; France.
- an* Also at Manhattan College, New York NY; United States of America.
- ao* Also at Moscow Institute of Physics and Technology State University, Dolgoprudny; Russia.
- ap* Also at National Research Nuclear University MEPhI, Moscow; Russia.
- aq* Also at Physics Department, An-Najah National University, Nablus; Palestine.
- ar* Also at Physics Dept, University of South Africa, Pretoria; South Africa.
- as* Also at Physikalisches Institut, Albert-Ludwigs-Universität Freiburg, Freiburg; Germany.
- at* Also at School of Physics, Sun Yat-sen University, Guangzhou; China.
- au* Also at The City College of New York, New York NY; United States of America.
- av* Also at The Collaborative Innovation Center of Quantum Matter (CICQM), Beijing; China.
- aw* Also at Tomsk State University, Tomsk, and Moscow Institute of Physics and Technology State University, Dolgoprudny; Russia.
- ax* Also at TRIUMF, Vancouver BC; Canada.
- ay* Also at Università di Napoli Parthenope, Napoli; Italy.
- * Deceased